Characterization of Defeat of Weaponized Biological Spores via Heat Transfer

by

Drew Rolader

A thesis submitted to the Graduate Faculty of
Auburn University
in partial fulfillment of the
requirements for the Degree of
Masters of Science in Mechanical Engineering

Auburn, Alabama
December 10, 2016

Keywords: thermal sciences, fluidized beds, heat transfer, fluid dynamics

Approved by

Jeffrey Suhling, Chair, Professor of Mechanical Engineering
Daniel Harris, Associate Professor of Mechanical Engineering
Jay Khodadadi, Professor of Mechanical Engineering
Daniel Mackowski, Professor of Mechanical Engineering

Abstract

During the past few decades, there has been concern that large amounts of weaponized Bacillus Anthracis (Ba) is being created and stored in 55 gallon barrels by potential adversaries of the United States. The most likely offensive solutions to deal with these stored agents is to just bomb the storage facility. While such an attack may prevent the Ba from being used as a weapon, it also could loft the agent into the air and disperse it into civilian populations. This "collateral damage" could kill thousands of innocent people. The objective of this thesis was to study a new low collateral damage method for defeating biological agents. Weaponized biological agents are typically in the form of spores. When inhaled, these spores vegetate and release toxins within the body. Only a very small amount of Ba spores inhaled can lead to death. For this thesis, two new methods to defeat a simulate for Ba spores (Bacillus Thuringiensis, Bt) were investigated. Both methods used thermite as a heat source inside of a barrel of agent simulate. The first method relies on the temperature generated by the thermite to kill the spores. The second method uses the heat from the thermite to burn the outer layer of the spores and the filler material. This burning releases sticky gasses throughout the barrel, and as they re-condense, these gases cause the spores to form clumps that are larger than the respirable limit. For this thesis, many experiments were performed and a theoretical model was developed. The aim was to use the experimental data to validate the numerical model and understand the basic phenomena occurring with simulate as it is exposed to high temperature. Temperature data was collected experimentally, and the model accurately predicted the measured distribution. In addition, the measured spatial distribution of the particle sizes in the mixture correlated very well with that predicted by the model. This analysis indicates the studied approach may be a viable solution to destroy weaponized biological agent in the future.

Acknowledgments

Most importantly, I would like to thank my Lord and savior for any and all opportunities I am blessed to have. I would not have been able to get through graduate school without his strength each and every day.

I would to thank my parents for raising me in an environment which encouraged learning and education. The sacrifices they have made for me and my siblings are something I will never fully understand. Family is very important to me, and I would not be where I am with each member of my family and how they have impacted my life. This accomplishment would have not been possible without them.

I would like to thank my job, IS4S, for allowing me this opportunity, not only for a job, but allowing me to turn my work into this thesis. Thank you to Dr. Charles Neely of Auburn Chemical, Dr. Eric Mentz and Dr. Kofi Bota of Clark Atlanta University for your guidance and direction throughout this thesis. I would also like to thank Jack Otto and Ryan Hill for always helping when I was stuck and steering me in the right direction whenever he thought I needed it. Thank you, again, to my dad, Dr. Glenn Rolader. He has shown me the importance of education and also working extremely hard in every area of life. Without his work ethic, I would not be able to present any of this work.

I would like to thank my thesis advisor Dr. Daniel Harris of the school of Mechanical Engineering at Auburn University. As well as the other professors on my committee: Dr. Daniel

Mackowski and Dr. Jay Khodadadi. Without their willingness to help this thesis would not have been possible.

Thank you.

Disclaimer

252.235-7010 Acknowledgment of Support and Disclaimer. (MAY 1995)

(a) The Contractor shall include an acknowledgment of the Government's support in the publication of any material based on or developed under this contract, stated in the following terms: This material is based upon work supported by the Defense Threat Reduction Agency under Contract No. HDTRA1-14-C-0028.

(b) All material, except scientific articles or papers published in scientific journals, must, in addition to any notices or disclaimers by the Contractor, also contain the following disclaimer: Any opinions, findings and conclusions or recommendations expressed in this material are those of the author(s) and do not necessarily reflect the views of the

Defense Threat Reduction Agency.

Table of Contents

List of Tables

List of Figures or Illustrations

Lists of Abbreviations of Symbols

Ba – Bacillus Anthracis

Bt – Bacillus Thuringiensis

C - Celsius

HE – High Explosives

K – Kelvin

Ms – Milliseconds

µm – Microns

Chapter 1: Intro/Purpose

Some nations and adversaries possess stored chemical and/or biological agents, and there is a growing risk that terrorists may obtain these agents. Current approaches to neutralize and/or functionally defeat these agents rely on extremes such as explosive blasts and high temperatures for neutralization. There has been progress over the past 15 years, but there is still no accepted method to neutralize large, or even small, quantities of bulk agents without the risk of undesirable collateral hazard.

The use of biological agents is a growing concern due to the fear that they can be packaged and used as weapons of mass destruction. The most effective method to functionally defeating these bio-agents is to use munitions and blow up the entire facility, rendering the material useless. Although this method is effective because the agent cannot be gathered and used, it is very dangerous to the surrounding population. The over-pressure from the munition creates an airborne plume that contains biological agent, which if breathed can be deadly. Therefore, there is a need for an innovation and optimized approach to neutralize bulk chemical and biological agents.

One known biological threat is Bacillus Anthracis (Ba) stored in large barrels. Due to the hazardous nature of this material, it is not an option for testing. Therefore, a simulant must be used. There are multiple types of bacillus, and their anatomy is very similar. Bacillus thuringiensis (Bt) is a common simulant for Ba because it has similar physical properties. The actual simulant for a weaponized agent is comprised of two materials mixed together: Javelin WG, which contains 80%, by weight, Bt, and precipitated silica. Javelin WG is a pesticide used to protect crops from insects such as caterpillars. Precipitated silica

is a material used as a filler in most application to improve performance in plastics and rubbers. In this case, it is used to give the Javelin a lofted property.

A new mechanism of defeat was conceived and developed to functionally defeat large quantities on Ba. This method of bulk neutralization requires the use of a heat source placed inside of a barrel filled with the biological agent. The material surrounding the heat source will be raised to a temperature which renders it useless. Thermite was used as the heat source due to the high levels of energy produced during the reaction. This method produces a low collateral damage solution.

The aim of this thesis is to quantify the effectiveness of the bulk neutralization method using Bt as a simulant for Ba. This investigation requires a closely coupled experimental and modeling effort to understand the fundamental physics and the overall system effectiveness of the method. Experiments were identified, planned, setup, and executed with the goal of validating the model. The model tracks temperature profiles and densities throughout the system. Acceptable temperature profiles and clump sizes were identified for kill/neutralization, and these were used to quantify the effectiveness of the method.

Chapter 2: Background

Bulk agent defeat concepts can be grouped broadly into the our classes seen in Table 1. The first class relies on High Explosives (HE) that produce significant fragments, opening agent containers, and aerosolizing the agents. These concepts strive to control collateral damage by using heat and/or chemicals to neutralize the aerosolized agents before they are able to "vent" out of the facility. However, analyses and sub-scale experiments with surrogates have shown this approach results in significant collateral hazards, as the agent is not fully killed before the pressure drives it out of the facility.

Table 1 - Agent defeat concepts can be broadly categorized into these four classes

(1) High Explosives Methods

- Use explosive warheads to open agent containers
- Kill agent inside and outside facility; order of milliseconds
- Potential for collateral hazards

(2) Disruption Methods

- Open containers
- Minimize over pressure and collateral damage
- Deployment challenges

(3) Radiative Methods

- Nuclear effects to kill agents
- May avoid opening containers
- Significant Policy challenges

(4) Bulk Neutralization Methods

- Does not require container opening
- Reduced collateral risk
- Potential for "complete" kill
- Relies on thermal kill
- Energy intensive due to inefficiencies

The second class, Disruption Methods, focuses on opening containers or destroying other facility components while generating minimal facility over-pressure. Without significant over-pressure, agent venting and collateral damage can be minimized. These concepts offer promise under some conditions of operation, but the deployment and scaling issues must be resolved.

The third class is Radiative Methods, which as the name suggests, relies on radiation for neutralization and/or facility denial. Some of these methods have promise, but the collateral damage and political sensitivities makes development and deployment very challenging.

Finally, the fourth class is Bulk Neutralization Methods, which attempts to neutralize and/or functionally defeat the agent in its bulk form. Research on these methods are not as advanced as other methods, but the potential of this method justifies further investigation and research.

Theoretically, more than enough energy can be delivered for bulk neutralization, but the challenge is getting the neutralizing heat and/or chemical to the desired location for the necessary amount of time. A proposed solution utilizing distributed thermal sources for localized functional defeat was developed. Figure 1 shows a relative comparison of different methods of biological agent neutralization as a function of temperature and time, and shows that the proposed approach operates in an intermediate time/temperature regime.

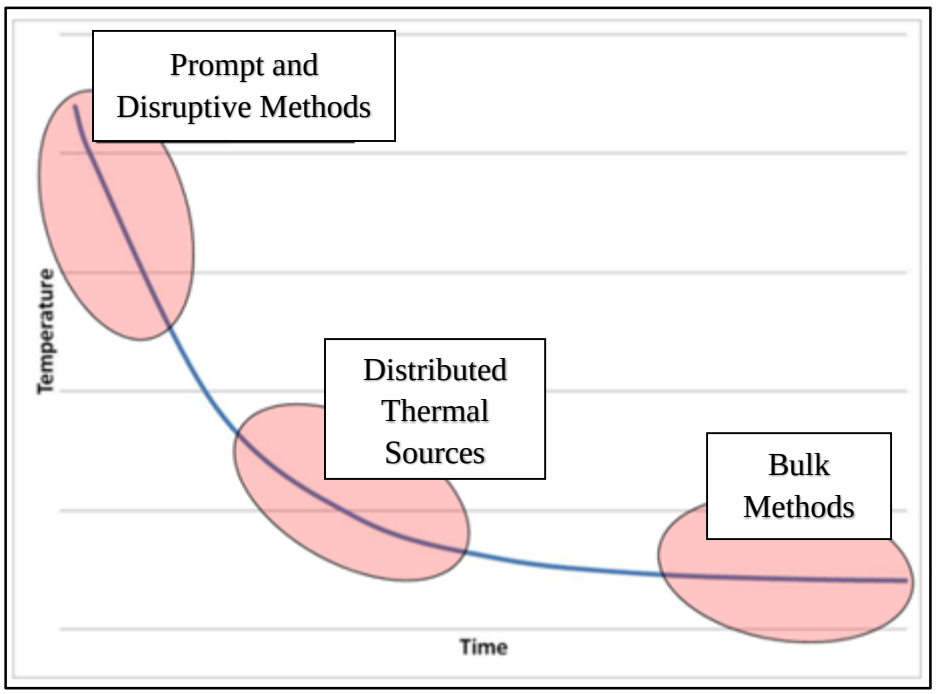

Figure 1 – Representation of the different methods of neutralization as a function of temperature and time

To understand how effective this new method is, a clear understanding of "effective" must be defined. There are multiple ways to prevent Ba from harming people. First, access to the agent can be prevented. For example, if the agent is buried in the rubble from an explosive, it is not accessible. Second, if the Ba spores are killed (neutralized), they are not harmful. Finally, if the Ba is "clumped" into groups that are too large to be respirable, they will not harm humans, and the material is considered functionally defeated. Research has shown that when Bt spores are airborne heat can kill them in a matter of milliseconds (ms). Figure 2 [1] shows the kill of a Bt spore as it is exposed to heat. Spores were exposed to 700 Kelvin (K) and 900 K. Different samples were exposed at these temperatures for a known time, and viability analysis was run on these samples to determine the amount that was still viable.

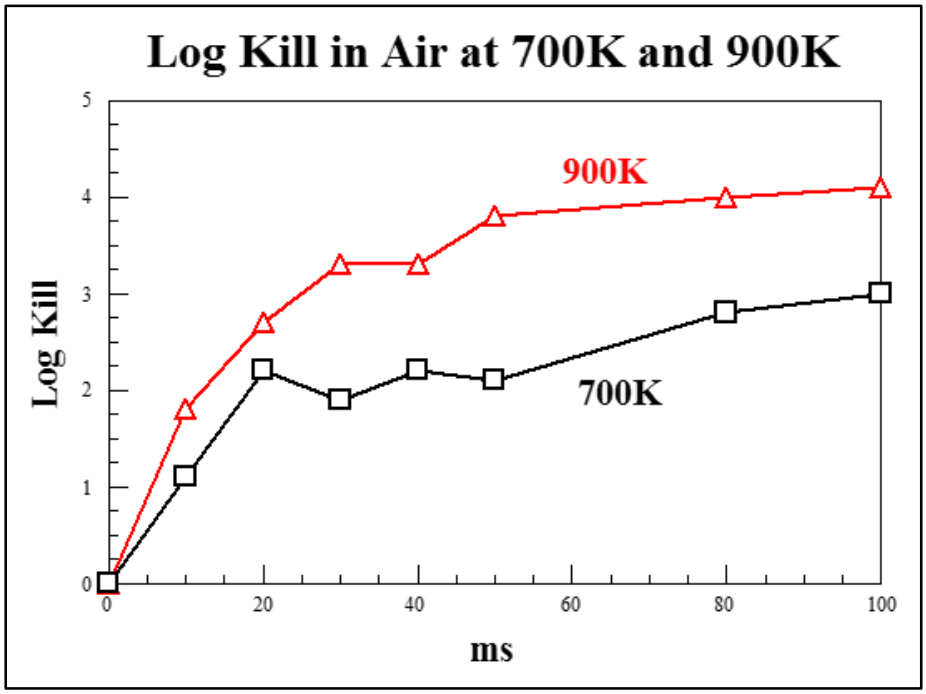

Figure 2– Short term agent neutralization at 700 K and 900 K

According to Figure 2, if a spore is held at 900 K for 100 ms there is a 4 log reduction in the viability. Although this data is useful, it must be understood these experiments are done in a lab, and are conducted in purified air. This does not accurately represent a real scenario because these results are from individual spores being heating, and not bulk spores. Inside of a large barrel there will be millions of these spores insulating each other, as well as silica. A major challenge for bulk heat neutralization is getting the energy to diffuse throughout the agent. These agents tend to be excellent insulators. If a barrel of Bt was placed in a room that was 900 K for 100ms, the surface of the spores on the outside would be killed, but effectively the barrel would be completely untouched by the heat. In order for the model to quantify the effectiveness, the correct thermal properties for the Bt must be found.

Ba is used in a powder form and is harmful in three ways: through the skin, eating the spores, or inhaling the spores. Although each can be very harmful and potentially fatal, inhalation is by far the most dangerous. When *Ba* is inhaled the spores become vegetative bacteria and release toxins within the body. The bateria can be killed, but the toxins remain in the blood and effect the heart and liver. For media of any kind to be inhaled, it must be very small. Figure 3 [2] shows a diagram of the size a particle must be to settle at different locations in the human respiratory system. For example, if a particle is between 9 microns (μm) and 5.5 μm it will not go farther than nose/throat.

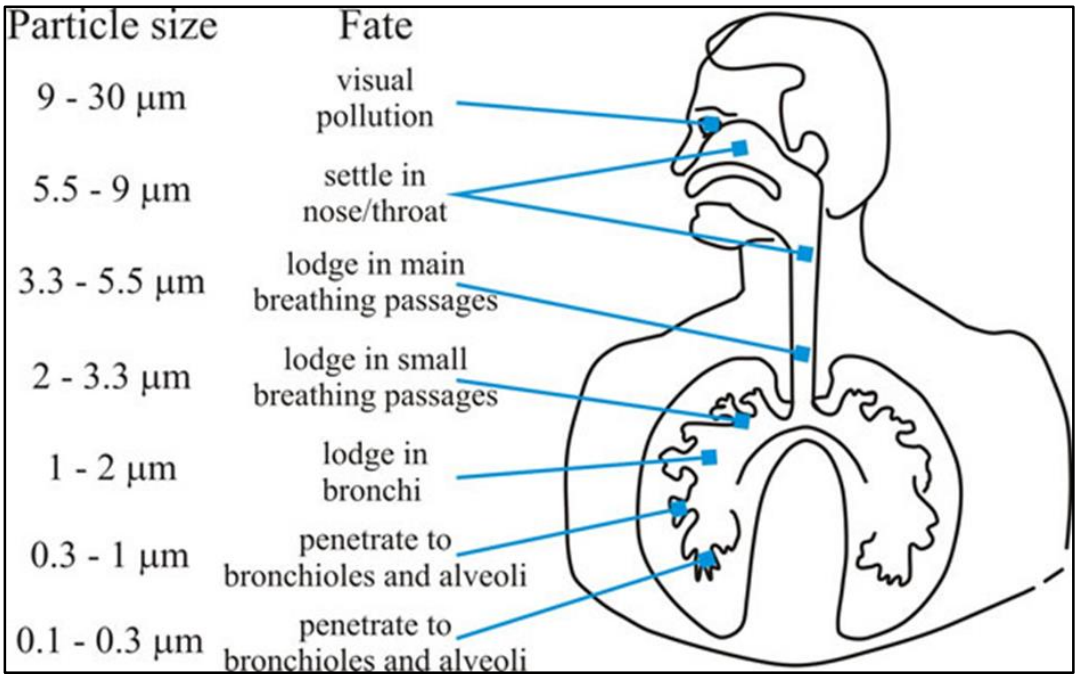

Figure 3 – Settling locations of particles as it passes through the respiratory system

Therefore, if spores of Ba could be aggregated into clumps bigger than 10 μm, they would not enter the respiratory system. This approach does not kill the spores, but it renders them functionally defeated and useless for an airborne weapon. To facilitate this effect, a concept was developed that exploits the fact the exotoxins on the outer layer of these spores

are naturally “sticky” and cause the agent to clump together. Once heat is introduced to the system these exotoxins begin to burn off. A sticky gas is produced and moves through the system. These gases will re-condense as they push through the barrel causing the spores to clump together.

The proposed method for bulk material defeat utilizes a heat source to locally raise the temperature of the material high enough to kill some spores, and causes release of the exotoxin gases throughout the system. This results in spores being killed from the heat as well as spores becoming “sticky” and clumping to one another. This renders the material not hazardous.

For this research, thermite was selected as the heat source. Thermite is comprised of an aluminum powder for fuel and a metal oxidizer. With different particle sizes and different oxidizers, the number of different thermite compositions is large. Thermite burns at temperatures well over 2000 °C, and it can reach as high as 3000 °C. When ignited, the thermite (powder form) undergoes an exothermic reaction, and generates molten iron which retains heat for an extended period of time. Thermite has an extremely high energy density, making it an ideal heat source.

With an understanding of the problem statement the question remains, what is the effect of a thermite burn inside a barrel of Bt? An experimental test series was developed to answer the question; however, these experiments require multiple days and is very expensive, and each experiment only gives results for one thermite composition. The number of different thermites, particle sizes, and additives that could be used would take a long time to optimize if each had to be investigated experimentally. Therefore, a theoretical model is needed to predict the effectiveness of untested thermites. This model must track

temperature profiles throughout the system, as well as predict the spatial amount of clumping within the barrel. With a validated numerical model, thermite properties and system parameters can be analyzed without the time consuming, expensive experiments.

A significant amount of work was performed by other research team members to lay the ground work for understanding the fundamental physics driven by placing a thermite inside a barrel of a Bt mixture. This work was done through a series of qualitative observations and results gathered from different test series to identify the optimum time/temperature regime for bulk neutralization. A brief discussion of these experiments follows.

The first experimental setup investigated Bt inside of a 1-gallon paint can wrapped with a "heat jacket" to apply a constant boundary temperature of 100-200° C, 200-300° C, and 300-500° C. To consider higher temperatures, the Bt filled paint can was placed inside a 1000 ° C preheated oven. The 1-gallon paint can was instrumented with thermocouples in the lid (at different depths and distances from the wall) to track the temperature profile (Figure 4). The locations are shown in Table 2.

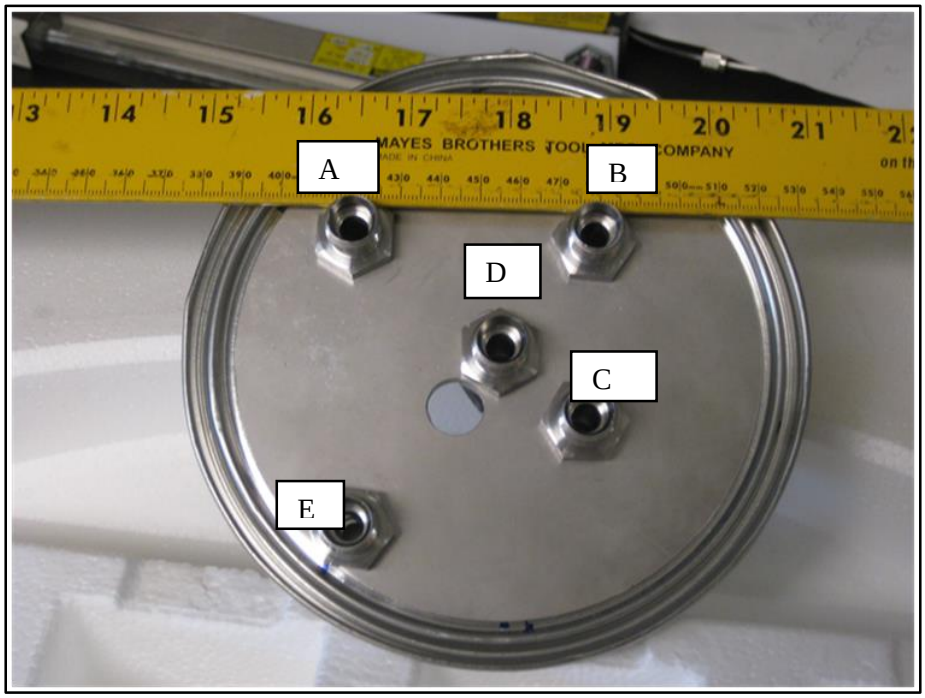

Figure 4 – Locations of thermocouples in the oven tests above 1000° C

Table 2 – Location of thermocouples in oven tests over 1000° C

Thermocouple Locations	Distance from Centerline (cm)
A	4.7
B	3.7
C	2.7
D	0.0
E	5.7

When higher temperatures were tested the results were not as expected. Temperatures at some locations inside the can were higher than temperatures closer the edge. The paint can was heated by conduction only, and should have shown higher temperatures decreasing from the outside to the middle. Figure 5 shows these results.

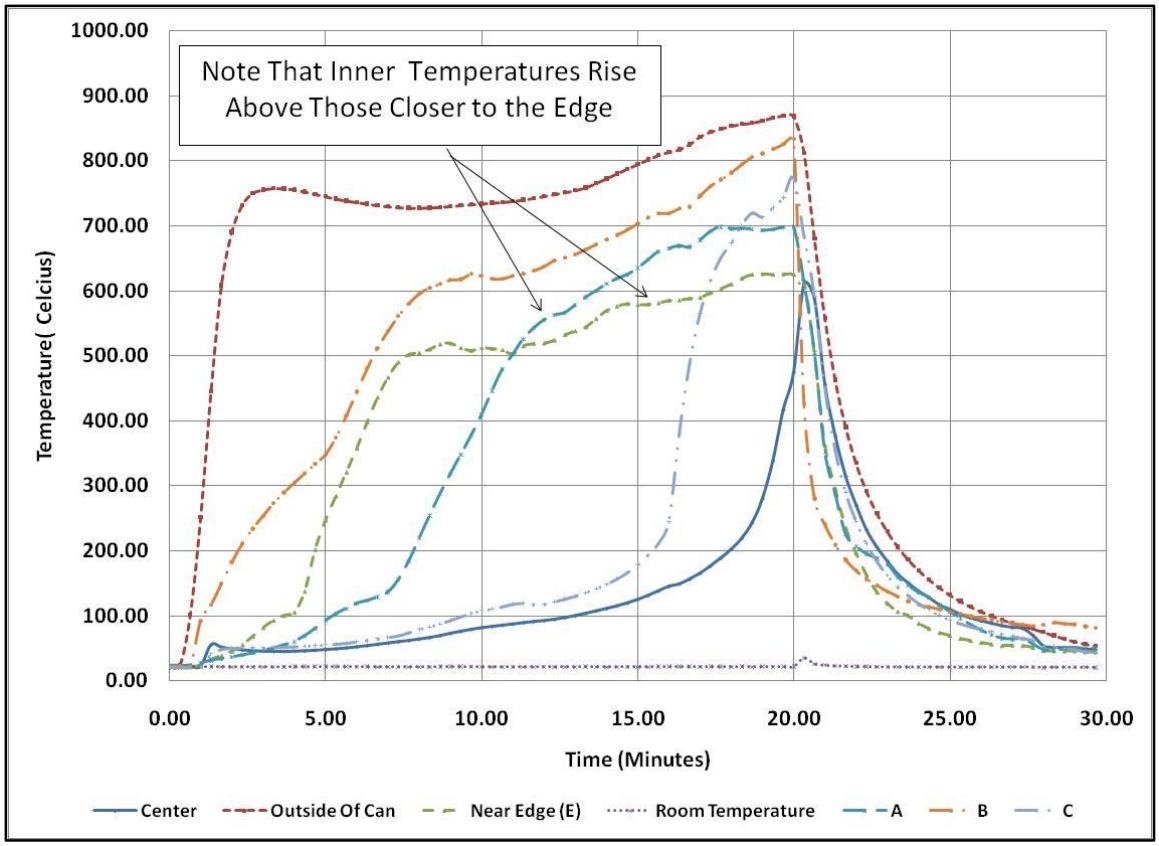

Figure 5 – Temperature profile from oven tests over 1000° C

The temperature inversion indicated that some type of transport phenomena was taking place inside the paint can when heat was applied, implying that "fluid like" movement was taking place with the addition of heat.

To gain a better understanding of this behavior, a test apparatus was built to view the movement inside of the Bt when heated. These experiments were named the "ant farm" test series, due to the shape of the test apparatus. Figure 6 shows the drawing and Figure 7 shows the final product before testing. The ant farm is made out of a steel bottom, 3 steel sides, and 1 side being glass to view the movement of spores.

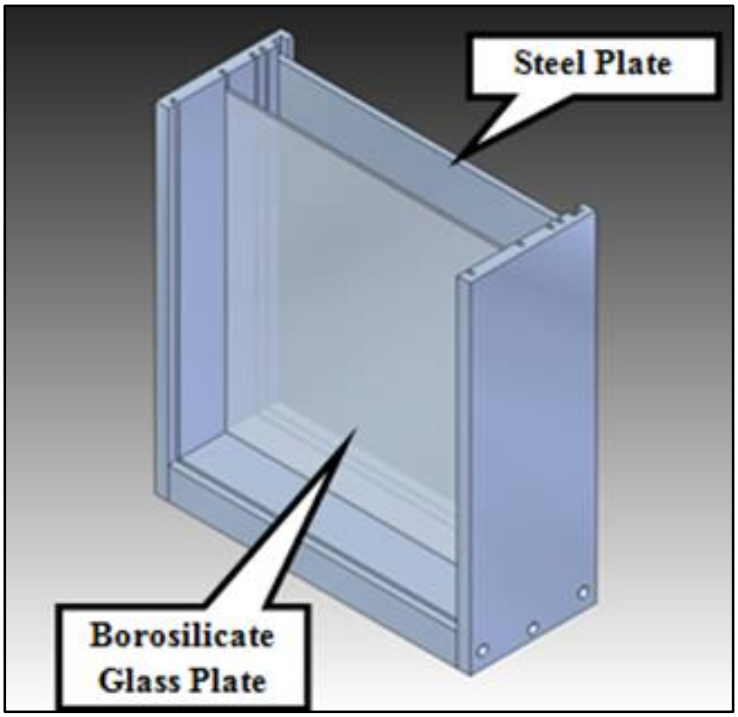

Figure 6 - Drawing of ant farm with glass plate for viewing

Figure 7 –Ant farm filled with Bt

A heat source was applied to the metal plate opposite of the glass viewing window and observation were made. Figure 8 shows that the Bt inside the system begins to move rapidly throughout the test apparatus. The top was left off the apparatus and the Bt can be seen bubbling and moving in a fluid like motion.

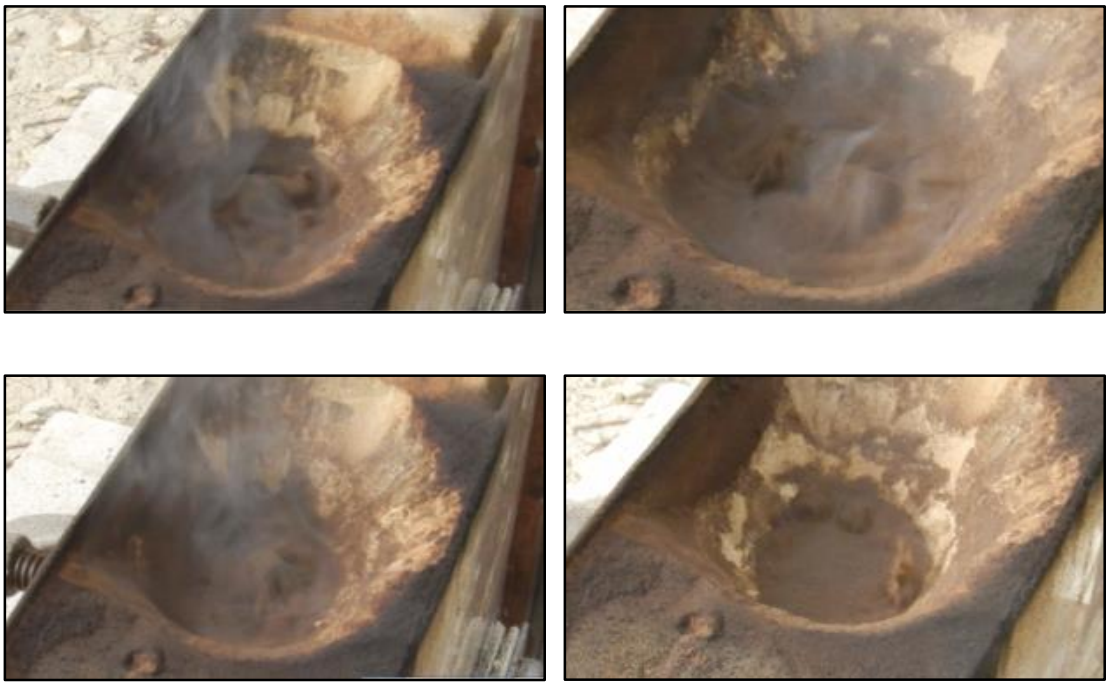

Figure 8 – This sequence of figures shows the Bt mix fluidizing after the thermite penetrated the spores and fell to the bottom. Note the "bubbling" and "boiling" effect.

Previous experiments showed deposition of a charred layer of spores on the top of the spore bed. At the time, it was uncertain if these spores were deposited due to fluidization or if the spores remained stationary but were charred from the heat. However, the ant farm test series showed that the charred spores are in fact deposited from the turbulence occurring at the wall due to the rapid heating. This newly identified phenomena was documented using photo/video tools. Allowing the heat from the thermite to enter the system leads to observable fluidization. The spores appear to "boil" similar to a pot of

water. Therefore, in order to properly model this problem, it must be viewed as a fluidized bed.

Chapter 3: Literature Review

Much of the information presented previously was derived from a detailed literature review, summarized in this section. In this literature review, three topics will be covered in detail: Bacillus thuringiensis, the chemical reaction of thermite, and necessary equations for the modeling of relevant phenomena. A better understanding of these three topics will not only help in understanding what is physically happening within the system, but it also aid in the development of the final results and conclusions.

3.1 Bacillus Thuringiensis

To investigate the basic phenomena occurring in the mixture requires a detailed understanding of the primary danger in weaponized, Ba. The threat is Ba, which is the primary causative agent of anthrax [3]. Since Ba cannot be safely used for bulk testing, a proper simulant must be identified. Ba is part of a genus which contains six recognized species. Those species are: B. cereus, B. thuringiensis, B. anthracis, B. mycoides, B. pseudomycoides, and B. weihenstepanensis [3]. DNA analysis shows that B. thuringiensis and B. cereus are more closely related to Ba [4].

B. cereus has been identified in two forms of food poisoning and is characterized by either abdominal distress or nausea and vomiting [5]. Therefore, it is not a safe simulate for Ba, and it is, therefore, eliminated from consideration. Bt is as an insect pathogen, and it is considered harmless to humans, which makes it an excellent choice as a Ba simulant. In addition, Bt is commercial available and can be bought as Bt Javelin WG from organic farms across America [6]. Consequently, Bt was selected as the Ba simulant for this research.

Biological weapons yield the most harm when they are airborne and can be breathed into the lungs. This period is called primary aerosolization [7]. Therefore, a lighter material is typically added to the agent to increase the mixture air dispersion. For this research, Aerosil R812 fumed silica was added to the Bt Javelin to create a simulated biological weapon mixture.

There are three distinct parts that make up a Bt spore: coat, cortex, and the core [8]. The coat portion of the spore is the outer most section. This section is resistant to lower temperatures and acts as a layer of protection. Although, when the temperature is raised to a higher value, the coat portion releases gasses and other materials which can cause the "clumping" effect.

3.2 Chemical Reaction of thermite

The word thermite was first used in 1908 by a German chemist named Dr. Hans Goldschmidt [9]. The name was chosen to describe the exothermic oxidation-reduction (redox) reaction in which there is rapid formation of Al-O bonds [10] from metals or alloys. When these powders undergo this reaction, the temperature can reach well over 3000° C. Thermite is known as a gasless reaction because there are no gaseous phases during the chemical process [11]. Therefore, the only relevant by-products of the metal powders after the process is completed is a molten iron.

While the thermite itself is a gasless reaction, the heat it creates does produce gases from the other solids in the control volume. When thermite is ignited in a barrel of Bt the direct result is instantaneous burning of the surrounding *Bt*; this burning produces a significant amount of gas vapor. This burning and pyrolysis results in permanent change in the system [12]. Thermogravimetric analysis (TGA), a process in which the physical and

chemical properties of a material are measured as a function of increasing temperature, has shown that the spores/silica mixture of Bt produce (i) permanent gases (oxygen, hydrogen, etc.), (ii) water, (iii) organic vapors, and (iv) char. This material characterization was verified using another technique, differential scanning calorimetry (DSC) where the temperature differential is measured between the amount of heat required to increase the sample and a reference baseline.

When the thermite is ignited solids (from the thermite reaction and Bt simulant material) and gases (condensable and non-condensable) move throughout the system. Once the Bt begins to burn and produce non-condensable gasses, those gasses move throughout the system and exit the barrel of Bt (the control volume) regardless of the rate of cooling. The non-permanent gasses, such as water and organic vapors, re-condense as the local temperature drops. The organic vapors re-condense as sticky material that cause clumping of bacillus spores/silica mix resulting in functional defeat.

Within the control volume, multiple materials must be tracked; these are known as species. Creation and destruction of these species, discussed in detailed in the modeling section, are a direct result of the chemical changes driven by the heat added thermite.

3.3 Model

Computer models, although not perfect, can be used to produce results much cheaper and faster than experiments. Heat transfer models have been used for years in applications ranging from the temperature profile of a lightbulb to the rockets on the Space Launch System. For this research, there is a need for a sufficiently detailed numerical computer model to simulate the detailed physics occurring in the system. There are two primary objectives of this model. First, it can be used to estimate performance without an

experiment. Second, and potentially more important, it can be used to better understand and explain the fundamental physics of the problem to help optimize the design and maximize effectiveness if the agent defeat concept.

Previous work provided insight into key aspects of the problem. It is known that multiple species exist in the system, and that fluid motion and phase change must be tracked. Furthermore, the "ant farm" experiments clearly showed that the system behaves, and should be modelled similarly, to a fluidized bed.

The physics of fluidized beds have been well documented and studied in many other areas such as pyrolysis of biomass. Since this process contains much of the same physics as the current research project, the typical fluidized-bed conservation equations provided a starting point for this effort. In several countries, the desire for clean hydrogen fuel has required research in biomass pyrolysis. That reaction is done in vessels filled partially with sand. The pyrolysis process is endothermic; therefore, the vessel is heated from injecting hot air at the bottom. Inside the vessel, the bed of material begins to obtain fluid-like properties and become a gas-solid mixture. Biomass is then fed into the vessel via a feeding mechanism, mixing throughout the fluidized bed. As the process continues the biomass begins to pyrolyze and produces gases, tar, and char. These gases work through the system while the tar and char products move through the exit and are allowed to cool [13].

"Fluidization is observed when a bed of solid particles comes into contact with a vertical upward fluid flow within a particular range of flow velocity [14]." As a thermite charge is ignited at the bottom of a barrel of simulant, energy and heat are released, burning the surrounding Bt. The Bt reacts very similarly to burning of biomass producing gases and char. The creation of tar is absent in Bt, and can be removed from the corresponding

equations. The gases created and released from the Bt forcefully move upward through the bed. Because the thermite is the source of disturbance, it can be modeled as the origin.

To explain the phenomena within the barrel, a detailed multi-species model must include the continuity equation, energy equation, and momentum equation. These equations will be used to track properties of each species as a function of distance from the origin (center of the thermite).

3.3.1 Continuity Equation

The continuity equation, found in [13], [15], and [16], is simply a mass balance within a control volume. The Boltzmann transport equation describes a fluid with the direction and rate of temperature change causing heat to flow from a source to cooler regions by the transport of particles. Multiple sources utilize the derived Boltzmann equation [17]. Equation (1) shows the Boltzmann equation before any simplification or assumptions.

$$\frac{\partial f_i}{\partial t} + \sum_i v_i \frac{df}{dx_i} + \sum_i g_i \frac{df}{dv_i} = \left.\frac{df}{dt}\right|_c \tag{1}$$

In order to turn the Boltzmann into a solvable continuity equation, both sides must be multiplied by the mass and integrated over d^3v, resulting in:

$$\frac{d}{\partial t}\int mfd^3v + \sum_i \frac{d}{dx_i}\int mfv_i d^3v + m\int \sum_i \frac{d}{dv_i}(g_i f)d^3v = \int m\frac{df}{dt}\Big|_c d^3v \tag{2}$$

First Term:

Using the mass density as defined as:

$$\rho = \int mf(\vec{x},\vec{v},t)d^3v \tag{3}$$

The results is:

$$\frac{d\rho}{dt} \tag{4}$$

Second Term:

The mass density is used again and simplified to the following:

$$\sum_i \frac{d}{dx_i}(\rho\langle v_i\rangle) \tag{5}$$

In equation 5, $\langle v\rangle$ is the mean fluid velocity at a point in time and can be written as u. Also using the del operator the second term can be simplified to:

$$\nabla\cdot(\rho u) \tag{6}$$

Third Term:

Using the divergence theorem this term can be re-written as a volume integral. After simplifying all three terms the continuity equation, from the Boltzmann equation, can be written as:

$$\frac{\partial \rho}{\partial t} + \nabla \cdot (\rho u) = 0 \tag{7}$$

Since the agent in the barrel has multiple species, a volume fraction, α, must be incorporated for each species. Equation 7 is then tailored for both the gas and solid phases, shown below.

Gas Phase:

$$\frac{\partial (\alpha\rho)_g}{\partial t} + \nabla \cdot (\alpha\rho \boldsymbol{V})_g = \Gamma_g \tag{8}$$

Solid Phase:

$$\frac{\partial (\alpha\rho)_i}{\partial t} + \nabla \cdot (\alpha\rho \boldsymbol{V})_i = \Gamma_i \tag{9}$$

α_g = volume fraction of the gas phase

α_s= volume fraction of the solid phase

Γ_g= mass conversion rate of the gas phase originating from pyrolysis

Γ_s= mass conversion rate of the solid phase due to condensation

ρ = Density

The first term in Equation 8 and Equation 9 is the time rate of change of density in the infinitesimal control volume. The second term is the outward flux of density due to the velocity field. The right-hand term (Γ), as stated above, is the rate of mass conversion within the control volume for each phase.

The first (gas) equation says that the time rate of change of gas density plus the net outward flux of gas density (due to the gas's movement) equals the time rate of change of gas density conversion. The same concept applies to the solid equation. The normal continuity equation is set equal to zero when no mass is being created. However, in this case gas is being created through pyrolysis, and solid is being created through condensation. Setting $\Gamma_g + \Gamma_s = 0$ ensures that the total amount of mass is constant.

Within the continuity equation the initial volume fraction terms and rate of change (Γ) terms must be found before these equations can be used in the model. The initial volume fraction is the amount of a given species as a percent of the total, i.e. the sum of the volume fractions shown in Equation 10.

$$\alpha_{s,i} + \alpha_{s,re} + \alpha_{g,bio} + \alpha_{g,st} + \alpha_{g,nc} = 1, \quad (10)$$

Where the subscripts indicate:

(i) s,i: the initial solid

(ii) s,re: re-condensed solid material

(iii) g: bio-biological gases

(iv) g,nc: non-condensable (permanent) gases.

(v) g,st: steam gases

3.3.2 Energy Equation

The thermal energy equation, found in [13], [16], for both the gas and solid phase are found in Lathouwers (2001) [13], and are shown in Equation 11 and Equation 12.

Gas:

$$\left(\alpha\rho C_p\right)_g \frac{D_g T_g}{Dt} = \nabla\cdot\left(\alpha_g k_g \nabla T_g\right) + \frac{6\alpha_s k_g}{d_s^2} Nu_s\left(T_s - T_g\right) + \Gamma_{tar}^{s-g}\left(C_p^{tar} T_b - C_{p,g} T_g\right) + \Gamma_{gas}^{s-g}\left(C_p^{gas} T_s - C_{p,g} T_g\right) \quad (11)$$

Solid:

$$\left(\alpha\rho C_p\right)_s \frac{D_s T_s}{Dt} = \nabla\cdot\left(\alpha_s \rho_s C_{p,s} D_{ss} \nabla T_s\right) + \frac{6\alpha_s k_g}{d_s^2} Nu_s\left(T_g - T_s\right) + \alpha_s \rho_s \left(\frac{Q_{r,s}}{m_s}\right) + \alpha_s \rho_s \left(\frac{dm_s}{dt}\frac{h_v - h_s}{m_s}\right) \quad (12)$$

C_p= specific heat capacity

k = thermal conductivity

d_s= particle diameter

Nu_s= effective Nusselt number

Γ= mass conversion rate

$Q_{r,s}$= radiative component of heat transfer

m_s= particle mass

D_{ss}= self-diffusion coefficient

h = specific enthalpy.

Both Equation 11 and Equation 12 are derived from conservation of energy, and state that the time rate of change of energy in the control volume is equal to the net flux of

all relevant forms of energy. For the gas equation, the first term on the right-hand side is the thermal conductive flux, where k_g is the thermal conductivity of the gas. The second term accounts for heat exchange with the solid through conduction or convection. The final two terms represent excess enthalpy flux entering the gas phase from the solid phase. In other words, as some reaction causes a phase change of solid to gas, the inherent enthalpy in that matter is accounted for in the gas equation.

3.3.3 Momentum Equation

The applicable momentum equations, found in [13], [18], for a gas and a solid are shown in Equation 13 and Equation 14.

Gas:

$$\frac{\partial(\alpha\rho V)_g}{\partial t} + \nabla V_g \cdot (\alpha\rho V)_g = -\alpha_g \nabla p_g + \nabla \cdot 2\alpha_g \mu_g S_g + \alpha_g \rho_g f_g + \frac{\alpha_s \rho_s}{\tau_{s,12}}\left(V_g - V_s\right) - \Gamma_s V_s \tag{13}$$

Solid:

$$\frac{\partial(\alpha\rho V)_s}{\partial t} + \nabla V_s \cdot (\alpha\rho V)_s = -\alpha_s \nabla p_g + \nabla \cdot \left(\Sigma_s + \Sigma_s^f\right) + \alpha_s \rho_s f_g + \frac{\alpha_s \rho_s}{\tau_{s,12}}\left(V_s - V_g\right) + \phi_s + \Gamma_s V_s \tag{14}$$

∇p_g= thermodynamic pressure

S_g= strain rate tensor

μ_g= shear viscosity

f_g= gravitational acceleration (or any other body forces)

$\tau_{s,12}$= fluid particle interaction time scale

Σ_s= solid stress tensor

Σ_s^f= solid stress tensor due to friction

ϕ_s= momentum exchange of various solid classes due to collision.

Both Equation 13 and Equation 14 state that the time rate of change of momentum for an infinitesimal control volume equals the sum of forces acting on it. For the gas equation, the first term is the time rate of change of gas momentum inside the control volume. The second term is the outward flux of momentum from the control volume. The right-hand side lists the forces acting on the fluid element. The first term on the right-hand side is the force due to the pressure gradient in the gas, the second term is the effect of shear stresses, the third is the effect of the gravitational (and any other) body force, the fourth is the drag force exerted on the gas particles by the solid particles, and the last term is the effect of mass transfer (gas converted to solid) on the momentum of the gas. The gas equation, then, says that the time rate of change of gas momentum inside the control volume plus the net outward flux of momentum is equal to the sum of all the forces acting on the gas at that point.

Chapter 4: Experimentation

4.1 Relevant data

To build a base of data points to ground the model, a test series was developed and evolved into a method of obtaining the effectiveness of a thermite burn inside a barrel of Bt. These tests were executed to gather a number of data points to help quantify the amount of the material either killed or rendered useless. Physical samples of Bt before and after a thermite burn were obtained and sent to a lab for viability testing. These tests showed the kill reductions in the spores from the virgin baseline Bt compared to the Bt that was burned inside the barrel during an experiment. Another set of samples were also taken and run through a sieving process to determine clump size. Temperature profiles (taken at the exact locations of the samples) are used to correlate the temperature with results from viability and clump size as a function of distance from the thermite origin.

4.2 Test Setup for Temperature and Sampling

A very detailed test setup was developed and can be seen in a 2-dimensional illustration in Figure 9. A 10 gallon barrel was instrumented with eight K-type thermocouples which are very precisely placed on four different radii from the center of the charge (0.5”, 3.75”, 7”, and 9.9”). In *Figure 9* the thermocouple is shown as red dots. Multiple thermocouples were placed on these spheres in order to check the uniformity of the temperature gradients. These radii are known as the “radii of influence” within the barrel tests. The three black lines are the sampling slits, which are pre-cut in the side of the barrel to allow sampling at known depths and location. A weather balloon is attached to a vent hole and catches all the off gasses and any material leaving the barrel. The barrel is only filled with 6 gallons of Bt in order to reduce the costs of each test.

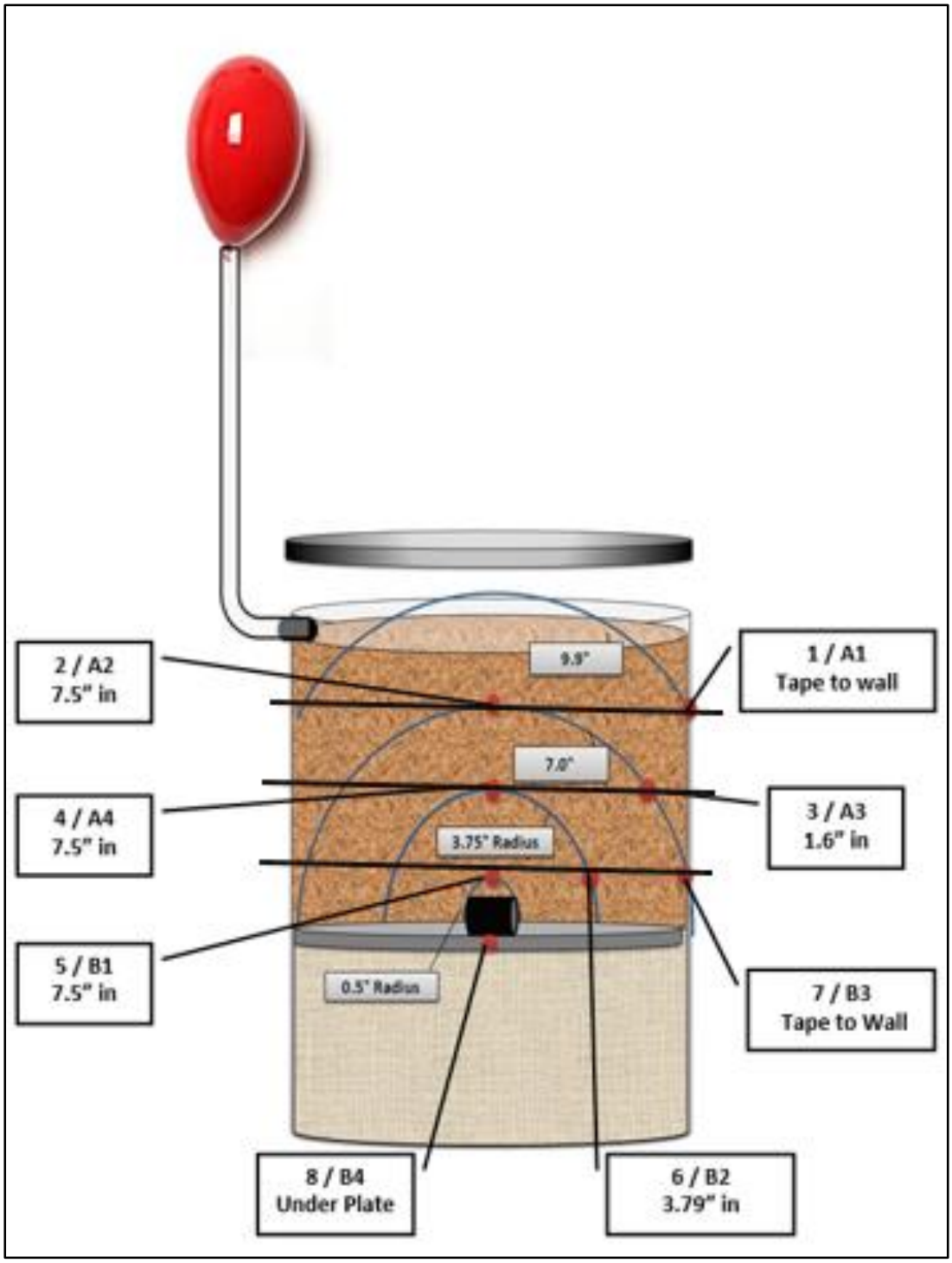

Figure 9 – Illustration of barrel test setup shown with sampling and thermocouple location (shown in red) with their distance and location from the origin, slit locations (shown as black lines), radii the samples are taken on (shown as blue half-circles), and each layer required for a barrel test.

Figure 10 shows the holes where the thermocouples are inserted. They are sealed with rubber gaskets and plumbing fittings. Thermocouple wire is run down the middle of a ceramic tube and welded together at the end to guarantee good connection. The ceramic tube is inserted into the plumbing fitting to the proper depth according to its radius to ensure the thermocouples fall on the proper radii from the origin of the thermite. This can be seen in Figure 11.

Figure 10 –Sealed thermocouple holes before ceramic tubes are put into place

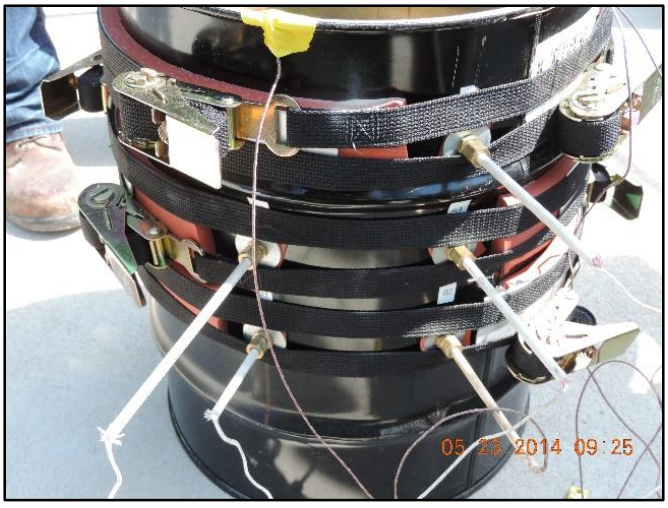

Figure 11 – Ceramic tubes with thermocouple wires run into the barrel.

Figure 12 shows the other side of the barrel where slits are cut before a test is executed. These slits are used for extracting samples after a test. They are sealed with a rubber gasket held in place with a metal band and ratchet strap. The gasket creates a seal that hold the material inside of the barrel during a test. The gasket is removed after the burn of the thermite and the barrel has cooled, seen in Figure 13.

Figure 12- Slits are cut into each barrel before a test is executed

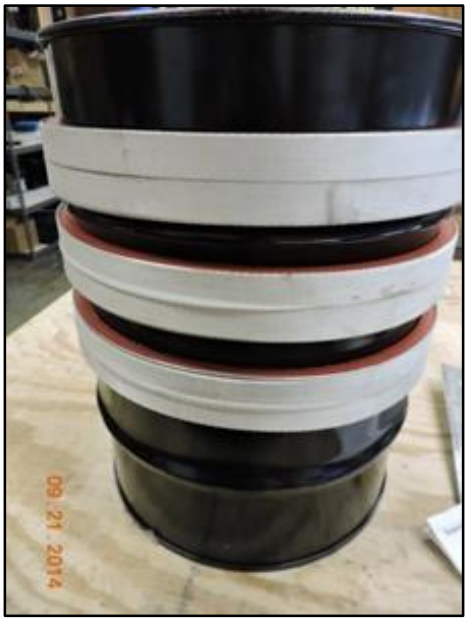

Figure 13 – Slits are sealed with a rubber gasket, metal strap, and a ratchet strap

Once the barrel is properly instrumented with thermocouples and sampling slits, a charge is placed in the middle of the barrel. The barrel is filled with Bt and executed. Temperature profiles are collected during the test using a data logger. While the particle size analysis requires the barrel to be sampled before producing any results.

4.3 Post Test Sampling Processes

Once the barrel is allowed to cool the sampling process begins. Each slit shown in Figure 9 are sampled. The rubber gasket is removed, a metal plate is inserted into the slit (one layer at a time), the Bt above the plate is vacuumed out, and the plate is removed. This provides spatially located samples. This process can be seen in Figure 14.

Figure 14 – Removing the Bt after the metal plate was slide into place.

Figure 15 – After removing the metal plate, a template is used to obtain samples.

After the material on top of the plate is removed using a vacuum the metal plate is slid out of the barrel. This process leaves an undisturbed cross-sectional layer of Bt at the desired sample locations. Figure 15 shows samples being taken using a template. This template has holes which directly line up to where the thermocouple locations are. It is extremely important to know the temperature profiles of the sample in order to correlate this data to the sample viability. (Ex. Sample "A" was raised to a maximum temperature of 850° C, and was held over 100° C for 4 minutes 30 seconds, experimentally. The results from the viability analysis show the sample was 99% killed. Therefore, it can be said that if the temperature of a location meets these conditions the percent kill can be correlated.) Further instrumentation includes a vent hole on the side of the barrel with a hose connecting it to a balloon. This allows the test to vent while still capturing any material that is escaping the control volume.

Samples are collected in triplicates, as seen in Figure 16. One set of samples are sent to a lab for viability. The second set is used to obtain clump size, and the third set is stored to in a temperature controlled area for any future analysis.

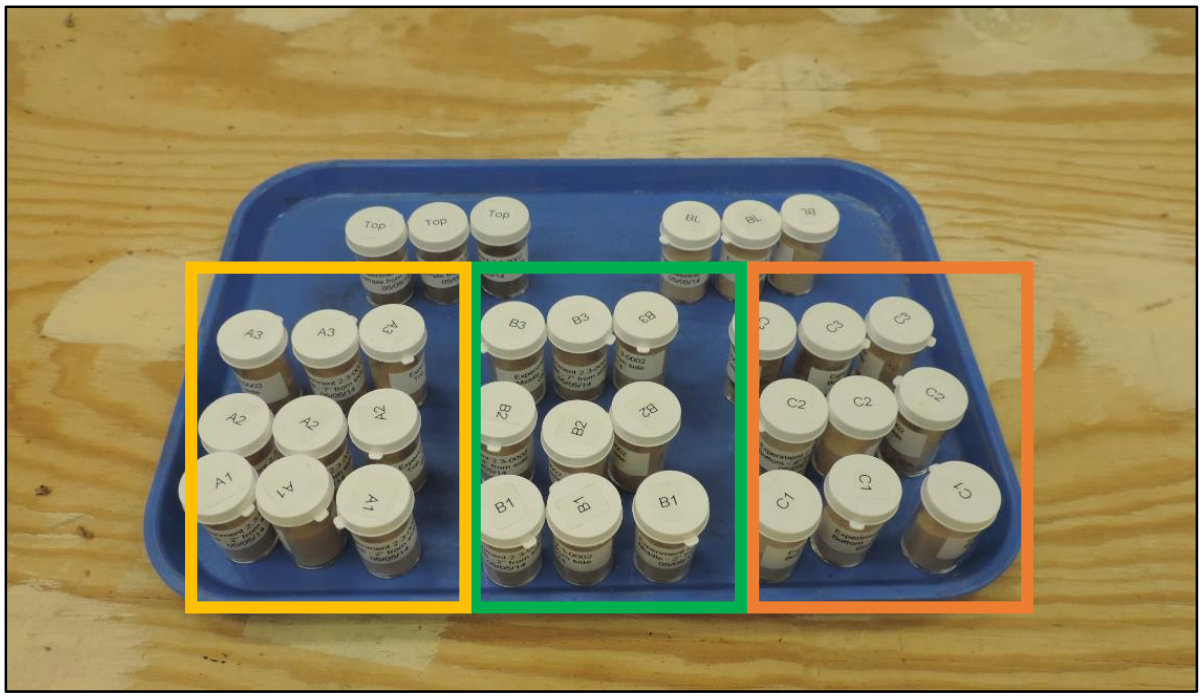

Figure 16 – Samples collected in triplicates

4.4 Initial Results and Validation

Although this sampling method produces samples that "appear" to be accurately taken from known locations, this sampling method must be validated. Sending samples to a lab for testing can be very expensive. A major area for concern is when the metal plate slides into the side of the barrel, the surface of the metal plate generates friction between the two, disturbing the sample. Furthermore, it is known that there will be movement of Bt within the barrel; what is unknown is how much movement and if that movement is negligible. To answer this question, a test series was developed using a powdered dye with a density which closely represents Bt. Barrels of Bt were mixed with different colored

powders. A plexi-glass divider was inserted into a barrel to create 4 quadrants. Each quadrant was filled with a different color Bt, and the plexi-glass divider was removed. This setup is shown in Figure 17.

Figure 17 – Top Left, Bt that was colored with powdered dye. Top right, plexi-glass used to divide the different colored Bt. Bottom Left, barrel filled with all four different dye filled Bt. Bottom right, barrel once the plexi-glass divider was removed.

Once the barrel setup was completed a "mock" sampling was done. The straps were removed to simulate an experiment completely, and the metal plate was slid into place. The Bt above the plate was vacuumed out, leaving a layer of Bt that appeared to shift slightly along with the plate as expected. This can be seen in Figure 18.

Figure 18 – From left to right: Before, during, and after the metal plate was slide into the barrel full of colored Bt.

A detailed template with 16 sample locations was used to validate this method. Figure 19 shows exact location from samples taken in the middle of the barrel. The middle picture is a “top-down” cross section with the template in place. The direction the plate was inserted into the barrel is shown with the red arrow. The movement of the Bt can be seen in the top two pictures, showing a zoomed in view of two sample location that were most effected by the overlap due to how close they were to different colored quadrants.

The layer of Bt that is nearest the plate is seen to shift a half of a millimeter of thickness. Therefore, when sampling after a thermite burn, the thin top layer is scrapped away and an accurate sample is taken just beneath the surface.

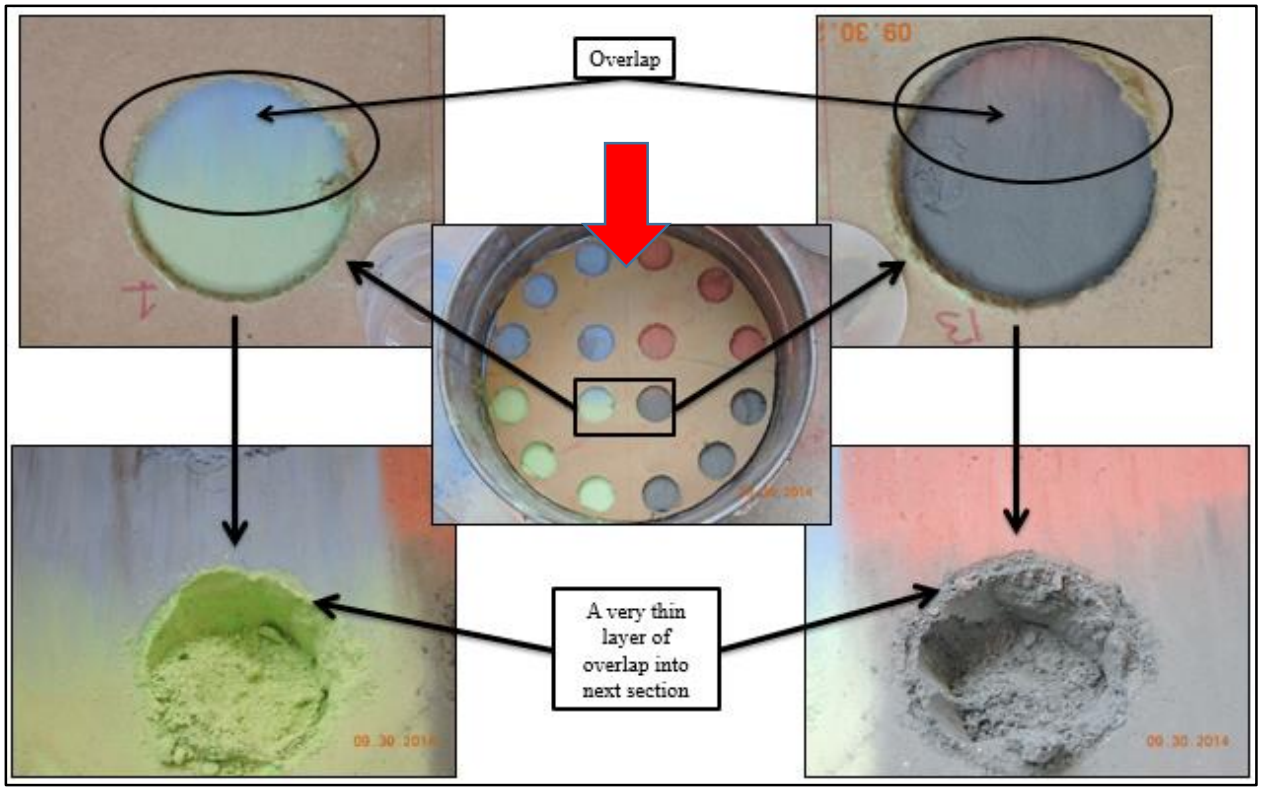

Figure 19 – A detailed schematic using pictures to show the thin layer of disturbed sample when a metal plate is inserted into a barrel of Bt.

In order to fix as many variables as possible, all the thermite charges are selected to be 100 grams. The charge is placed directly in the middle of the barrel onto a steel plate. It is ignited remotely with a system that drops a voltage through a filament that becomes white hot and starts the ignition. Once the charge is ignited, the barrel is left for 30 minutes to allow for cooling before it is opened and sampled. Figure 20 shows a barrel test before ignition.

Figure 20 –Barrel test setup

The purpose of these barrel tests are to validate and feed into the model. Therefore from each test the temperature profile correlated with the viability and the clump size are the two desired data points. Figure 21 shows the maximum temperatures of each thermocouple location while an example of a complete temperature profile can be seen in Figure 22. The viability results come from an off-site laboratory.

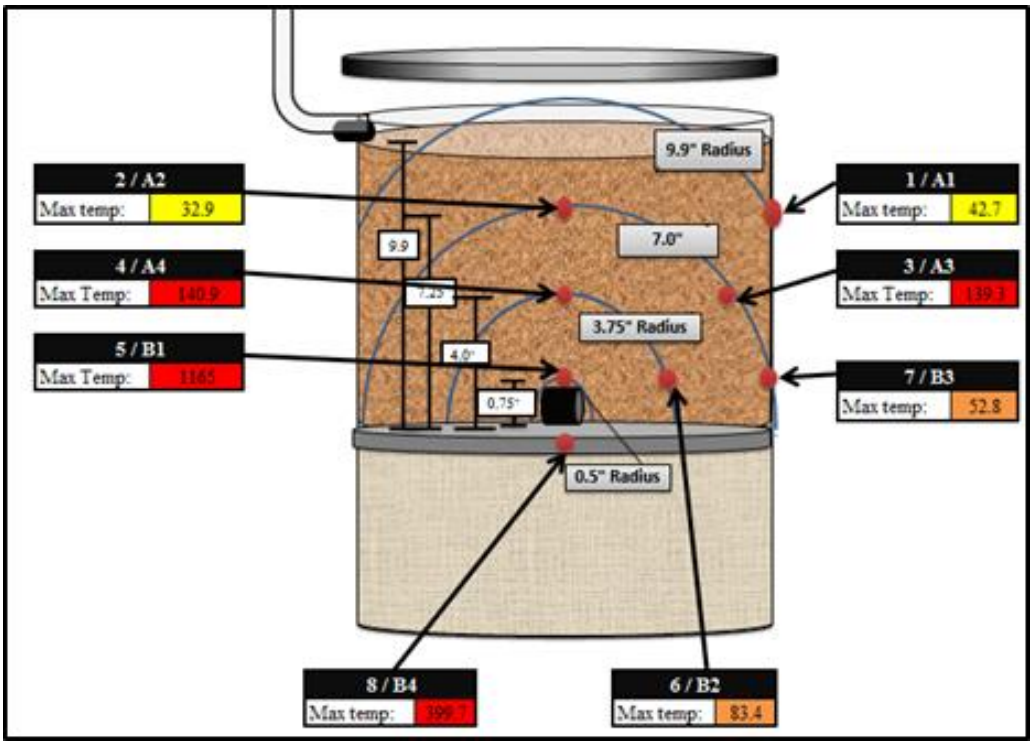

Figure 21 – Maximum temperature of locations throughout the barrel

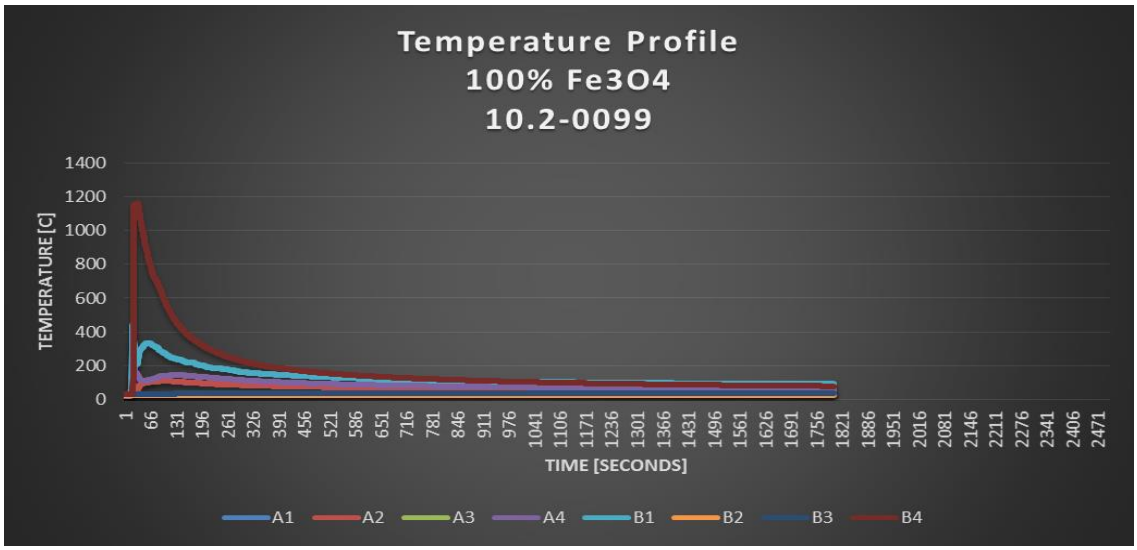

Figure 22 – Example of a complete temperature profile of a barrel test

After initial testing and data collection it was seen that the temperature profile of the thermite was distributed proportionally. Meaning that even though a thermite burn is a

chaotic event, temperature profiles along the same radius should be consistent. However, this was tested for validation. A test was constructed which could give a more complete temperature profile to test the validity of this assumption. Figure 24 shows the test setup. A 10 gallon barrel was instrumented with 24 k-type thermocouple placed on 3 different radii. Samples could not be obtained from this test because the amount of holes needed for the thermocouples did not allow anywhere for the slits to be placed. The 3-D drawings for this test setup can be seen in Figure 23.

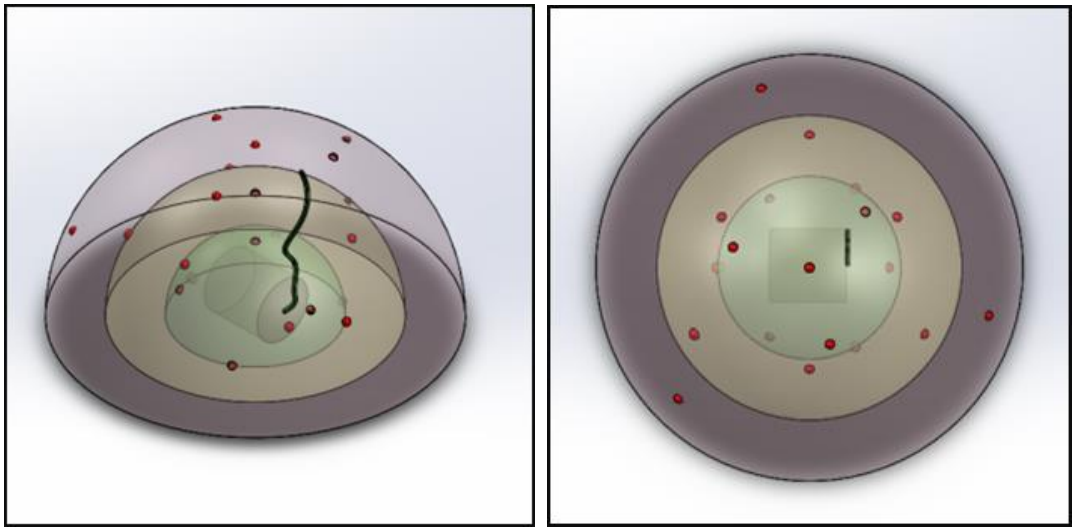

Figure 23 - 3-D drawings of the locations of each thermocouple were used to ensure exact locations of the thermocouples.

Figure 24 –A top-down view of the thermocouple test set-up.

Figure 24 is a picture taken from the physical test setup. Results from the data loggers showed that the temperatures remained consistent along each radius. There are 7 thermocouple along a 3” radius, 7 thermocouples along a 5” radius, and 7 thermocouples along a 9” radius. The largest variation in temperature was found on the 3” radius. There was a temperature difference of about 50° C in one location to another. Using this test, it was proven a barrel could be instrumented to only take temperature profiles on one side. Thus, allowing a slit to be placed on the other side for sampling. It is important to note that even though temperature profiles are taken on one side of the barrel and the slit for the samples are taken on the other side, the physical sample is still taken at the exact location the temperature profile is recorded.

To ensure confidence in the temperature profiles being taken, a completely independent thermocouple and data logger were used to take temperatures of samples right

after they are pulled from the barrel. That temperature is compared to the last known temperature of the sample taken while still inside the control volume. A Flir infrared camera is also used on those same samples to triple check the temperatures. This is done to validate that the data logging equipment is operating correctly, and the correct samples are being taken. These methods are shown in Figure 25.

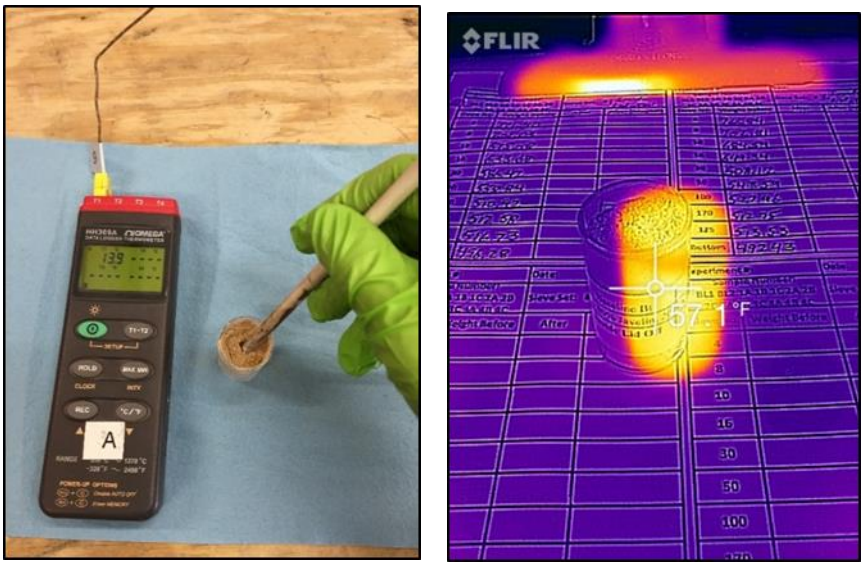

Figure 25 – Other methods of validating temperatures of sample taken. Left, data logger with a k-type thermocouple. Right, a Flir infrared camera.

These samples are then sent to an off-site lab to be tested for viability. Viability testing shows the amount of the sample that is still alive. Bt is made up of spores that are living, and viability will show the percent of the sample killed. Viability testing is done on a baseline sample taken from each barrel before the thermite is ignited, and compared to all the samples pulled from different locations throughout the given barrel, giving a percent kill of the agent. Viability analysis is a very detailed process which requires each sample be plated, treated, grown, and counted multiple times. The samples are plated in a petri dish filled with a solution which allows the spores to grow. The petri dish is incubated

overnight. The spores start to grow and form colonies overnight which are visible, and they are counted the next morning. The number of colonies is compared to the baseline, and each sample is given a percent kill.

In order to validate the viability process and find the minimum temperature needed to kill Bt spores initial lab tests must be done. To simulate a thermite charge inside a bed of Bt a pre-heated oven was used. The oven was pre-heated to capture the heat produced by the thermite charge. The samples were held at a known temperatures for 5 minute increments. Published kill temperatures of 100° C, 125° C, 150° C, 175° C, 200° C, and 225° C were tested. The results can be seen in Figure 26. The y-axis is the viable spores (the amount of the sample alive), and the x-axis is the time. As seen, no significant kill was shown until 150° C was reached. These tests showed that the higher the temperature, the faster the spores would be killed. Although these tests provided an accurate graph that show the kill of samples at known temperatures and times, it does not account for the impulse of much higher temperatures instantaneously after ignition. Due to the limitations of conventional convection ovens, this impulse of heat cannot be achieved using an oven test. Therefore the results of the oven test can be viewed as a "worst-case-scenario" because they do not account for the highest temperatures reached.

Figure 26 – Viability results from samples placed in a convection oven and held at known temperatures for a set amount of time.

The second set of samples collected are for clump analysis. Recall from Figure 3, particles above 10µm cannot travel into the human respiratory system past the nose/throat therefore, rendering them functionally defeated. Obtaining the percent increase (in clump size) of a sample after a thermite charge is ignited will allow a comparison of the effects between charges.

After the charge is ignited and the lid of the barrel is removed, visible charring and clumping can be seen throughout the surface of the barrel. These clumps can be roughly the size of marbles. Figure 27 shows the top of the barrel before and after a thermite charge was ignited at the bottom. Even though some of the spores inside these clumps did not reach a high enough temperature to kill them, they are functionally defeated because the clumps are above 10 µm and cannot enter the lungs.

Figure 27 – Left, view of the top of the barrel filled with Bt before the charge is ignited. Right, same view of the top of the barrel after the charge is ignited

Analysis to determine the size of the particles is done in two stages: large particles and small particles. Large particles are defined as anything above 300 µm and small particles defined as anything below 10 µm. Four different layers are sampled on the same radii the viability samples are taken. Each layer has three samples taken and run through the clump identification process. These three samples are then averaged together to obtain a particle size distribution for each layer. Quantifying the large particle size is done with three sieves consisting of different size screens: 300 µm, 600 µm, and 1180 µm. The sieves are weighed before the sample is poured in; the sample is evenly distributed onto the screen and hand tamped. After the loose material has fallen through the sieve, both the sieve and the sample (which fell to the bottom) are weighted. This gives a percent (by mass) of the sample that is above the mesh size. The material that fell through the mesh is passed through two more sieve, the last being 300µm. This process is illustrated in Figure 28. This is not a clean and/or perfectly accurate method, but it is repeatable and over the course of 50 tests and the numbers prove to be consistent.

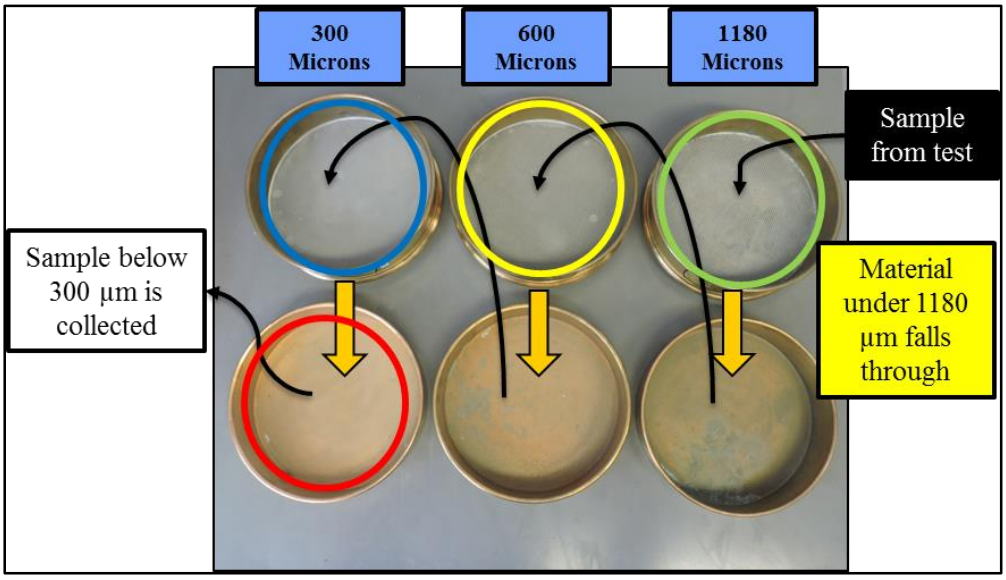

Figure 28 – Illustration of quantifying larger particle sizes (>300µm)

Each sample that passed through the last sieve is collected and sent to the off-site laboratory. Those samples are run through a very precise instrument called a hydrocyclone (cyclone), seen in Figure 29. The cyclone has a constant stream of air blown into the top of the device (from the left inlet in the figure). The air rotates around the interior walls and eventually exits through the hole at the top. A sample is fed into the stream of air just before it enters the cyclone, and follows the same trajectory of the air around the interior wall. These walls are very precisely machined to allow a certain size particle to fall to the bottom or float out of the exit at the top. This is known as the cut point of the cyclone. For this application a cyclone with a cut point of 10µm was used. The material that is above 10µm falls into a dish at the bottom while the remaining sample floats to the exit in the top. The sample is weighted before it is introduced and the dish at the bottom is weighted at the end of the run to obtain a percent above and below 10µm. To ensure an accurate number, 3 samples at each layer are passed through this process and are averaged together. For example, for the layer directly above the thermite (0.5” for the origin) 3 homogeneous

samples are taken. Each of those samples are individually run through the large particle and small particle quantification process and averaged together to give 1 representative number for the layer.

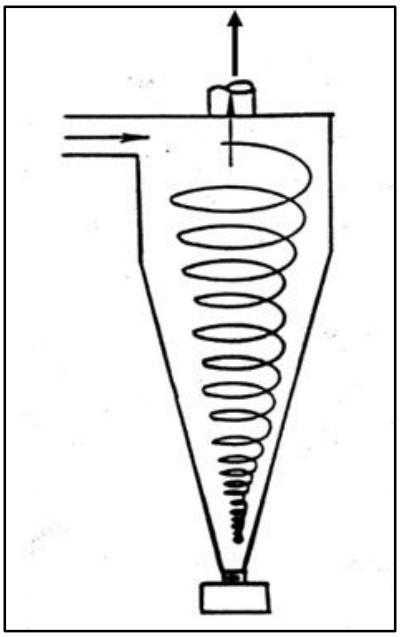

Figure 29 – Schematic of a cyclone

The entire experimental process of finding temperature data and particle size is done for every thermite composition. The process is trusted, reliable, and proven to give an accurate temperature profile and clump size along with samples that are confidently taken at known locations. Using the temperature profile a correlation can be drawn between the viability results (percent killed) and the clump percentage (percent functionally defeated). This is no small achievement, and takes a large amount of money and time for each thermite composition. For example, if one parameter of the thermite is modified (i.e. increase the burn time by 0.5 seconds) the whole process must be repeated. Though a numerical model would never completely take the place of testing, the development of such a computer program would save time/money and eliminate numerous tests.

Chapter 5: Modeling

To better understand the physics and predict the results of a thermite burn, a detailed coupled heat transport finite element model was developed. To allow the user to code the individual source terms, Finite Element Solver, FlexPDE was used. The complexity of the problem makes it difficult to solve from first principles. Consequently, experimental measured properties were used to simplify the numerical calculations.

An understanding of what is happening inside the barrel is needed before the model can be developed. As stated previously, when the thermite is ignited solids and gases are generated from the burning Bt. The initial solids created are defined as char. There are two different gases created: permanent and re-condensable. Permanent gases are those which are incapable of being in a liquid form, therefore leaving the system once created regardless of temperature profiles throughout. The re-condensable gases are burned off the outer layer of the individual Bt spores. As the system begins to cool, the re-condensable gases form a new solid (sticky material). From this process, the number of species that need to be tracked for the purposes of this model is 5: initial solid, re-condensable solid, biological gas (re-condensable gases), steam gas (perfect gases), and non-condensable gas.

The energetic is located inside the barrel of biological material, which is defined as the initial solid. As the energetic burns water vapor and non-condensable gases, such as carbon dioxide which do not naturally re-condense back into a solid, move throughout and exit the system. The final gas includes higher molecular weight sugars that re-condense into a solid below their boiling temperature. The steam and biological gases re-condense back into a solid state (Re-condensable Solid). This is illustrated in Figure 30.

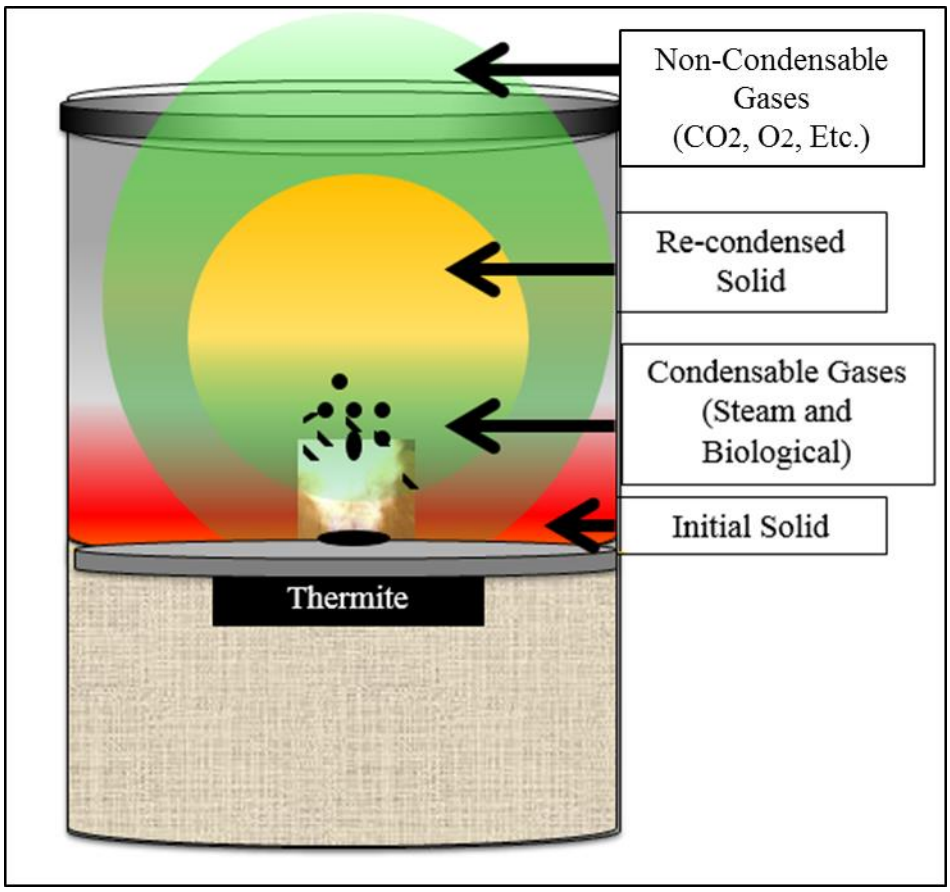

Figure 30 - Illustration showing barrel phenomena includes five different species.

Using these five species, a model was developed to solve for the density and temperature. The density is correlated to the particle size (clumping) and shows the percent above 10µm. The temperature is linked to the experimental results sent to the lab for viability testing and shows the percent of the spores (per sample) that were killed. This is achieved with the use of the continuity, energy, and momentum equations for each species.

Before simplifications and assumptions, each of the five species has a continuity, energy, and momentum equation, totaling 15 first-order partial differential equations. Within the time-dependent model, variables are selected in order to hold as many conditions constant (and as close to experimental data) as possible.

Table 3 – Species included in the model

	Species
1)	Initial Solid
2)	Re-condensable Solid
3)	Biological gas
4)	Steam Gas
5)	Non-condensable gas

For development of the model, the burn time, maximum temperature, and ambient (initial) temperature identified throughout experimental data. Although these numbers change slightly from test to test, the range is considered negligible. Parallel to the experimental setup, the boundaries of the control volume and radius of the thermite are set to represent the inside walls of the barrels used in the experiments. It can also be said for the sake of the model, the thermite reaction is uniform along a given radius from the origin, therefore making this problem one-dimensional.

For simplicity, within the model, the density (ρ) of each species and volume fraction (α) are tracked together and called Beta (β). These can be seen:

$$\beta_{s,i} = \alpha_{s,i}\rho_{s,i} \tag{15}$$

$$\beta_{s,re} = \alpha_{s,re}\rho_{s,re} \tag{16}$$

$$\beta_{g,nc} = \alpha_{g,nc}\rho_{g,nc} \tag{17}$$

$$\beta_{g,bio} = \alpha_{g,bio}\rho_{g,bio} \tag{18}$$

$$\beta_{g,st} = \alpha_{g,st}\rho_{g,st} \tag{19}$$

There are no known values for the porosity (volume fraction) of Bt in any literature; therefore some assumptions must be made. Porosity is the amount of space between the grains and cracks in a material. Numbers from alternative materials can be used from other literature sources. Various soils and sands have been well documented, and sand most

resembles Bt for this application; depending on the type of sand, the porosity ranges from 0.25-0.5 [19]. The lower limit represents smaller particles, and it is chosen. It is also acceptable to assume Bt starts at 70% (0.7) solid and 30% (0.3) air; the other species are set to zero. These values were found from compression tests, consist of placing a known amount of Bt inside of a 35mm diameter pressing die and using a 25 ton press to squeeze all the air out. The ratio was found by marking the volume before and after pressing. This gives the following volume fractions:

$$\alpha_{s,i} = 0.7 \tag{20}$$

$$\alpha_{s,re} = 0 \tag{21}$$

$$\alpha_{g,bio} = 0 \tag{22}$$

$$\alpha_{g,st} = 0 \tag{23}$$

$$\alpha_{g,nc} = 0.3 \tag{24}$$

Any gas can be used to calculate the total pressure locally. For example, $\rho_{g,nc}R_{g,nc}T_{g,nc} = \rho_{tot}R_{tot}T_{tot}$, which holds true for all gas species (R being the specific gas constant). All species' partial pressures sum to the total pressure, shown in equations

$$\rho_{g,nc}R_{g,nc}T_{g,nc} = \rho_{g,st}R_{g,st}T_{g,st} \tag{25}$$

$$\rho_{g,bio}R_{g,bio}T_{g,bio} = \rho_{g,st}R_{g,st}T_{g,st} \tag{26}$$

To enter these into the code, however, they must be solved explicitly in order, as shown below:

$$\rho_{g,bio} = \frac{1}{1-\left(\alpha_{s,i}-\alpha_{s,re}\right)}\left[\frac{R_{g,nc}T_{g,nc}\beta_{g,nc}}{R_{g,bio}T_{g,bio}} + \beta_{g,bio} + \frac{R_{g,st}T_{g,st}\beta_{g,st}}{R_{g,bio}T_{g,bio}}\right]$$

$$\alpha_{g,bio} = \frac{\beta_{g,bio}}{\rho_{g,bio}}$$

$$\rho_{g,st} = \frac{R_{g,bio}T_{g,bio}}{R_{g,st}T_{g,st}}\rho_{g,bio}$$

$$\alpha_{g,st} = \frac{\beta_{g,st}}{\rho_{g,st}}$$

$$\rho_{g,nc} = \frac{R_{g,bio}T_{g,bio}}{R_{g,nc}T_{g,nc}}\rho_{g,bio}$$

$$\alpha_{g,nc} = \frac{\beta_{g,nc}}{\rho_{g,nc}}$$

From [13] the continuity equation for both a gas (8) and a solid (9) can be developed for each species. These equations are shown in Equations 27 through 31.

Initial Solid	$\frac{\partial \beta_{s,i}}{\partial t} = \Gamma_{\mathrm{s,i}} - \nabla \cdot \left(\beta_{s,i} V_{s,i}\right)$	(27)
Re-condensable Solid	$\frac{\partial \beta_{s,re}}{\partial t} = \Gamma_{s,re} - \nabla \cdot \left(\beta_{s,re} V_{s,re}\right)$	(28)
Re-condensable Biological gas	$\frac{\partial \beta_{g,bio}}{\partial t} = \Gamma_{g,bio} - \nabla \cdot \left(\beta_{g,bio} V_{g,bio}\right)$	(29)
Re-condensable Sticky gas	$\frac{\partial \beta_{g,st}}{\partial t} = \Gamma_{g,st} - \nabla \cdot \left(\beta_{g,st} V_{g,st}\right)$	(30)
Non-Condensable Gas	$\frac{\partial \beta_{g,nc}}{\partial t} = \Gamma_{g,nc} - \nabla \cdot \left(\beta_{g,nc} V_{g,nc}\right)$	(31)

Note: $*\beta = \alpha\rho$

Within the continuity equation the initial volume fraction terms (α) and rate of change (Γ) terms must be found before these equations can be used in the model. The initial volume fraction is the amount of a given species as a percent of the total, i.e. the sum of the volume fractions equal 1.

$$\alpha_{s,i} + \alpha_{s,re} + \alpha_{g,bio} + \alpha_{g,st} + \alpha_{g,nc} = 1 \quad (32)$$

Since there are five species, there is a need for five gamma terms (rate of change of species). Gamma terms are assigned the nomenclature Γ_1, Γ_2, Γ_3, Γ_4, and Γ_5. The definition of these gamma terms can be seen below in Table 4.

Table 4 –Defining the gamma terms

Γ_1	Initial Solid → Non-Condensable
Γ_2	Initial Solid → Biological gas
Γ_3	Initial Solid → Steam gas
Γ_4	Biological Gas → Re-condensable Solid
Γ_5	Steam Gas → Re-condensable Solid

Table 5 – Gamma equations for each species

Initial Solid	$\Gamma_{s,i} = -(\Gamma_1 + \Gamma_2 + \Gamma_3)$
Re-condensable Solid	$\Gamma_{s,re} = \Gamma_4 + \Gamma_5$
Re-condensable Gas (Biological)	$\Gamma_{g,bio} = \Gamma_2 - \Gamma_4$
Re-condensable Gas (Steam)	$\Gamma_{g,st} = \Gamma_3 - \Gamma_5$
Non-condensable Gas	$\Gamma_{g,nc} = \Gamma_1$

To solve, an algebraic equation for the change of species is required. These equations, shown in Table 5, are described below.

- Gamma for the initial solid ($\Gamma_{s,i}$) is the negative sum of what the thermite does initially. Immediately after ignition, the thermite produces non-condensable and re-condensable (steam and biological) gases. The initial solid gamma is the sum of all three of those.
- Gamma for the re-condensable solid ($\Gamma_{s,re}$) is the addition of the biological and steam gases, which turn back into a solid as they migrate through the system.
- To find gamma for the re-condensable biological gas ($\Gamma_{g,bio}$), subtract the rate of change of what is re-condensed from the rate at which it was produced from a solid.
- Gamma for the re-condensed steam ($\Gamma_{g,st}$) is found using the same method as finding gamma for the biological gas.
- The rate of change for the non-condensable gas ($\Gamma_{g,nc}$) is simply Γ_5.

Γ_1, Γ_2, and Γ_3 were determined experimentally via TGA and pyrolysis analysis. This is the process of measuring the physical and chemical properties of a material as a function of increasing temperature. First, samples of *Bt* were raised to a known temperature and the rate of gas release measured. This processes was use to generate Figure 31 using experimentally obtained data.

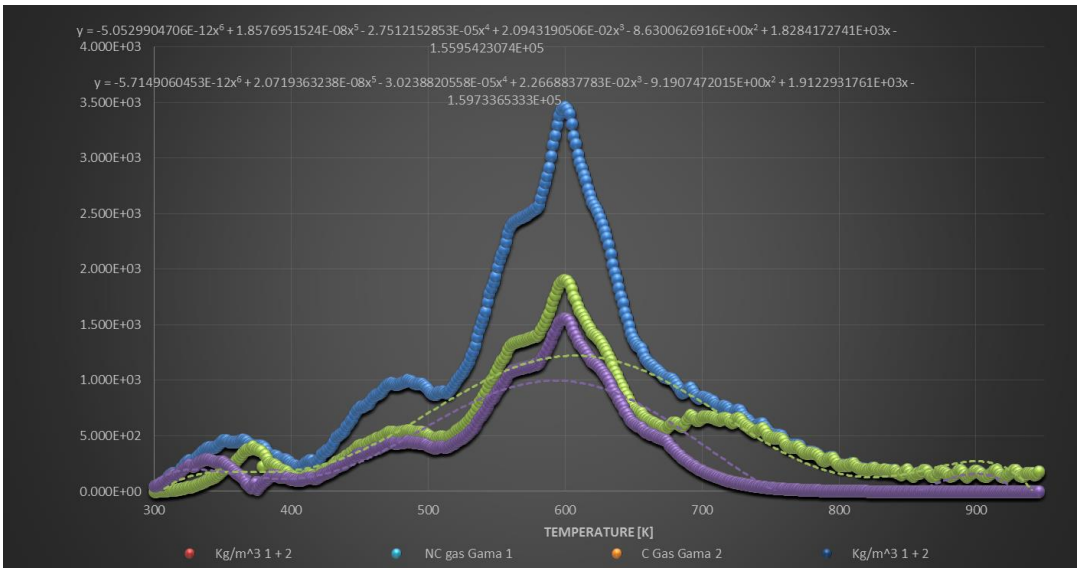

Figure 31 – Experimental results for Γ_1, Γ_2, and Γ_3.

This figure shows the rate in which the initial solid changes to gas, both condensable and non-condensable. The green dots show gamma one (Γ_1), and the purple dots show gamma two plus three (Γ_2+ Γ_3). The blue dots show of all gamma terms (Γ_1+Γ_2+ Γ_3). A curve fit was used to create a sixth order equation for each term. The equation from the purple dots (Γ_2 and Γ_3) is adjusted to account for the gamma terms separately. This separation is done fairly easily by determining a percent fraction.

Γ_1, shown in green, is the rate in which the initial solid turned into non-condensable gas. The data from the TGA shows that the there was no generation of gas until 300K, and the system produced gas until roughly 900K. A 6th order polynomial curve fit equation was generated and is seen in equation (33).

$$\Gamma_1 = -5.0529904706x10^{-12} * Temp^6 + 1.8586951524x10^{-8} * Temp^5 - 2.7512152853x10^{-5} * Temp^4 + 2.0943190506x10^{-2} * Temp^3 - 8.6300626916 * Temp^2 + 1.8284172741x10^3 * Temp - 1.5595423074x10^5 \quad (33)$$

The raw equations for gamma from Figure 31 need to be converted from $1/min$ to $1/sec$ to show the percent difference$(1/100)$. Beta is a nomenclature used to simplify equations within the model. $\beta_{g,nc}$ is equal to the volume fraction of the non-condensable gas times the density of the non-condensable gas. Representing the local mass of this individual species in an individual control volume divided by the total volume of that control volume. This is not the same as the density term which represents the local mass divided by the volume occupied by the particular species. Therefore importing the raw data into the model would not account for the assumption the measured density is $250kg/m^3$. Equation (34) shows the equation as it is entered into the model. The term $\left(\frac{\beta_{s,i}}{250}\right)$ produces a proportionality to the local amount of mass in the element at any given time.

$$\Gamma_1 = \left(\frac{\beta_{s,i}}{250}\right)\left(\frac{1}{6000}\right)[-5.0529904706x10^{-12} * Temp^6 + 1.8586951524x10^{-8} * Temp^5 - 2.7512152853x10^{-5} * Temp^4 + 2.0943190506x10^{-2} * Temp^3 - 8.6300626916 * Temp^2 + 1.8284172741x10^3 * Temp - 1.5595423074x10^5] \quad (34)$$

For purposes of the model it can be said that before the temperature reaches 300K Γ_1 is zero and until it reaches 900K it follow Equation 34. After the temperature is raised past 900K an assumption can be made that the rate of change is negligible.

Γ_2 and Γ_3 were found using the same method, fitting a 6th order polynomial equation, shown in equation (35) and (36). Γ_2 and Γ_3 come from the same line and therefore are the same equation. Both Γ_2 and Γ_3 start as initial solid and turn into biological gas and steam gas, respectively shown by Equation 35 and Equation 36.

$$\begin{aligned}\Gamma_2 = {} & -5.7149060453x10^{-12} * Temp^6 + 2.0719363238x10^{-8} \\ & * Temp^5 - 3.0238820558x10^{-5} * Temp^4 \\ & + 2.2668837783x10^{-2} * Temp^3 - 9.1907472045 \\ & * Temp^2 + 1.9122931761x10^{3} * Temp \\ & - 1.5973365333x10^{5}\end{aligned} \quad (35)$$

$$\begin{aligned}\Gamma_3 = {} & -5.7149060453x10^{-12} * Temp^6 + 2.0719363238x10^{-8} \\ & * Temp^5 - 3.0238820558x10^{-5} * Temp^4 \\ & + 2.2668837783x10^{-2} * Temp^3 - 9.1907472045 \\ & * Temp^2 + 1.9122931761x10^{3} * Temp \\ & - 1.5973365333x10^{5}\end{aligned} \quad (36)$$

Figure 31 shows Γ_2 and Γ_3 start turning to gas at approximately 300 K. An assumption is made that all of the gasses created below 400 K are biological (Γ_2). Above 400K, the amount of biological and steam gasses created are assumed to be the same, and are on a one to one comparison. Γ_2 and Γ_3 go to zero at approximately 750K, generating Equation 37 and Equation 38.

$$\Gamma_2 = \left(\frac{\beta_{s,i}}{250}\right)\left(\frac{1}{6000}\right)[-5.7149060453x10^{-12} * Temp^6 + 2.0719363238x10^{-8} * Temp^5 - 3.0238820558x10^{-5} * Temp^4 + 2.2668837783x10^{-2} * Temp^3 - 9.1907472045 * Temp^2 + 1.9122931761x10^3 * Temp - 1.5973365333x10^5] \quad (37)$$

$$\Gamma_3 = \left(\frac{\beta_{s,i}}{250}\right)\left(\frac{1}{6000}\right)[-5.7149060453x10^{-12} * Temp^6 + 2.0719363238x10^{-8} * Temp^5 - 3.0238820558x10^{-5} * Temp^4 + 2.2668837783x10^{-2} * Temp^3 - 9.1907472045 * Temp^2 + 1.9122931761x10^3 * Temp - 1.5973365333x10^5] \quad (38)$$

Γ_4 and Γ_5 are the rates in which the biological gas and steam gas are re-condensing, respectively. Equations for these terms are set to zero until the temperature drops below 100° C. Once this temperature is reached both terms are set as the ratio of density over the temperature to give the rate in which these different gases re-condense into a solid, shown in Equation 39 and Equation 40.

$$\Gamma_4 = \frac{\beta_{g,bio}}{T_{g,bio}} \quad (39)$$

$$\Gamma_5 = \frac{\beta_{g,st}}{T_{g,st}} \quad (40)$$

Similarly to the continuity equation, there must be 5 separate energy equations, one for each species. For the solid equation diffusive heat transport (in the first term on the right-hand side of equation 42) is modeled with a self-diffusion coefficient. The second term is equivalent to the respective gas equation term (heat exchange between solid and

gas phases by convection or conduction). The third term is the energy source due to thermal radiation. The final term is equal to the total average heat of reaction of all reactions taking place in the solid.

Before equations (11) and (12) can be tailored to each specific species, the material derivative is decomposed by its definition:

$$\frac{D}{DT} = \frac{\partial}{\partial t} + V \cdot \nabla \tag{41}$$

Substituting Equation 41 and $\beta = \alpha\rho$ into the energy equation for a gas (11), yields the following for a gas:

$$\frac{\partial T_g}{\partial t} = \left(\frac{1}{C_{p,g}\beta}\right)\left[\underbrace{\nabla \cdot \left(k_g \alpha_g \nabla T_g\right)}_{1} + \underbrace{\sum_i \frac{6\alpha_i k_g \left(T_i - T_g\right)}{d_i^2} Nu_i}_{2} + \underbrace{\sum_i \left\{\Gamma_{tar}^{s\to g}\left(C_p^{tar} T_b - C_{p,g} T_g\right) + \Gamma_{gas}^{s\to g}\left(C_p^{gas} T_i - C_{p,g} T_g\right)\right\}}_{3}\right] \underbrace{- V \cdot \nabla T}_{4} \tag{42}$$

In the Equation 42, the circled "1" is the Conduction Term, the circled "2" is the Convection Term, the circled "3" is the Phase Change Term, and the circled "4" is the Velocity Term. When this equation is applied specifically to the five species, the five equations are shown as Equation 43 through Equation 47.

(1) Gas, Non-Condensable:

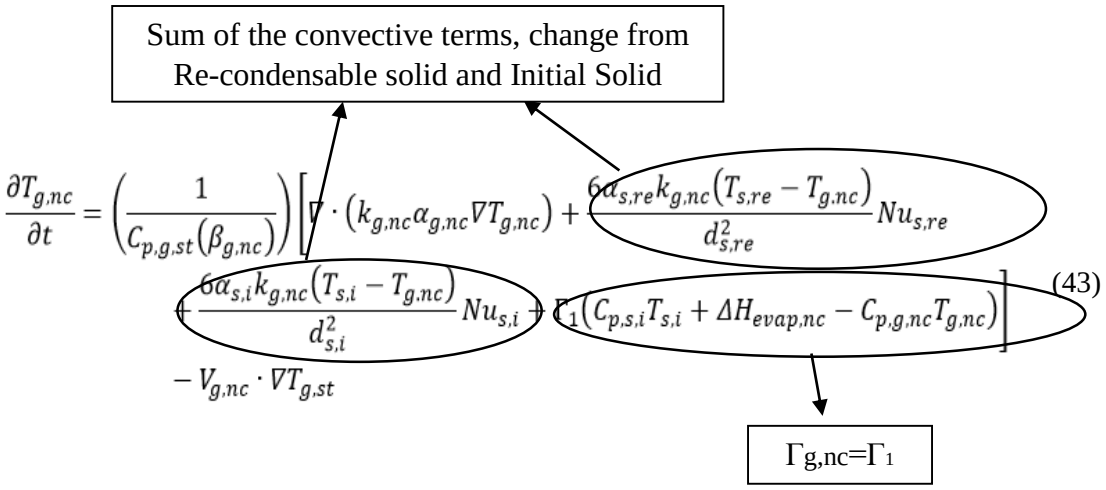

(43)

The energy equation for the other four species can be found in the similar way as described below. First, the gases and solids are assumed to be different temperatures.

(2) Gas, Steam:

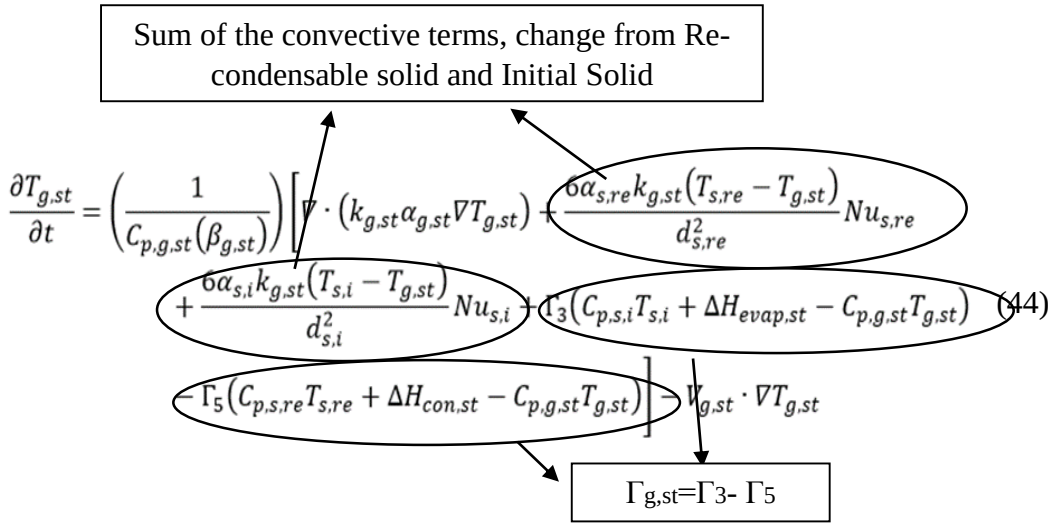

(44)

(3) Gas, Biological:

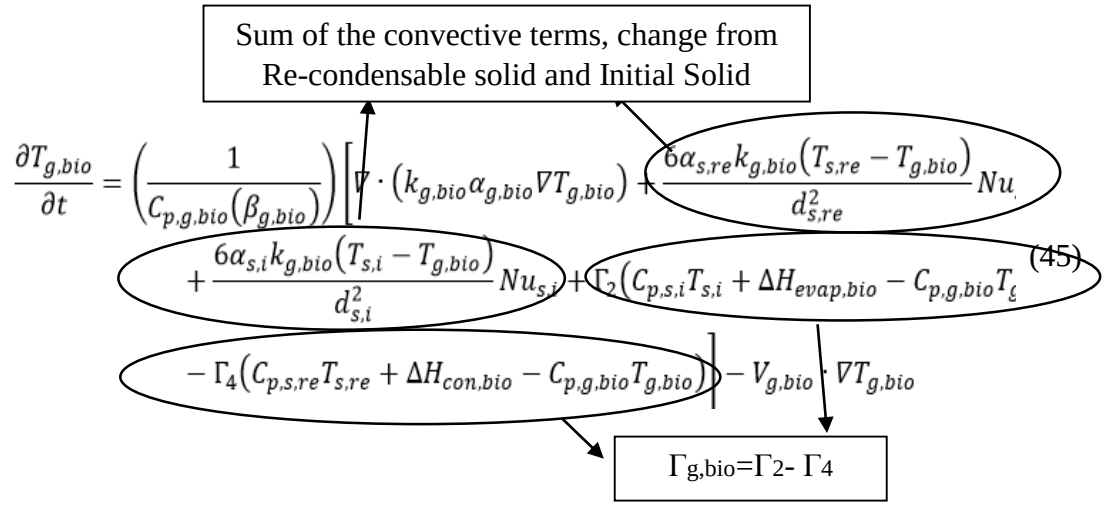

(45)

(4) Solid, Initial:

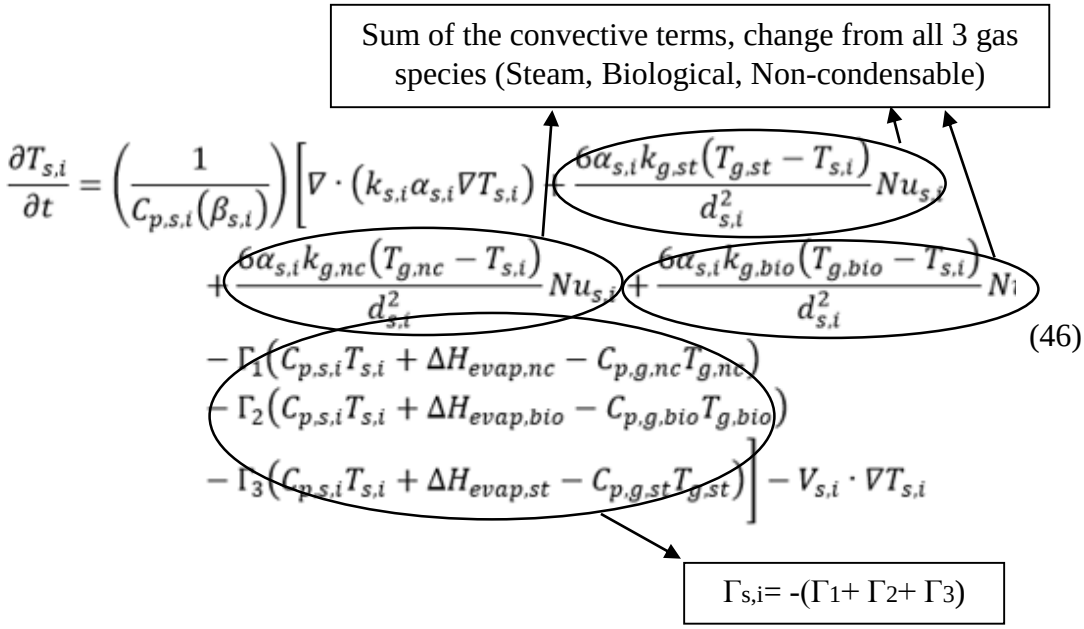

(46)

(5) Solid, Re-condensable:

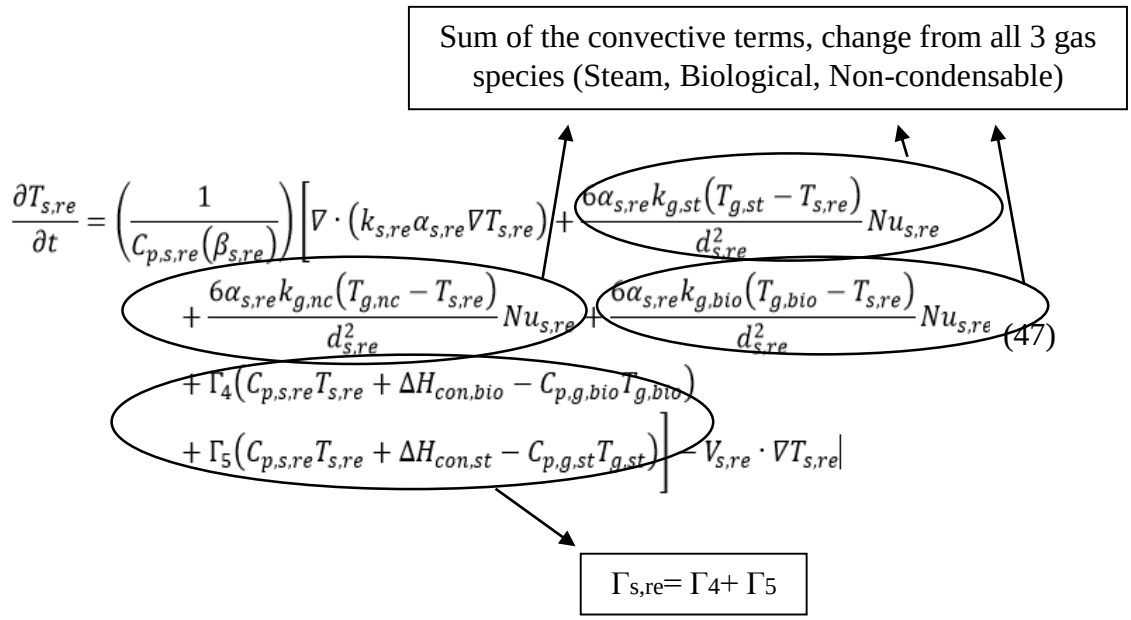

A number of unknowns must be found and terms defined in order for the energy equations above to be solved. The first is defining the specific heat (C_p) term. The specific heat is the amount of heat needed to raise the temperature of the given mass. Literature suggested values which most closely resembled the given species were used.

Table 6 – Specific Heat Values for each Species

Gas, Steam	2000 $\frac{J}{Kg*K}$
Gas, Biological	1500 $\frac{J}{Kg*K}$
Gas, Non-condensable	1500 $\frac{J}{Kg*K}$
Solid, Initial	1300 $\frac{J}{Kg*K}$
Solid, Re-condensable	1300 $\frac{J}{Kg*K}$

Thermal conductivity (k) for each species is defined as the materials' ability to conduct heat. A report generated by SAIC [20] simulated a container which captured some

of the governing properties, such as thermal conductivity. Modeled was done by heating a cylindrical element with natural convection at one edge and low convection at the other, seen in Figure 32.

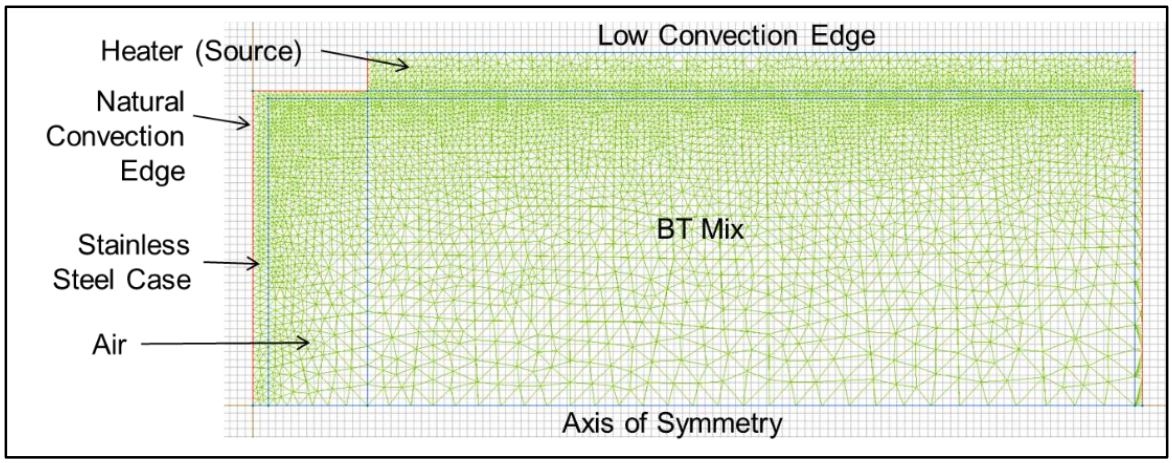

Figure 32 – Model from SAIC report to find properties of each species in the model .

The results for the thermal conductivities for each species can be seen in Table 7, taken at 293K.

Table 7 – Thermal Conductivity for each Species

Gas, Steam	$0.0188\frac{w}{m*k}$
Gas, Biological	$0.024\frac{w}{m*k}$
Gas, Non-condensable	$0.024\frac{w}{m*k}$
Solid, Initial	$0.1\frac{w}{m*k}$
Solid, Re-condensable	$0.1\frac{w}{m*k}$

The particle diameter must also be defined. This was done/estimated using a microscope and ImageJ software. Digital pictures are taken of samples of Bt, and a pixel map is created. The software uses the pixel map to estimate the size of the particle. The diameter of the initial solid particle was determined to be 0.0005 meters and the re-condensable solid is 0.0009 meters. An example image can be seen in Figure 33

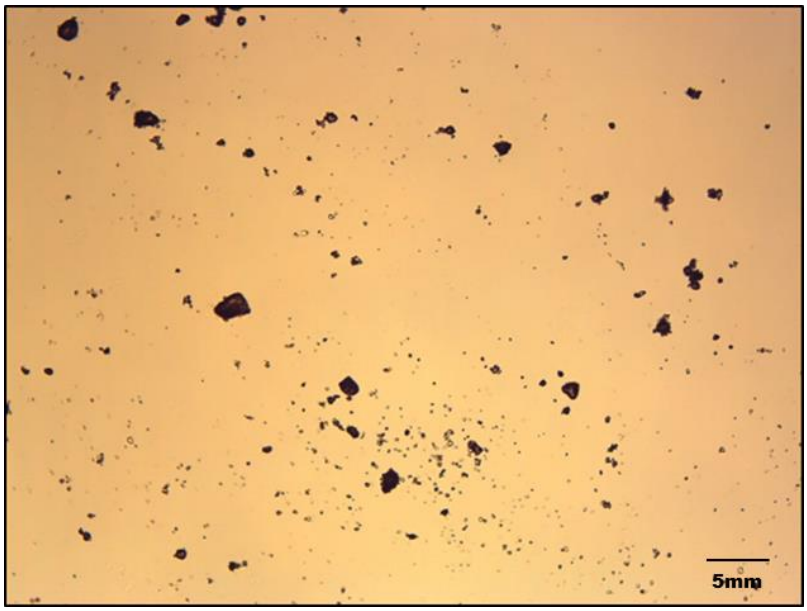

Figure 33 – Image taken using ImageJ software to determine the diameter of the particle size.

The appropriate Nusselt number equation can be found in the paper by Lathouwers [18], and depends on the Reynolds and Prandtl number.

$$Nu = 2 + 0.66Re^{1/2}Pr^{1/3} \tag{48}$$

The Reynolds number was found using the equation for fluid flow through a bed. Assumptions made are that the particles are spherical and approximately the same size diameter. The equation used can be seen in Equation 49.

$$Re = \frac{\rho \Delta v d}{\mu} \tag{49}$$

The Prandtl number equation used for the Prandtl number is shown in Equation 50.

$$Pr = \frac{C_p \mu}{k} \tag{50}$$

The final term to be defined for the energy equation is the heat of evaporation and condensation. This term is the heat needed for a material to be vaporized or condensed back into that material. The energy of condensation is the inverse of evaporation. For this effort, it is assumed these terms balance and cancel each other out.

From the momentum equation, the unknown velocity terms are expected as the output. Equations 51, 52, and 53 are using Equations 13 and 14 for a gas and solid, respectively, and making them unique to each species.

(1) Gas, Biological:

$$\begin{aligned} &\frac{\partial(\beta_{g,bio}\boldsymbol{V_{g,bio}})}{\partial t} + \nabla \boldsymbol{V_{g,bio}} \cdot \left(\beta_{g,bio}\boldsymbol{V_{g,bio}}\right) \\ &= -\alpha_{g,bio}\nabla p_{g,bio} + \alpha_{g,bio}\mu_{g,bio}\nabla^2\left(\boldsymbol{V_{g,bio}}\right) + \beta_{g,bio}\boldsymbol{f_{g,bio}} \\ &+ \frac{\beta_{s,i}}{\tau_{si,12}}\left(\boldsymbol{V_{s,i}} - \boldsymbol{V_{g,bio}}\right) + \frac{\beta_{s,re}}{\tau_{sre,12}}\left(\boldsymbol{V_{s,re}} - \boldsymbol{V_{g,bio}}\right) - \Gamma_{s,i}\boldsymbol{V_{s,i}} \\ &- \Gamma_{s,re}\boldsymbol{V_{s,re}} \end{aligned} \tag{51}$$

(2) Gas, Non-Condensable:

$$\begin{aligned}&\frac{\partial(\beta_{g,nc}\boldsymbol{V_{g,nc}})}{\partial t}+\nabla\boldsymbol{V_{g,nc}}\cdot\left(\beta_{g,nc}\boldsymbol{V_{g,nc}}\right)\\&=-\alpha_{g,nc}\nabla p_{g,nc}+\alpha_{g,nc}\mu_{g,nc}\nabla^2\left(\boldsymbol{V_{g,nc}}\right)+\beta_{g,nc}\boldsymbol{f_{g,nc}}\\&+\frac{\beta_{s,i}}{\tau_{si,12}}\left(\boldsymbol{V_{s,i}}-\boldsymbol{V_{g,nc}}\right)+\frac{\beta_{s,re}}{\tau_{sre,12}}\left(\boldsymbol{V_{s,re}}-\boldsymbol{V_{g,nc}}\right)-\Gamma_{s,i}\boldsymbol{V_{s,i}}\\&-\Gamma_{s,re}\boldsymbol{V_{s,re}}\end{aligned}\tag{52}$$

(3) Gas, Steam:

$$\begin{aligned}&\frac{\partial(\beta_{g,st}\boldsymbol{V_{g,st}})}{\partial t}+\nabla\boldsymbol{V_{g,st}}\cdot\left(\beta_{g,st}\boldsymbol{V_{g,st}}\right)\\&=-\alpha_{g,st}\nabla p_{g,st}+\alpha_{g,st}\mu_{g,st}\nabla^2\left(\boldsymbol{V_{g,st}}\right)+\beta_{g,st}\boldsymbol{f_{g,st}}\\&+\frac{\beta_{s,i}}{\tau_{si,12}}\left(\boldsymbol{V_{s,i}}-\boldsymbol{V_{g,st}}\right)+\frac{\beta_{s,re}}{\tau_{sre,12}}\left(\boldsymbol{V_{s,re}}-\boldsymbol{V_{g,st}}\right)-\Gamma_{s,i}\boldsymbol{V_{s,i}}\\&-\Gamma_{s,re}\boldsymbol{V_{s,re}}\end{aligned}\tag{53}$$

Both solid species have zero velocity because it is assumed that they are stationary.

(4) Solid, Initial:

$$\boldsymbol{V_{s,i}}=0\tag{54}$$

(5) Solid, Re-condensable:

$$\boldsymbol{V_{s,re}}=0\tag{55}$$

Initially, the stiffness of the momentum equation caused instabilities in the numerical model. In addition, it is a common assumption in fluidized beds to assume the velocity is constant. As a trade between complexity (solving the momentum equations) and the simplest approximation (a constant velocity profile), a series of tests could generate a representative velocity profile experimentally.

A number of experiments were executed to measure the gas velocity profile both within and leaving a barrel. The test within the barrel were designed to understand the internal physics, and the tests with the material leaving the barrel was designed to understand the physics of the material leaving the barrel. Each test used a high-speed camera to capture the frames at which the Bt was either leaving or moving through the control volume. A velocity board was used to measure the distance of the surging particles, and using the frame rate, the velocity was calculated. The purpose of the first series of experiments, shown in Figure 34, was to measure the gas and particle velocity as it leaves the barrel as a function of time.

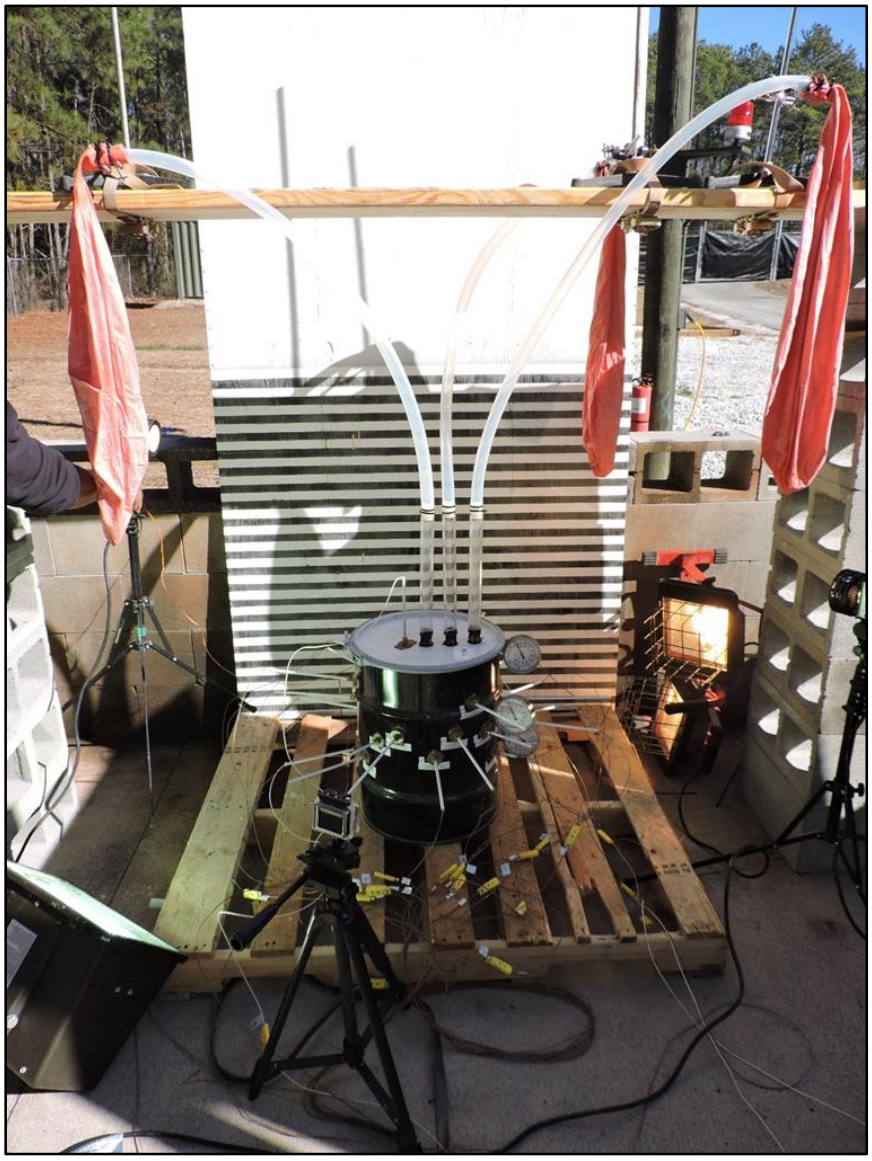

Figure 34 – Test setup to find the velocity profile of the off- gasses and Bt leaving the system after a thermite ignition

As shown in the figure, three holes were cut in the top of the barrel and 3 transparent tubes were secured to those holes. The first tube was located directly over the center of the thermite and the other two were spaced equally to the wall. As the thermite ignited, the reaction pushed material through these tubes into weather balloon. The field of view of a high speed camera was placed on these three tubes. The camera was shooting at 2,000 frames per second. The velocities in each tube were tracked, as shown in in Figure 35. The

red lines indicate the leading as it crosses the velocity lines on the velocity board in the background.

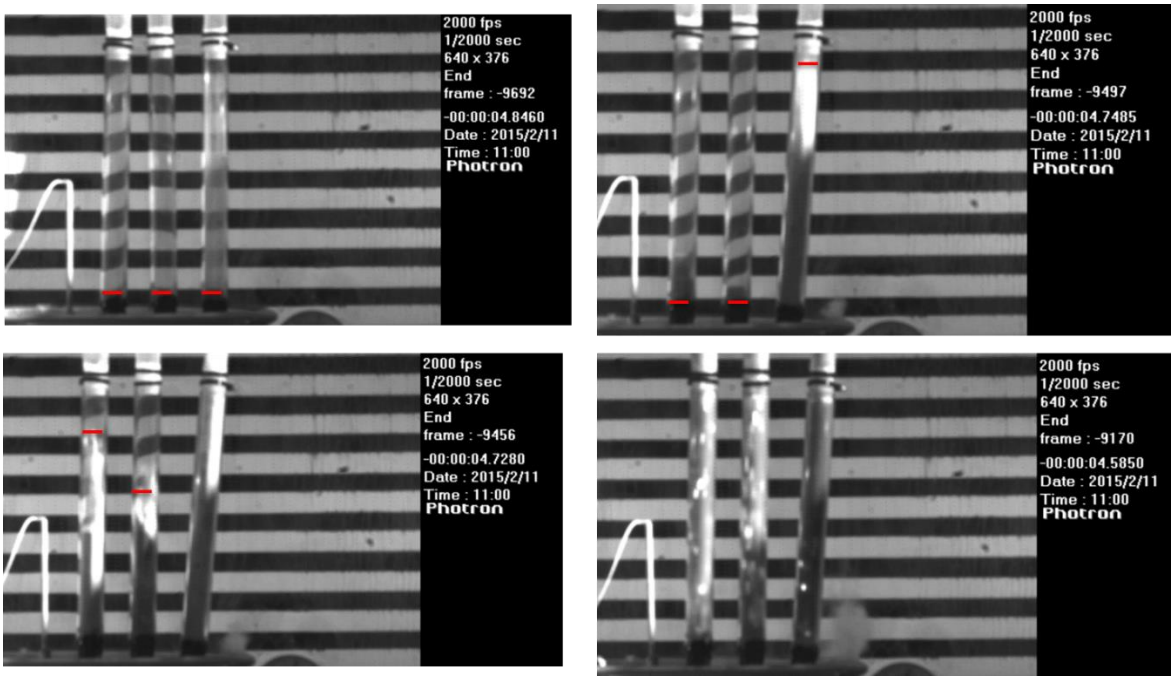

Figure 35- Images from the high-speed camera showing material as it moves through tubes.

The experimental velocities leaving the barrel are shown in Figure 36. In this figure, the blue line corresponds to the tube in the center of the barrel, the orange line corresponds to the middle tube, and the gray line corresponds to the tube closest to the wall. The yellow line provides an average of the three velocities, and a linear curve fit is shown in yellow.

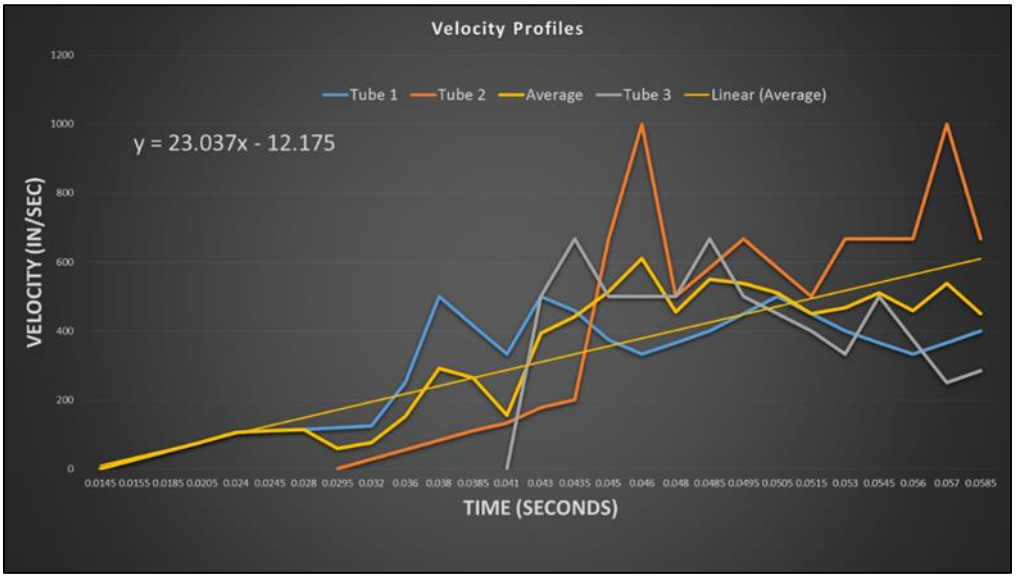

Figure 36 – Velocity results from experiments with tubes to allow Bt to vent from the system

The purpose of the second test series was to measure a velocity profile within the barrel. This experimental set-up is shown in Figure 37. Glass containers were filled to different depths with Bt and allowed to vent freely. A high-speed camera filmed the top of each jar against a velocity profile board to capture the speed at which the Bt was ejected.

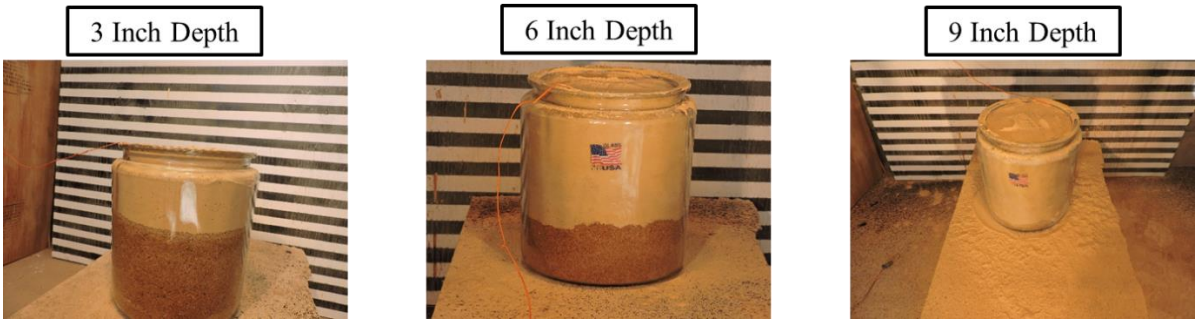

Figure 37 – A glass jar was filled to different depths of Bt and a thermite charge was ignited sending the Bt out of the barrel allowing a velocity profile to be calculated to capture a velocity profile

The material and gas velocity can be approximated by tracking three different events: (1) the ignition flame front, (2) the sparks generated as the thermite burns, and (3) the thermite reaction front as it leaves the containers. All three events were tracked for all three depths. Figure 38 through Figure 40 illustrate each of these events separately; for brevity only the depth of 6 inches is shown. In these figures, the horizontal white line shows the front being tracked as a function of time. In summary,

Figure 38: Shows the ignition flame front.

Figure 39: Shows the front of the sparks generated as the thermite burns.

Figure 40: Shows the thermite reaction front as it leaves the container.

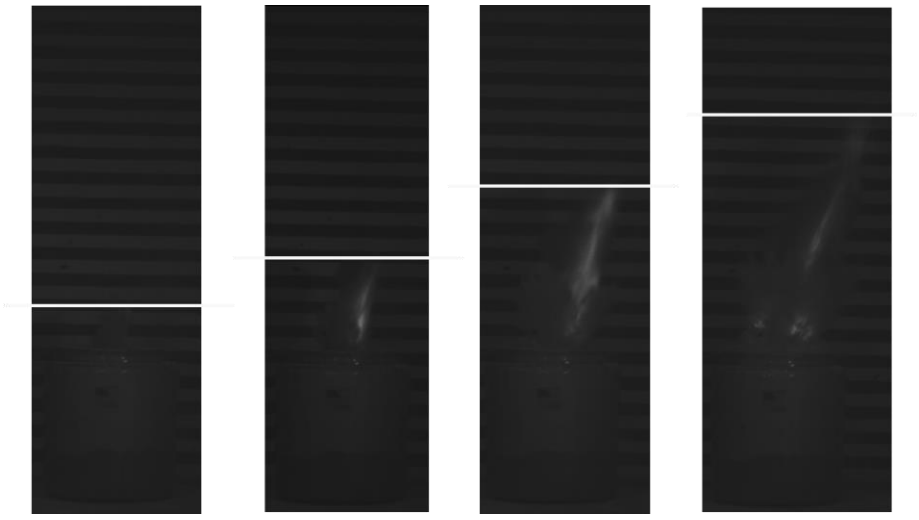

Figure 38 – Ignition flame front.

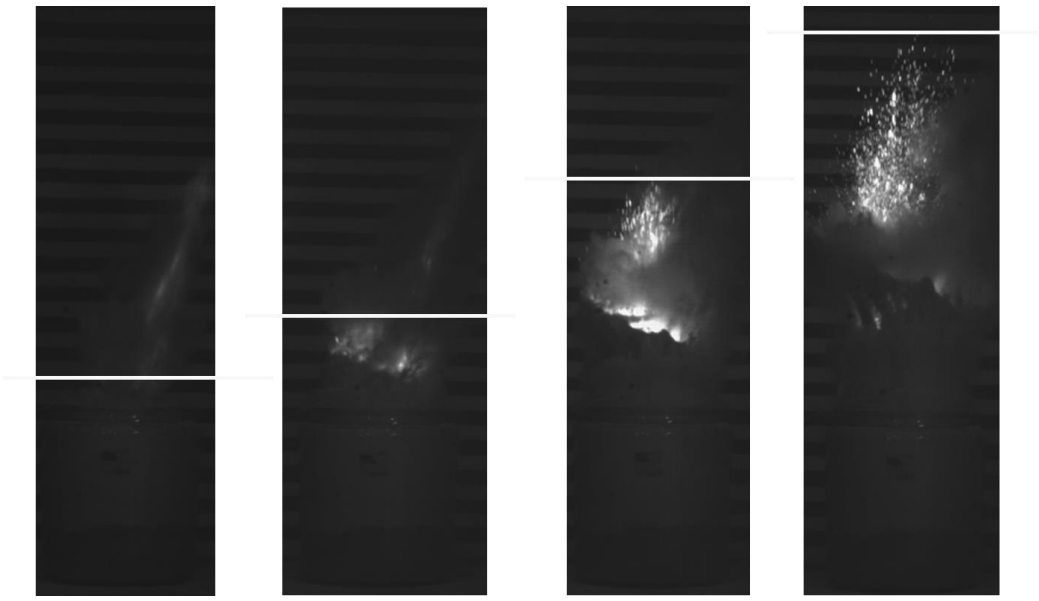

Figure 39 – Gasses and initial sparks of the thermite burn

Figure 40 – Thermite reacting and burning out of the system

Using the time between frames and the measured distance, velocity profiles were calculated for all three events, and presented for each depth:

Figure 41: Velocity profiles with the thermite at a 3 inch depth.

Figure 42: Velocity profiles with the thermite at a 6 inch depth.

Figure 43: Velocity profiles with the thermite at a 9 inch depth.

Figure 41 is first of the three depths (3”). The orange line represents the ignition flame front. The white line represents the sparks generated as the thermite burns, and the yellow line represents the final of the three events, the thermite reaction front as it leaves the container. The same can be seen in Figure 42 and Figure 43 for 6 inches and 9 inches, respectively. Note for 9 inches the ignition flame front is missing; the high speed camera has a small viewing area at high speeds and was not able to capture the entire field of view.

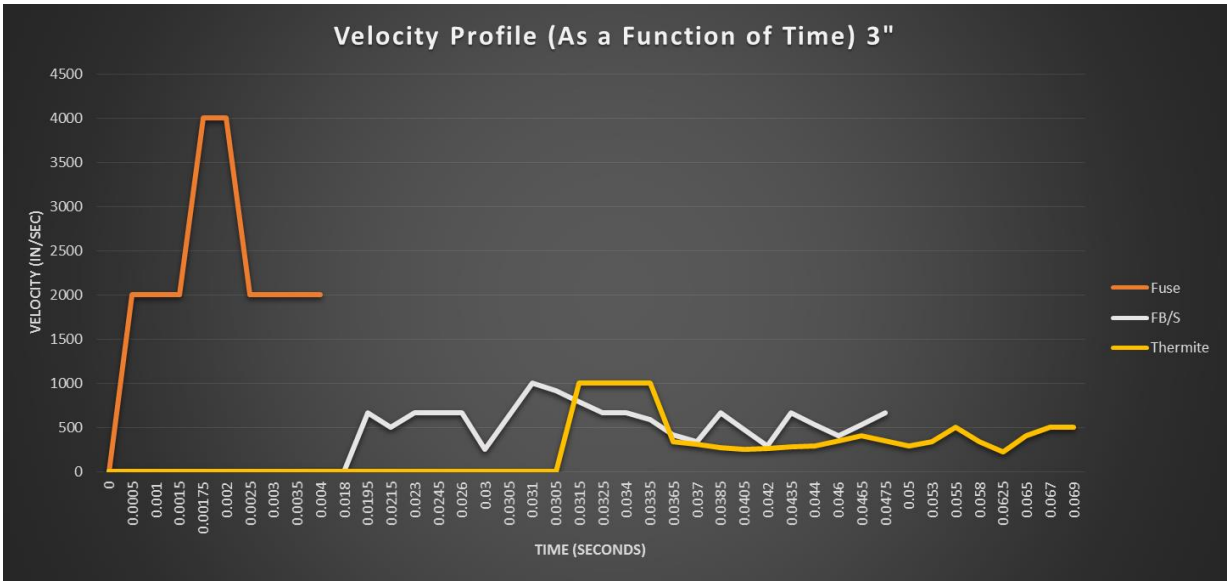

Figure 41 – Velocity profile of the fuse, gasses/initial sparks, and thermite at a depth of 3 inches.

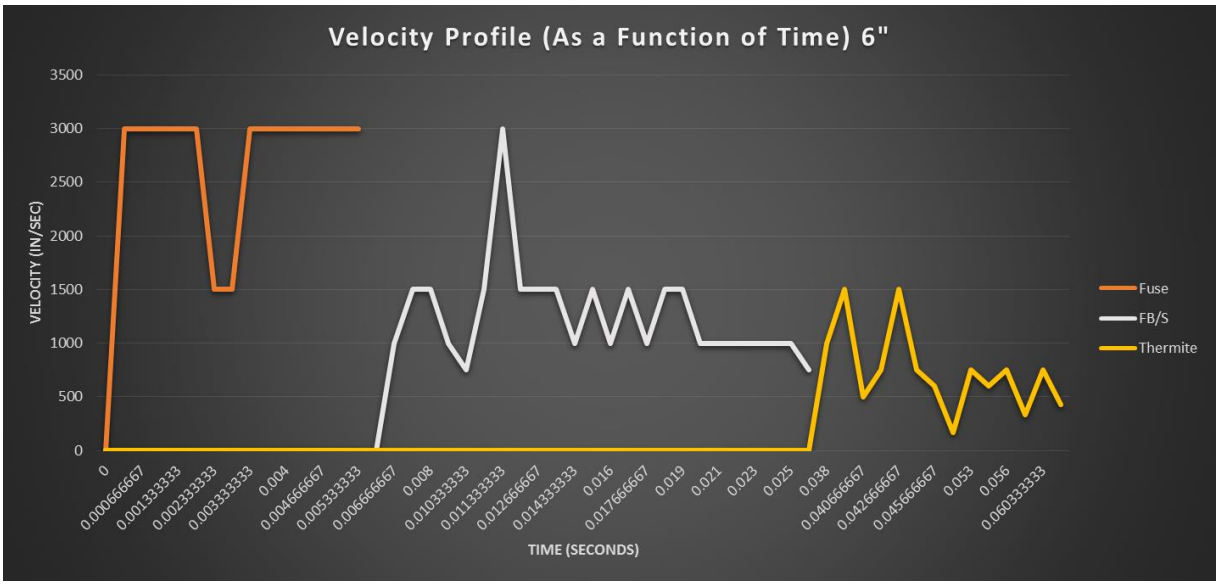

Figure 42 - Velocity profile of the fuse, gasses/initial sparks, and thermite at a depth of 6 inches.

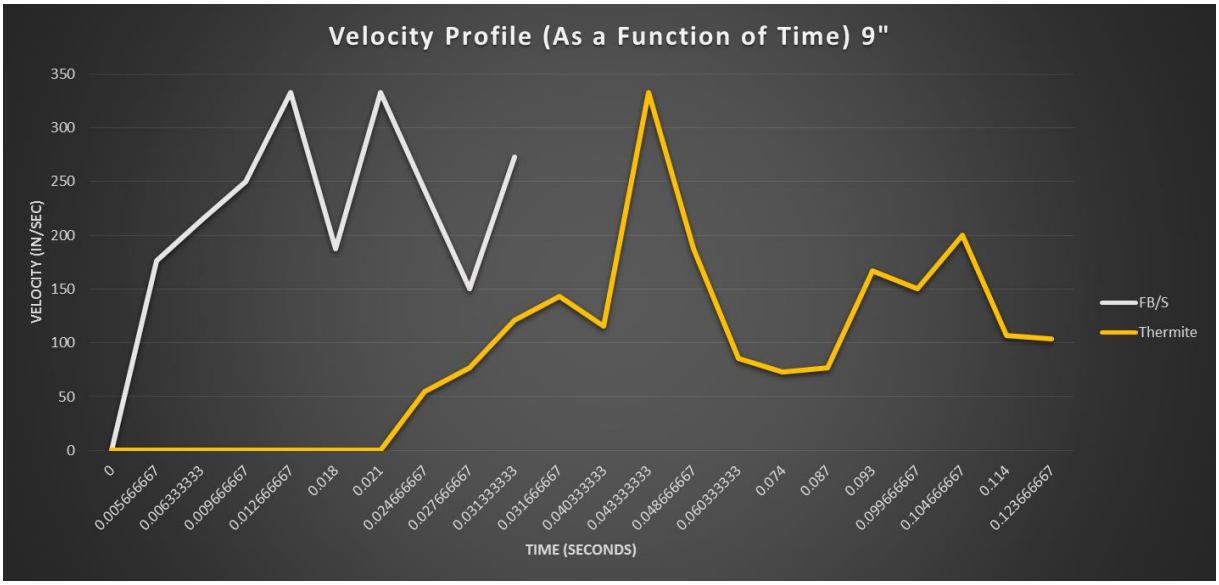

Figure 43 - Velocity profile of the gasses/initial sparks and thermite at a depth of 9 inches. Note that there is no orange line for the fuse, this is because the camera field of view did not capture the burn.

Figure 41, Figure 42, and Figure 43 show at all three depths the order that the reactions occur is consistent. Analysis of these curves provides numerous assumptions. The first is that the velocity of the fuse can be neglected (orange line). Even though the fuse

causes minor disturbance within the system, it is insignificant compared to the reaction of the thermite. The initial burn and the thermite fronts are averaged together and shown in green in Figure 44, Figure 45, and Figure 46 for each depth.

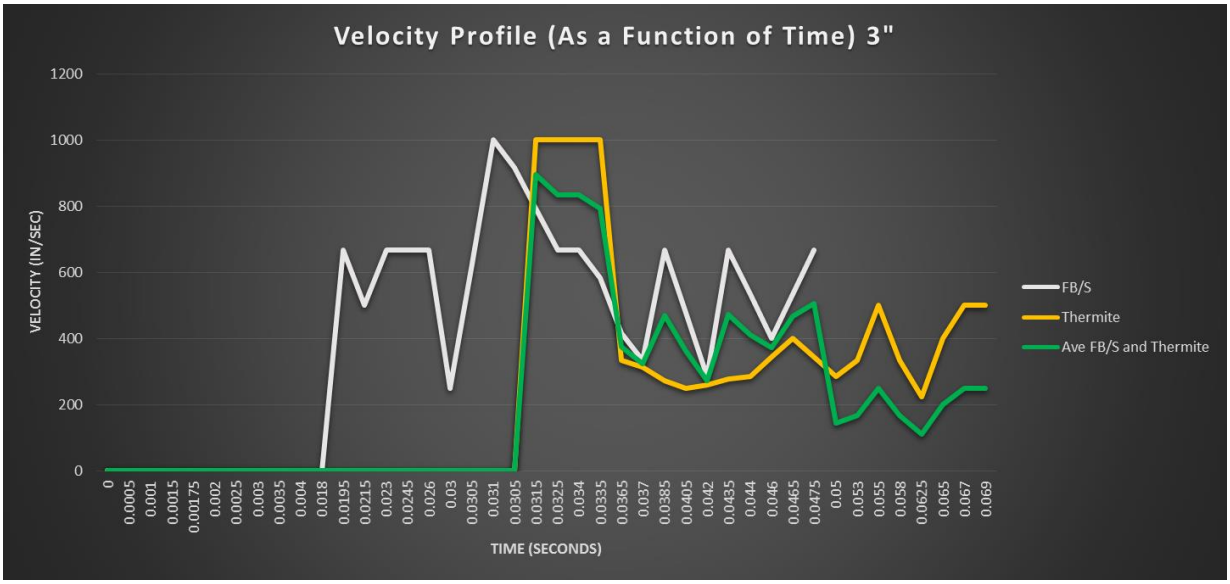

Figure 44 – Velocity Profile of the gasses/initial sparks, thermite, and the average of the two at a depth of 3 inches

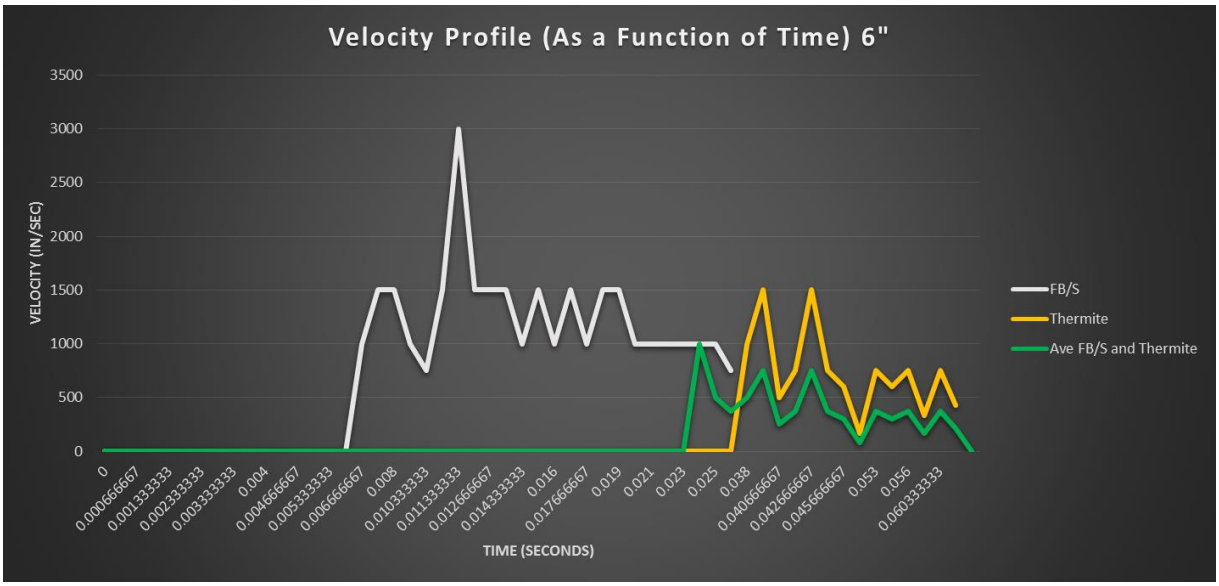

Figure 45 - Velocity Profile of the gasses/initial sparks, thermite, and the average of the two at a depth of 6 inches

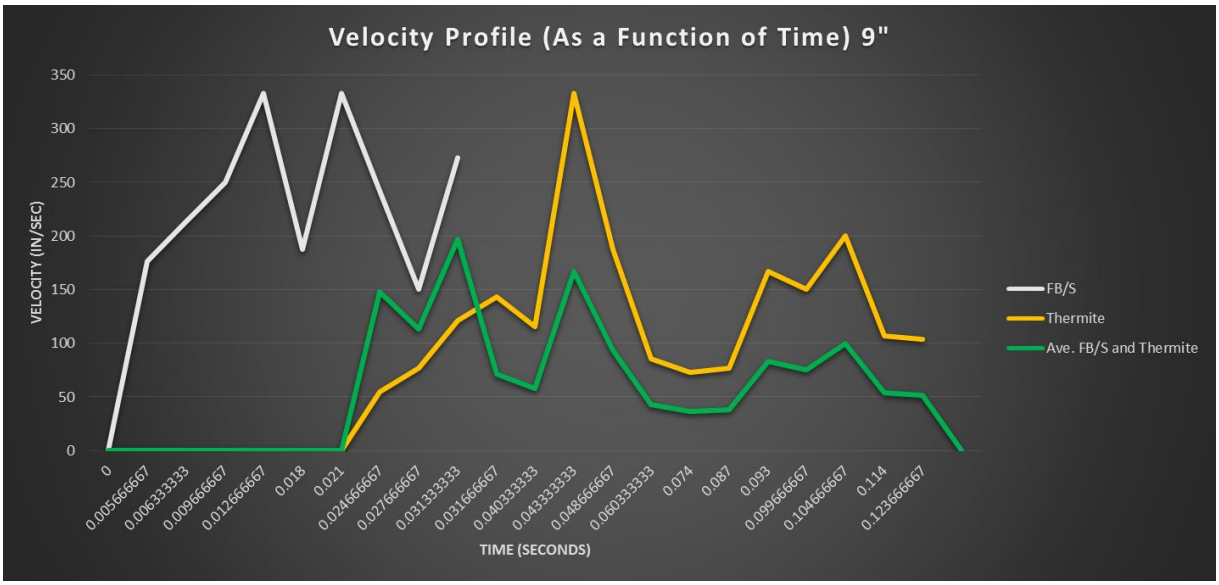

Figure 46 - Velocity Profile of the gasses/initial sparks, thermite, and the average of the two at a depth of 9 inches

The velocity profile is taken from these three figures. Figure 47 combines velocity profiles taken from their corresponding depths onto the same time scale. From the origin of the thermite to 6" the profile is taken from Figure 44 (Green line). From 6"- 9" the profile was taken from Figure 45, and the remaining profile was taken from Figure 46.

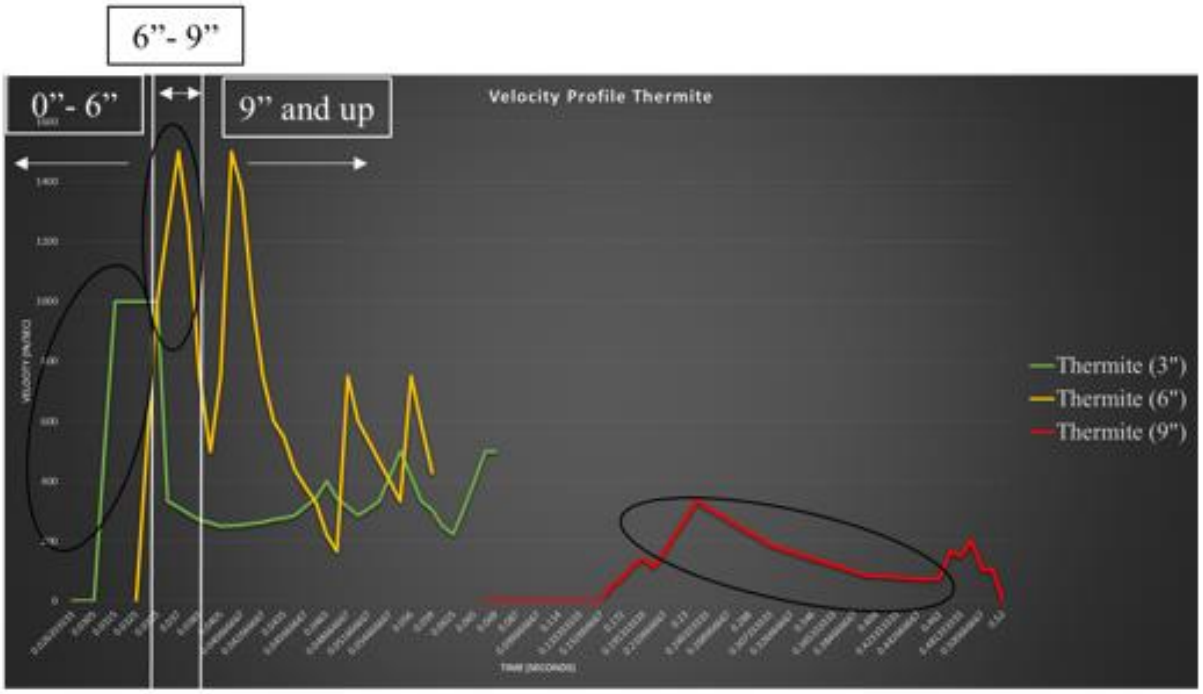

Figure 47 – The velocities for the FB/S for all three depths are placed on the same graph

The independent test profiles are merged together on one time dependent figure and shown in Figure 48.

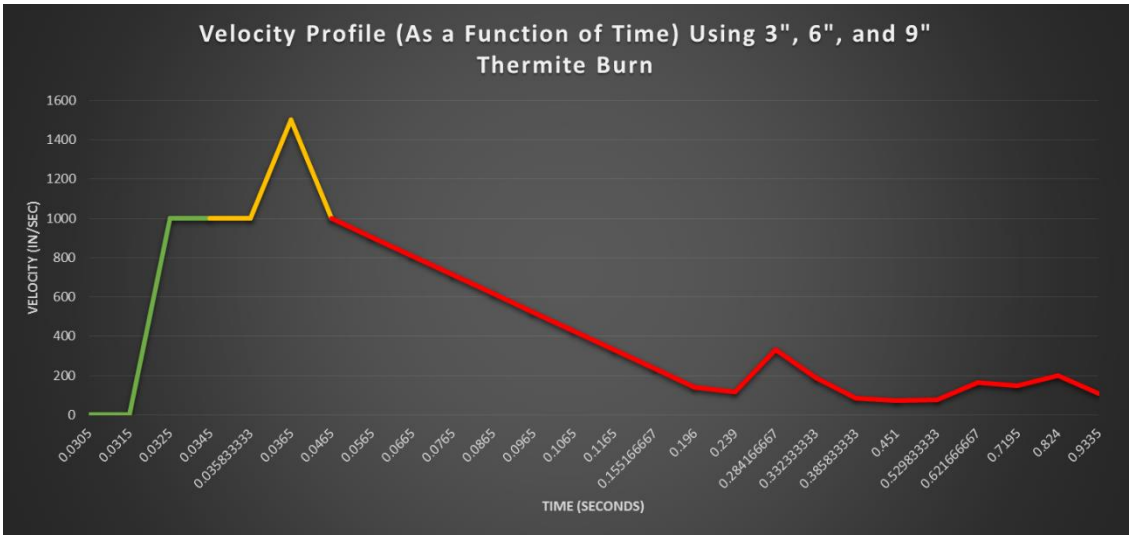

Figure 48 – The final velocity profile of the FS/B using all three depths

Equation 56 is the trend line taken from all three depths combined, and is the accepted velocity profile for a thermite burn inside of a barrel of Bt. The depths above 9 inches were compared to the profiles found in the "Transparent Tubes" and showed to be slightly high in velocity profile found in Figure 48. This is due to the lid decreasing the surface area that the pressure had to vent out of. The differences were very minimal and considered negligible, but validated the trend line found in Equation 56.

$$y = 0.0001x^6 - 0.009x^5 + 0.097x^4 + 4.0757x^3 - 112.05x^2 + 857.08x - 907.99 \quad (56)$$

Having found experimental data to support an accurate velocity profile, equations must be defined for FlexPDE. From Figure 48 a maximum velocity in the system is said to be 1,500 $^{in}/_{sec}$. With the maximum velocity known an equation must be found from as a function of both time and radius from the thermite. Equation 57 is found is a function of time.

$$Velocity_t = \frac{V_{max}}{(t_{max})^{16}}[t - t_{max}]^{16} + 0.1 \quad (57)$$

Using this profile controls the function of the time step as FlexPDE progresses through the problem. An important difference to note is that equation 57 uses the maximum amount of time defined by the operator. Equation 58 is used to account for the velocity profile in terms of time and radius.

$$Velocity_r = \left[\frac{(^{-9}/_{10}) * Velocity_t}{Problem\ Radius}\right] * r^{10} + Velocity_t \quad (58)$$

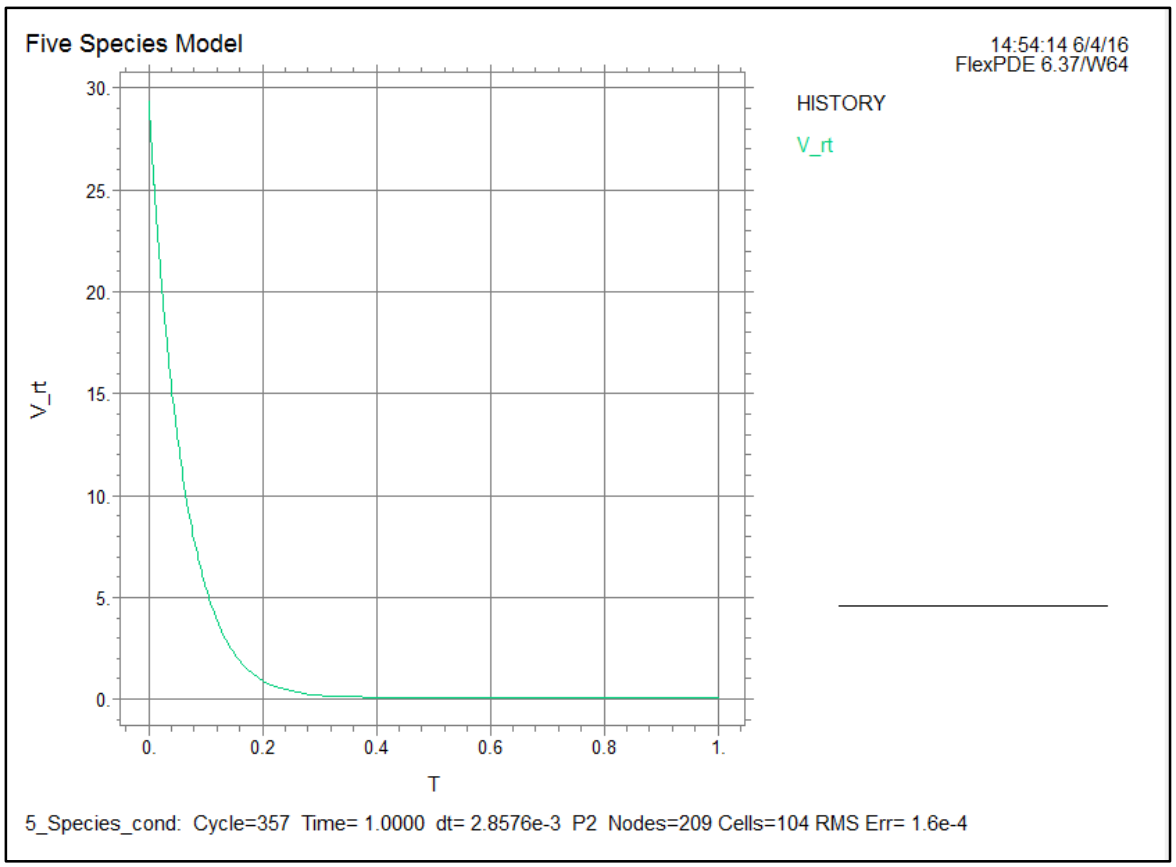

Figure 49 – Velocity Profile used within the model

The velocity profile found experimentally (Figure 48) is shown in inches per second while the velocity profile used in the model is shown in meters per second. The time on both graphs is shown in seconds. The difference between the two graphs is that the velocity found experimentally starts at zero and shows the rapid velocity rise, while the velocity profile used in the model starts at the maximum velocity found experimentally. This deviation has a dual-purpose. First, when a high temperature impulse is added to the velocity profile the model cannot account for the rapid change. Secondly, the model expects a temperature input upon initialization. Therefore, any velocity input of zero would create an unsolvable condition.

Before the equations can be solved, boundary conditions must be established for the outer edge of the control volume and the edge of the thermite. The outer edge of the control volume, in reality, is the wall of a steel barrel that nothing can cross. Therefore the velocity is set to zero. Regarding the thermite boundary layer, thermite does not produce any gas, but burning Bt does. During the ignition of thermite the Bt burning sends these gases throughout the system creating a pressure gradient outward into the barrel. If it is assumed the inner boundary for densities is a natural boundary (like the outer edge), then all the gas densities will quickly go to zero because there is not source of gas from the vaporization of the Bt at the origin to replace the gas that is being pushed through the system.

In order to provide a pressure gradient that will keep the densities of the gases above zero, a thin layer (or shell) around the thermite (origin) is modeled. This shell is the zone in which Bt is continually being vaporized and those gasses produced are being sent into the system. An equation for the amount of all three gasses produced (non-condensable, biological, and steam) was found experimentally using the rate of generation data (Γ_1, Γ_2, and Γ_3) and listed as Equation 34, Equations 37, and Equation 38.

The inner boundary starts with the assumption that no gasses are being created. The instant the thermite is ignited there is a small shell of Bt surrounding the thermite that is vaporized over a set amount of time. This shell of Bt produces non-condensable, biological, and steam gases that are sent through the Bt. After the set amount of time has expired the densities of the Bt inside the small shell return back to their original values. Effectively the inner boundary assumes that the surrounding Bt has been fully vaporized and is flowing into the system at the velocity defined by the velocity profile.

Other variables defined within the model are listed as follows:

- Maximum run time: This can be adjusted depending on what variables are being checked.
- Thermite radius: This is taken from physical properties of the thermite charge being used in testing.
- Problem radius: This is the distance from the origin (center of the thermite charge) to the wall of the barrel.
- Density of the initial solid: This was measured by taking by pouring the material into a known volume and dividing the mass by that known volume.
- Density of the re-condensable solid: This was found using data taken from TGA.

Figure 50 shows the results from TGA analysis done on samples of Bt. Those samples were raised to temperatures above 500° C. The data shows that there was a reduction of roughly 75% to 80%.

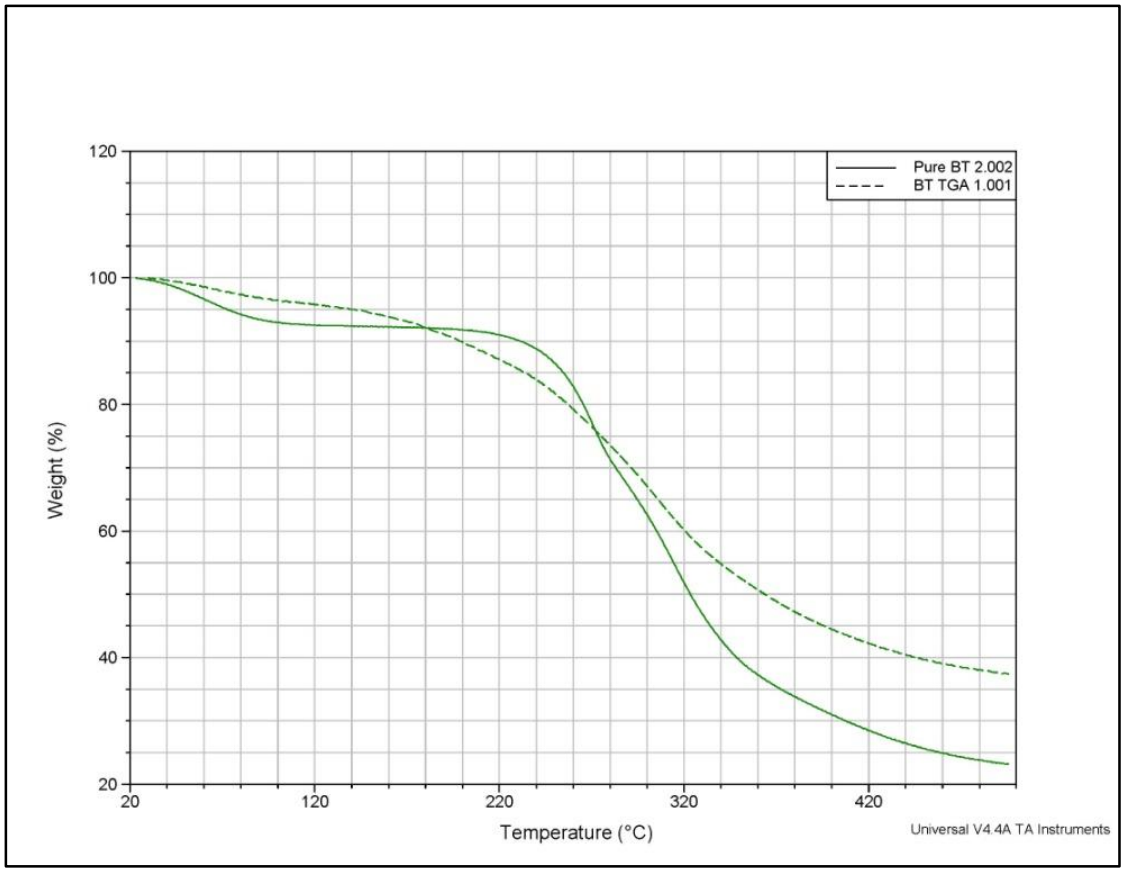

Figure 50 – TGA data from heating of Bt. Showing a reduction of roughly 75% - 80%

Using experimental data to fill unknowns the continuity and energy equations can be solved within FlexPDE. The momentum equation can be replaced with a velocity profile that was found experimentally. This produces plots what will be linked to the results found experimentally.

Chapter 6: Results

To quantify the effectiveness of a thermite charge ignition inside of a barrel of Bt, a figure of merit must be established. A figure of merit is numerical value that represents the effectiveness of a given procedure. In the middle of Figure 51 is a thermite mid-burn. The two circles represent the two different ways to render this material useless. The first circle (smaller of the two) is the area that the Bt spores are heated to a temperature that kills them. The second circle is the area where the temperatures did not get high enough to kill the spores within the material, but still experienced a different method of defeat. This is the area where the gases from the burning Bt re-condense and form sticky clumps above the respirable limit. Even though the Bt in this area is still considered viable it is considered useless as an aerosolizable weapon.

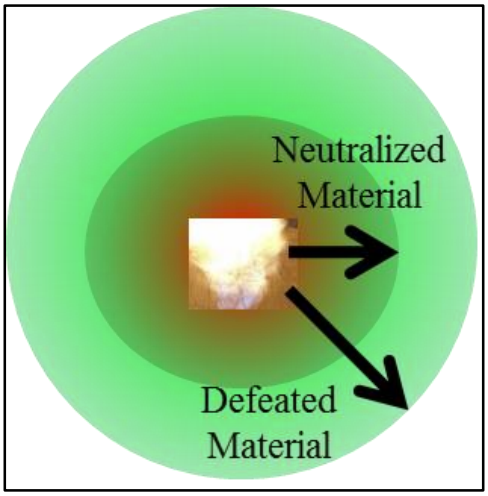

Figure 51 – Two different effects of a thermite burn are shown as the material neutralized and the material defeated.

Chapter 4 states the experimental results are used to feed not only back into the model, but they are used to establish an accurate figure of merit. The neutralized region relies almost exclusively on the temperature profiles the material in that area is exposed to.

Higher temperatures allow for less exposure time, while lower temperatures require there to be consistent heat. Because the temperatures do not get hot enough in the defeated material region, this area relies on the sticky re-condensed gases in the system. As the gases begin to re-condense the density in these areas begin to increase.

The two key parameters of the figure of merit are the temperature profile and the density (particle size) of the gases as they re-condense throughout the system. Temperature profiles in Section 6.1 are shown with the time (in seconds) on the x-axis and the temperature on the y-axis. Generally, tests show an instant increase in temperature when the thermite is ignited, and a slow decrease over time. Clumping results show an increase in particle size at all four levels sampled. The bottom two layers showed the most increase in particle size, while the top layer showed more functional defeat than the layer below it. Examples of temperature profiles and particles size are shown in Section 6.1.

6.1 Temperature

The locations at which temperature profiles were taken are shown again in Figure 52. The Bt sits, undisturbed, in the barrel for 30 minutes after ignition and samples are taken. Three samples are taken from each location (red dots). The sampling process is standardized to limit variance from test to test.

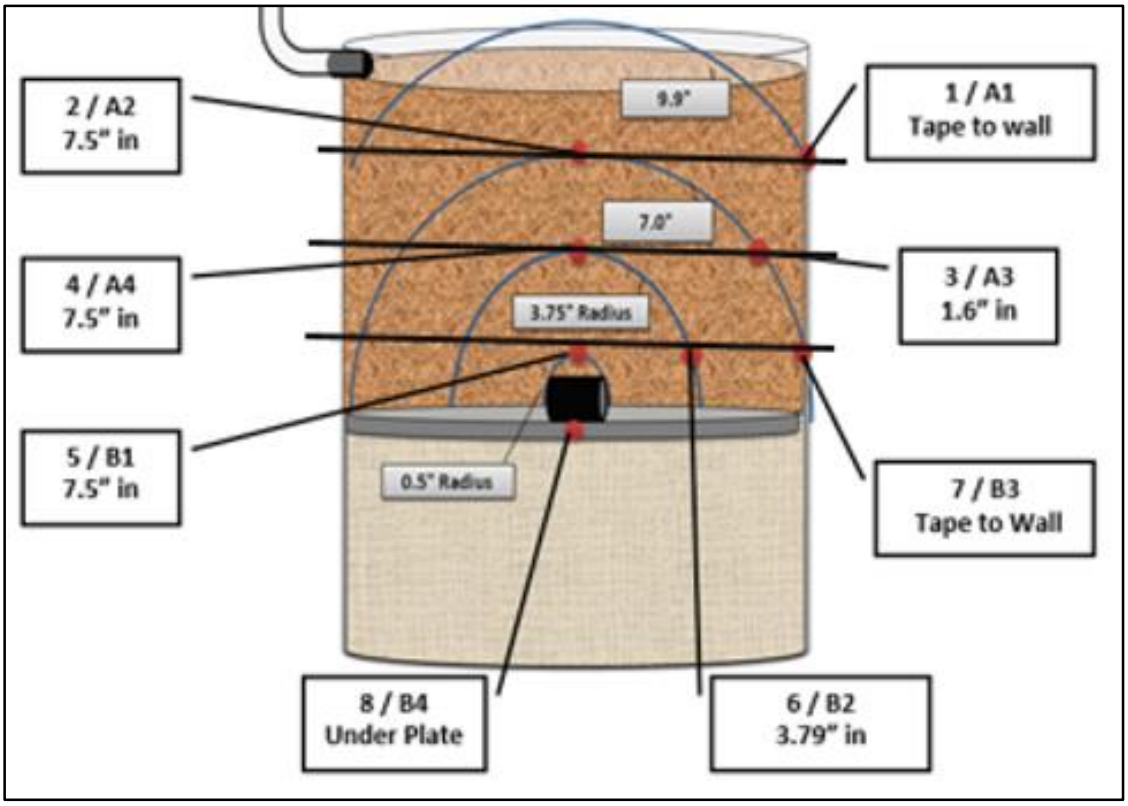

Figure 52 – Location of temperature profiles taken, shown by red dots.

Results from an experimental temperature profile can be seen in Figure 53. The light blue curve shows the measured temperature at the location closest to the thermite. The peak temperature at this location is just under 1000°C. Other curves, such as the purple, show a slight increase in temperature. Anywhere a dark red line is seen can be disregarded; this is located underneath the thermite charge and only serves to validate whether or not the charge ignited. Other locations see a slight increase in temperature, but remain just above ambient for the duration of the test.

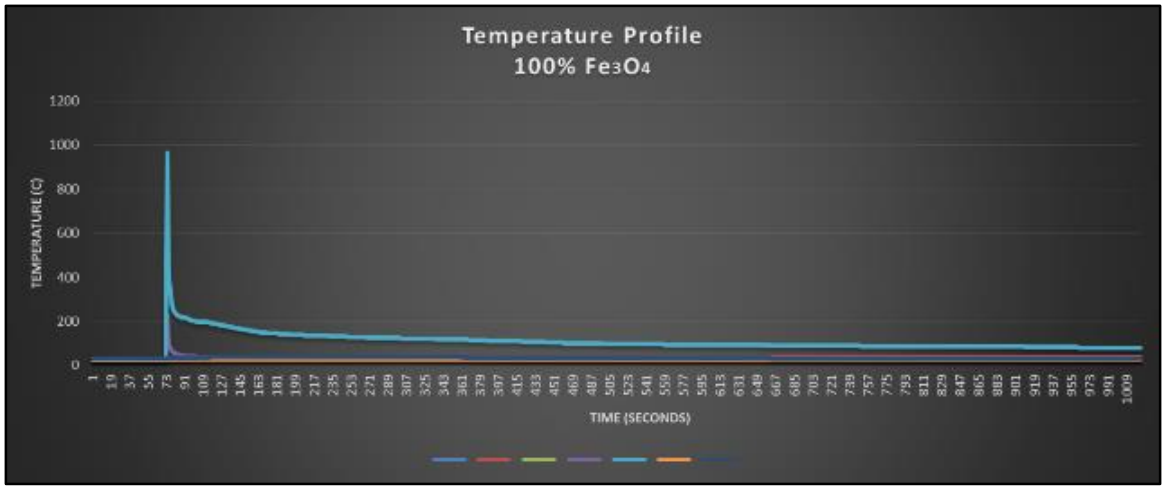

Figure 53 – Temperature profile logging different locations shown in barrel diagram.

Due to the chaotic reaction of a thermite ignition and burn, multiple tests were executed to provide confidence in the temperature profile data. Figure 54, Figure 55, Figure 56, and Figure 57 show four more profile from four more tests which are consistent to the one shown in Figure 53.

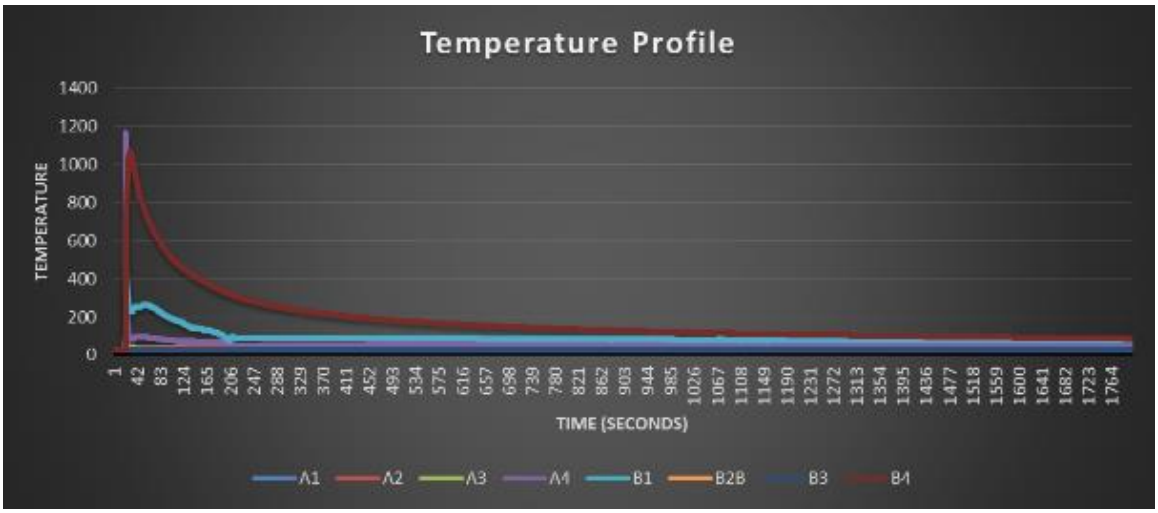

Figure 54 – Temperature profile of fast thermite experiment.

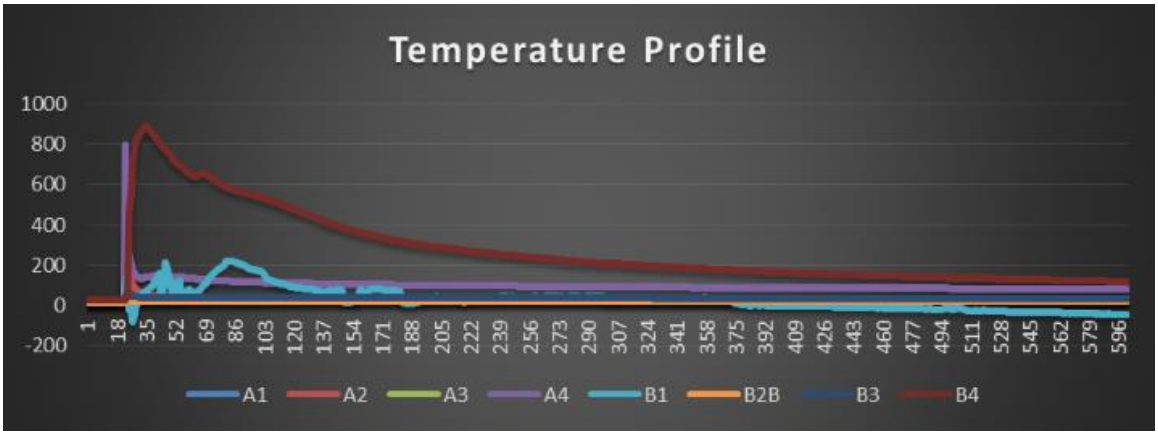

Figure 55 - Temperature profiles of fast thermite experiment.

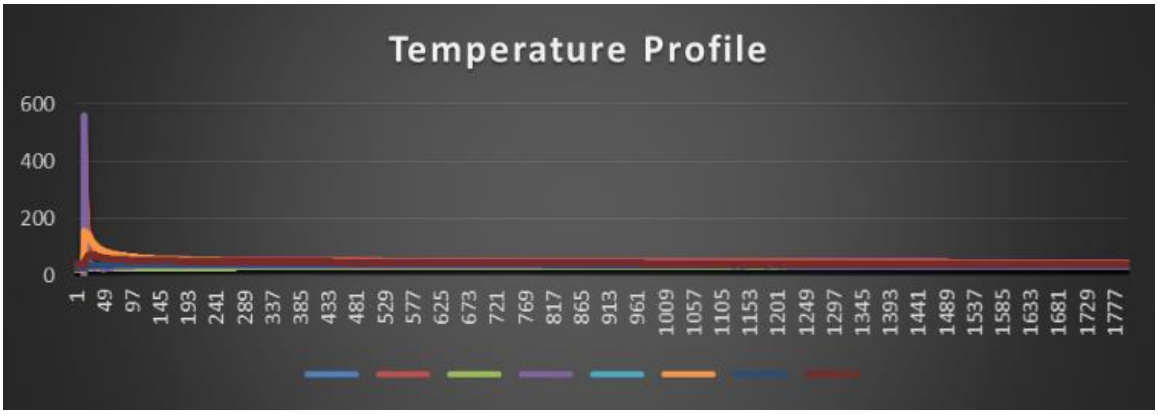

Figure 56 -Temperature profiles of fast thermite experiment.

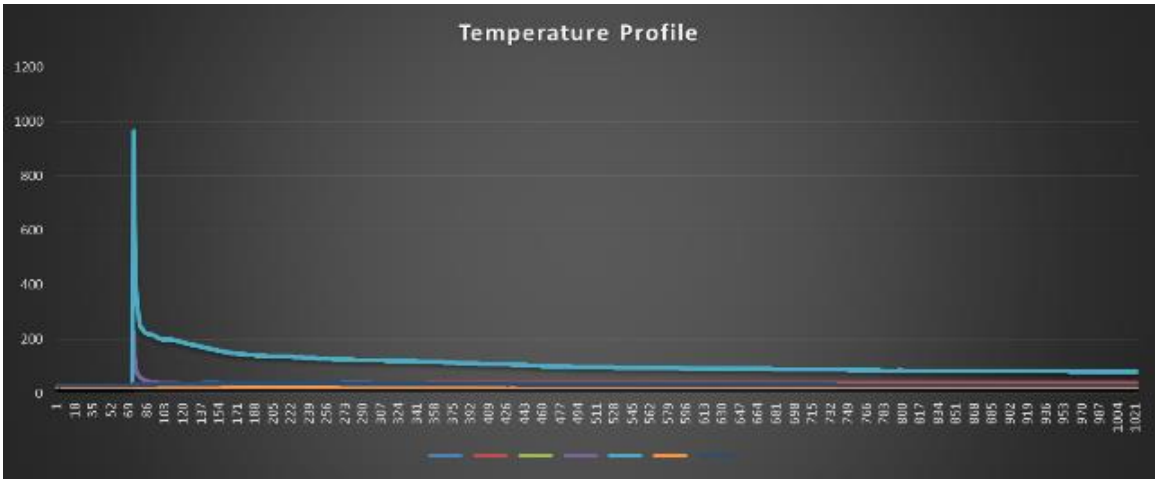

Figure 57 - Temperature profiles of fast thermite experiment.

The model produces a very similar figure to the experimental plots. Figure 58 shows the predicted temperature from the model. To the right of the graph is a 2-D representation of where the temperatures are taken in relation to the thermite charge. The charge is shown as a grey cylinder and a representation of the barrel is shown as black lines. The letters correspond to the locations where the temperatures are being taken. These letters span the distance from the origin to the wall of the barrel (total of 10 inches). For example, the letter ‘a’ is shown in pink. The location of this letter is half of an inch beside the thermite charge. Therefore the temperature at location ‘a’ is 0.5 inches away from the thermite. Figure 59 shows an alternative view of the control volume. This is a top down view. The red dot is the thermite (origin), and the letters ‘a’, ‘b’, and ‘c’ are the locations where temperature profiles were recorded and samples were taken for particle size analysis and viability.

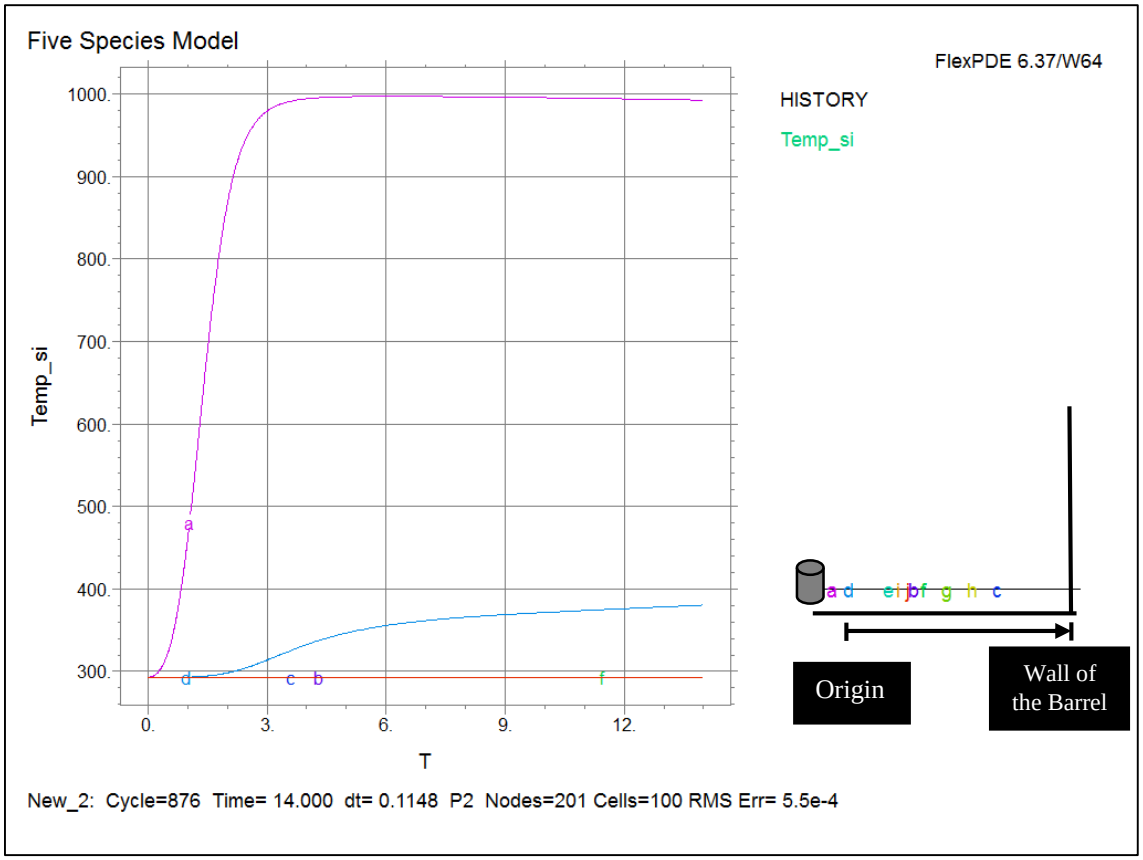

Figure 58 – Temperature profile generated using developed model.

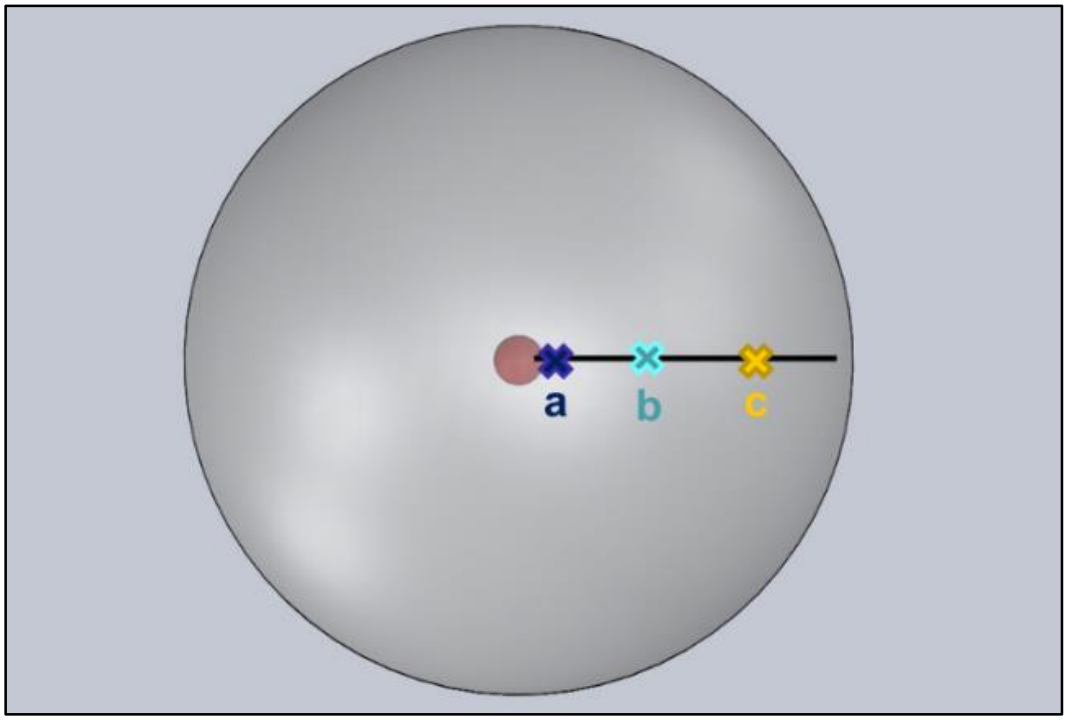

Figure 59 – Top down view of the barrel. The red dot is the thermite (origin) and the letters ‘a’, ‘b’, and ‘c’ are the locations that temperature profiles were recorded and samples were taken for particle size analysis.

Figure 58 is the modeling equivalent to the experiments that were run. The burn time was set to 1 second (recall this was determined by watching video of the experimental thermite burns). Comparing the model to the experimental results the curves are very similar. At location ‘a’ the experimental data shown in Figure 53 is almost exactly the same as it was in the modeling data. Figure 60 shows this comparison.

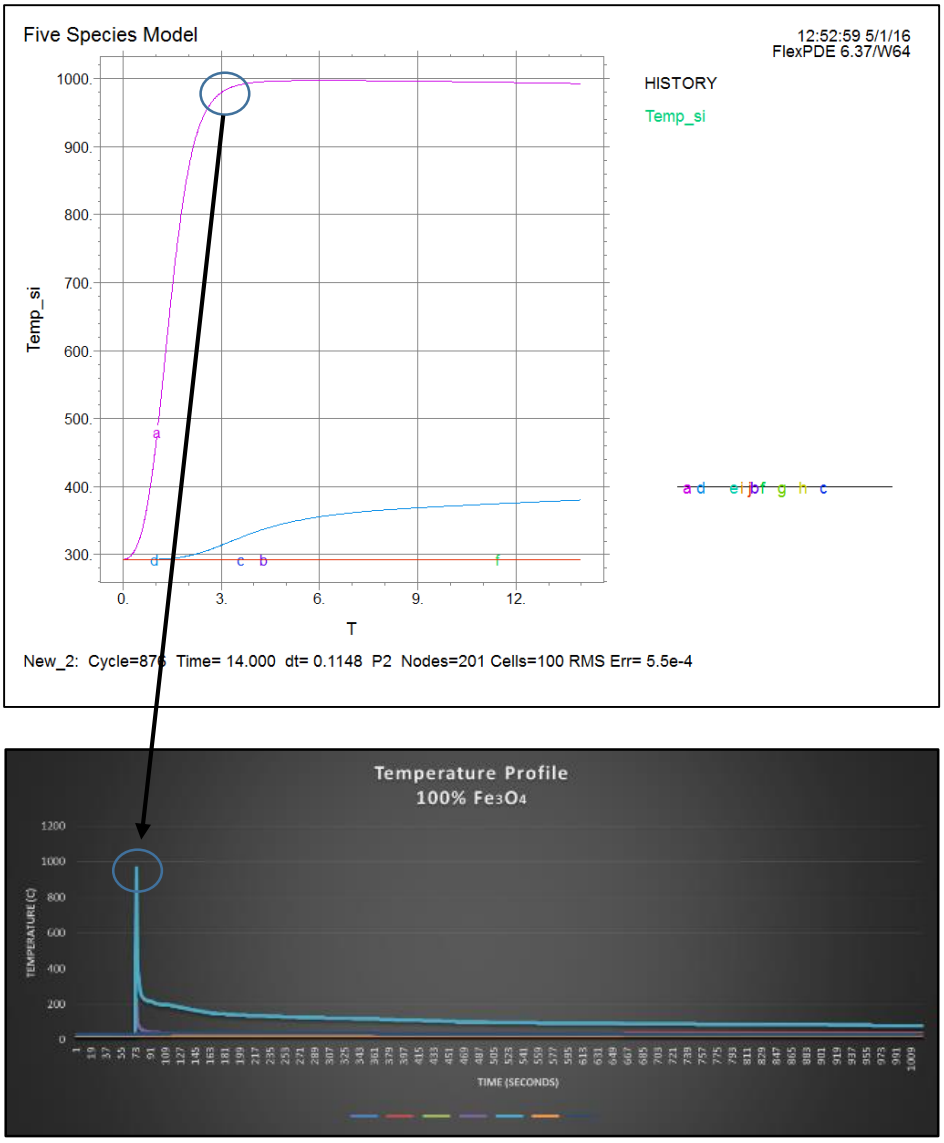

Figure 60 – Comparison of experimental data (bottom) and modeling temperature profile (top). Both temperatures reached a maximum around 1000 degrees Celcius.

Other experimental test data showed the maximum temperature of this location peaking at values of 1200° C, 800° C, and 600° C, likly due to the chaotic phenomena of a thermite ignition and burn. Using averaged data from multiple tests, it can be said that this model is a good representation of the expected temperature.

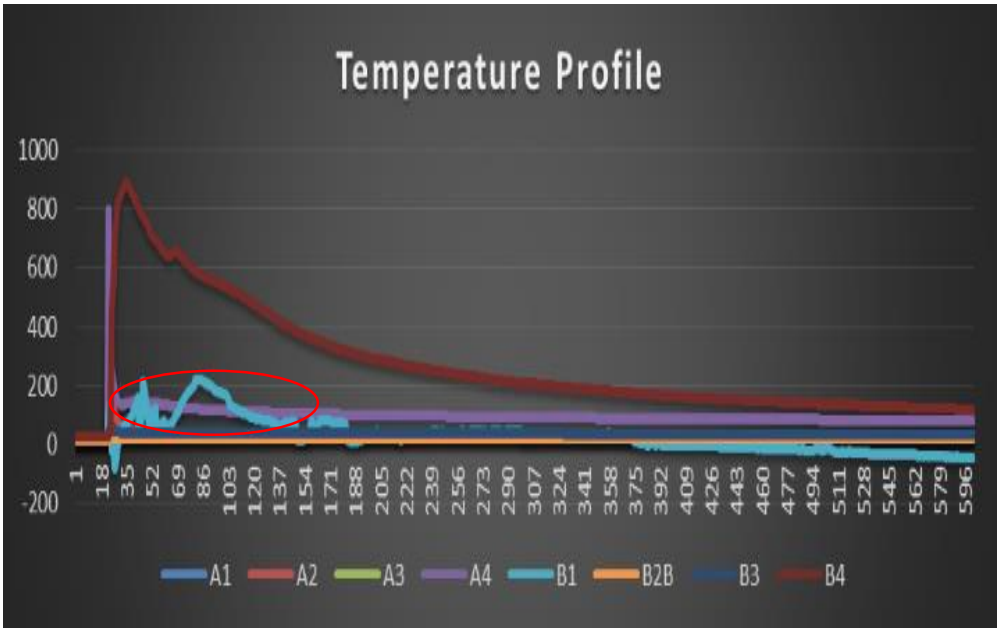

Figure 61 – Irregularities in experimental data. Increase in temperature profile that were not seen in other experiments or in the modeling data. These irregularities are shown with red circles.

While the model does generally track the experimental data, Figure 61 show irregularities in experimental data. These areas are shown with a red circle. When a thermite mixture burns the oxide reacts with the aluminum powder and produces a highly exothermic reaction, which can be violent. When seen in slow motion, little glowing particles of molten iron can be seen flying through the air. The model represents a single heat source which produces heat from one spot. These little balls of molten iron shooting into the system will occasionally land on the thermocouple wire and give a false temperature reading. This effect can be seen in Figure 62. In the left picture, the thermocouple wires are slid into place directly above the charge. In this test a piece of thermite reacted and pushed through the Bt onto the thermocouple wires. Because the thermite is molten iron, it welds to the wires. This causes much higher temperatures, and are not an accurate representation of the temperature rise in the Bt.

Figure 62 – Left, thermocouple wire before ignition. The wire is twisted and welded together at the end. Right, a piece of thermite shot out from the reaction and landed on the wire. This gives the thermocouple a temperature reading of the thermite, and not the material bed.

Different thermite compositions can be modeled by changing burn properties. One of these properties is the burn time. Most thermites tested experimentally in this work have a burn time of 1 second. A slight change in the particle size of the thermite can raise the burn time to roughly 5 seconds. Figure 63 and Figure 64 show the difference when the burn time is changed from 1 second to 5 seconds, respectively.

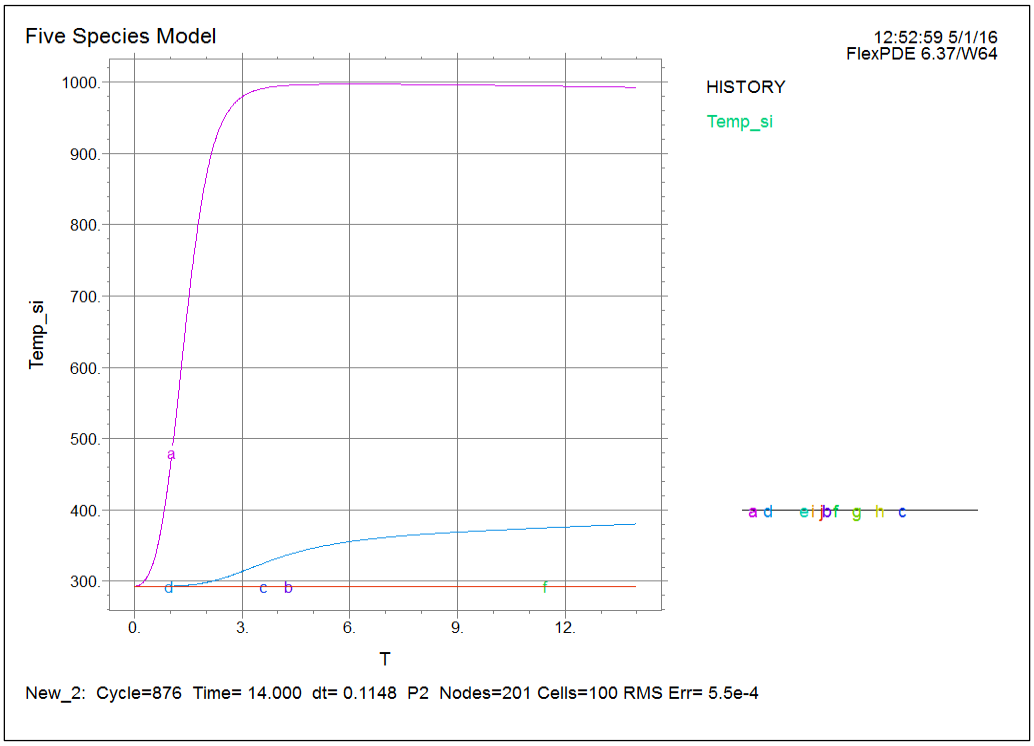

Figure 63 – Simulation with a thermite burn time of 1 second.

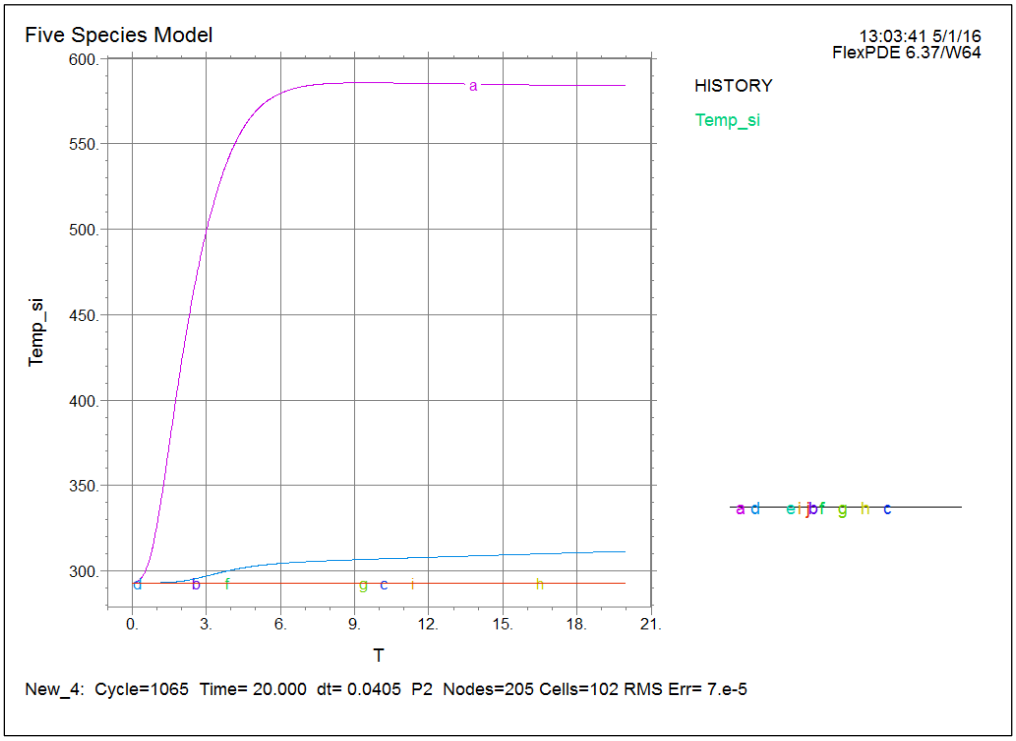

Figure 64 – Simulation with a thermite burn time of 5 seconds.

These simulations show that slowing the burn rate down will result in the temperature decreasing. It is also worth noting that the slower burn rate took longer to reach its maximum temperature before starting to decrease. This is done with the assumption that both charges still produce the same amount of energy.

6.2 Particle Size

As outlined in section 4.1, once a test is executed samples are taken at the same location as the temperature profiles being tracked. These samples are approximately 7-8 grams of material. To obtain the particle size these samples are examined to achieve two key data points: large and small particle size. Each sample is passed through a series of sieves with different size mesh (hole size) screens. This allows for the larger particles/clumps to be retained and the smaller ones to pass through (This process is explained in detail in section 4.4). Once the data is recorded for all 4 layers sampled, plus the baseline, it is presented in a bar graph that shows the percent of the sample that is above 300 microns, seen in Figure 66. The entire particle size process can be seen in Figure 65.

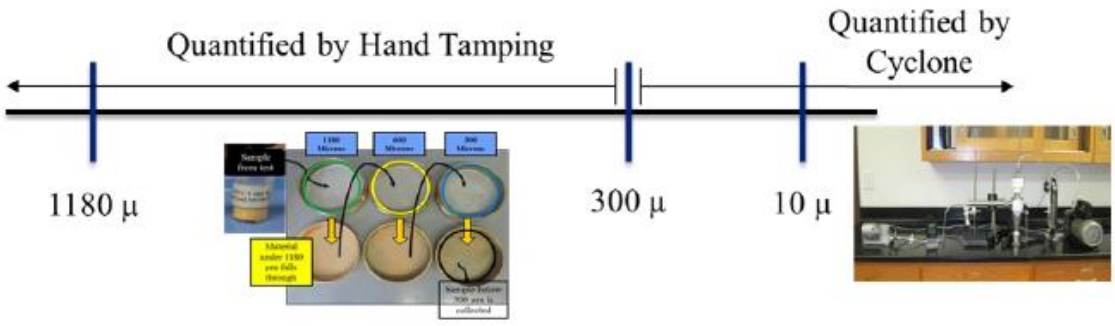

Figure 65 – Illustration of large and small particle size quantification process

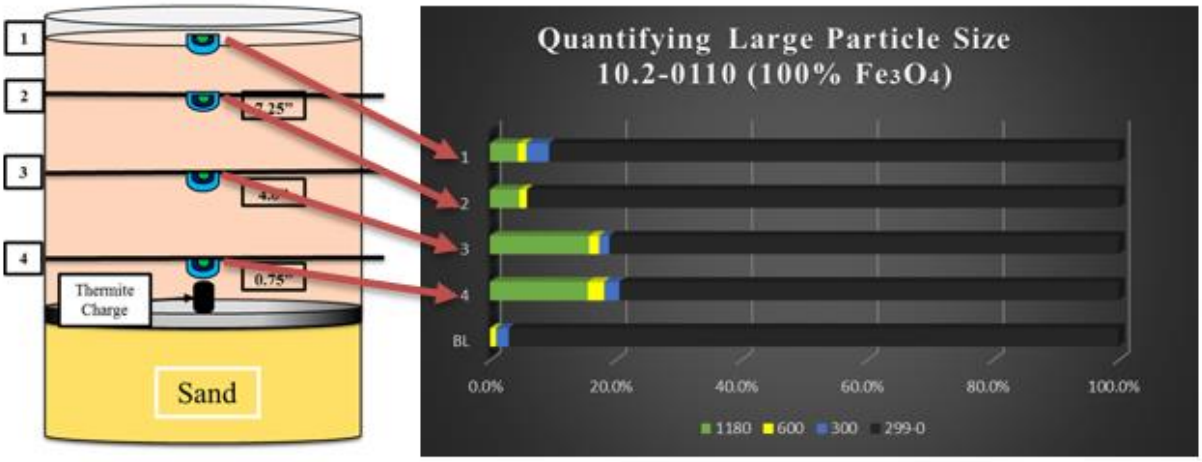

Figure 66 – Experimental clumping results from the 100% Fe_3O_4 thermite at different layers throughout the barrel. Left, an illustration of a barrel tests showing where the samples were taken. Right, Bar graph showing the percent of each sample above 300 microns, at each of the barrel levels.

The barrel in the left of Figure 66 is an illustration of where the samples are taken after a test is executed. The locations are at 0.75", 3.75", and 7.25" from the thermite. Samples are also taken off the top layer of the barrel after the burn and a baseline/virgin sample taken from the top before the thermite is ignited. These sample location correspond to the same location the temperature profiles are taken. The graph in the right of the picture is the data taken from the material that is passed through the sieves. Each bar on the graph corresponds to an individual layer in the barrel; the red arrows show each location the data represents.

Each "bar" on the graph represents 100% of the sample (by weight). The x-axis is the percent of that sample, staring at 0% on the left and going to 100% on the right. Each color of the line represents a different sieve size and the percent of the material that got caught in that sieve and did not pass through: the green portion is the 1180 micron sieve, the yellow portion is the 600 micron sieve, the blue portion is the 300 micron sieve, and

the black is everything was small enough to fall through all three sieves. For example, the top line is the sample from the top of the barrel after the thermite is ignited and the test is finished. The data says that roughly 7% of the sample was caught in the first sieve (1180 microns), 2% was caught in the second sieve (600 microns), and 5% of the sample was caught in the third sieve. Therefore, 14% of the sample was larger than 300 microns. This is compared to a baseline sample for each tests, the bottom line in the graph. The baseline of this test showed that only 4% of the sample was larger than 300 microns. Therefore it can be said that at the top of the barrel there was a 10% by weight increase in particles over 300 microns after the thermite burn. The results from this test show that the layers 4 and 3 (closest to the thermite) increased clumping from 4% to almost 20%.

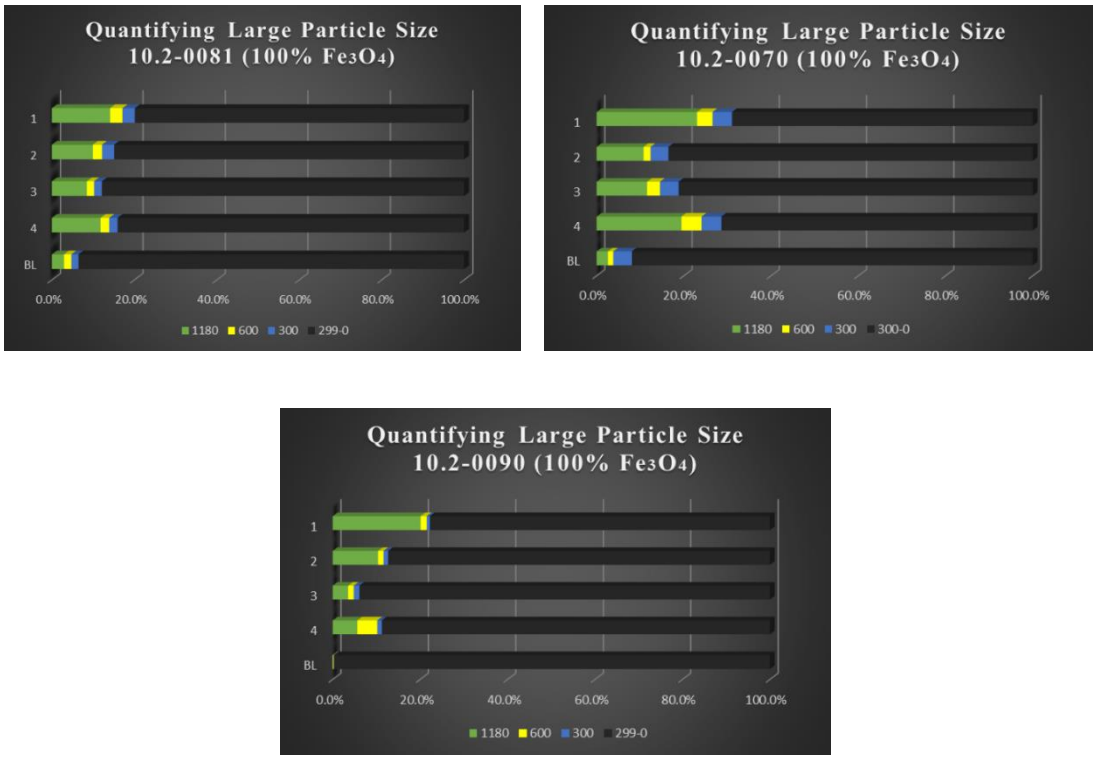

Figure 67 – Data from multiple tests showing the increase in particle size related to the baseline for different barrel layers

Figure 67 shows the results from three more tests that were executed. There are slight variations from test to test, but the trends are consistent. The layer directly above the origin (number 4 on the y-axis) and the top layer (number 1 on the y-axis) showed the largest increase in particle size.

The portion of the sample that passes through the last sieve is processed further to determine the "small" particle percentage. The samples are sent to an off-site lab that uses a hydrocyclone to determine the percent of the sample under 10 microns. This process is also explained in detail in section 4.4. Figure 68 shows the hydrocyclone used for analysis. The sample is introduced into the system from the left of the picture and fed into the cyclone. There is a collection plate at the bottom that catches all the material that is over 10 microns, while the material less than 10 microns is carried out through the tube on the right.

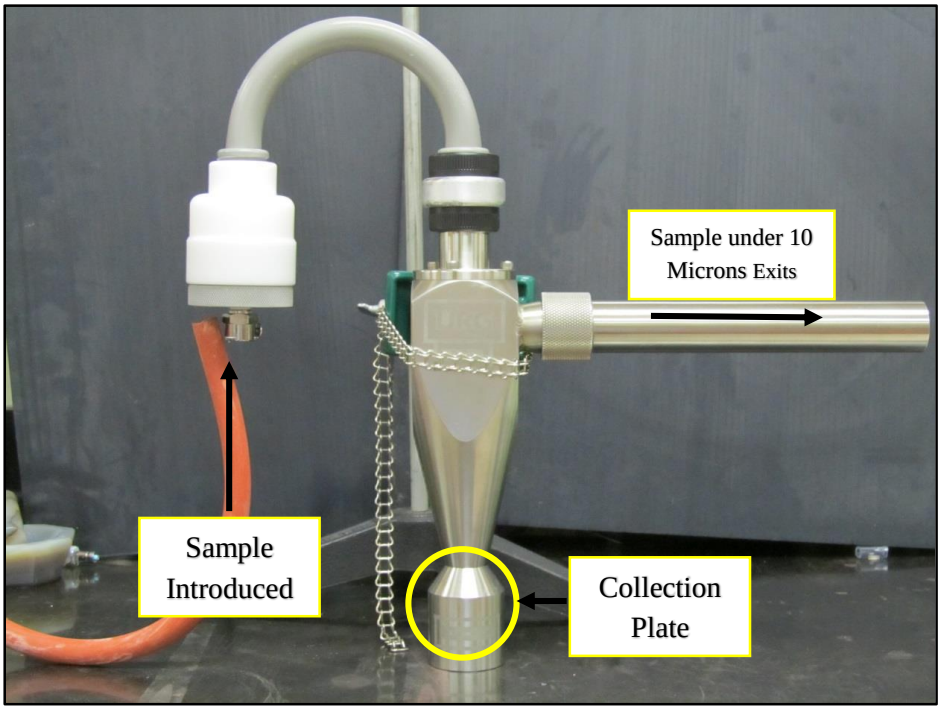

Figure 68 – Hydrocyclone used to determine small particle size.

Due to the time required for test preparation and cleaning of the apparatus, only a few samples were sent for analysis of small particle size. A baseline sample and the sample closest to the thermite (0.75” away from the origin) were analyzed using this method. Figure 69 shows the small particle size results from these samples, showing 26-27% of the baseline was under 10 microns. After the thermite burn, the small particles dropped to 18%, a reduction of almost 10%.

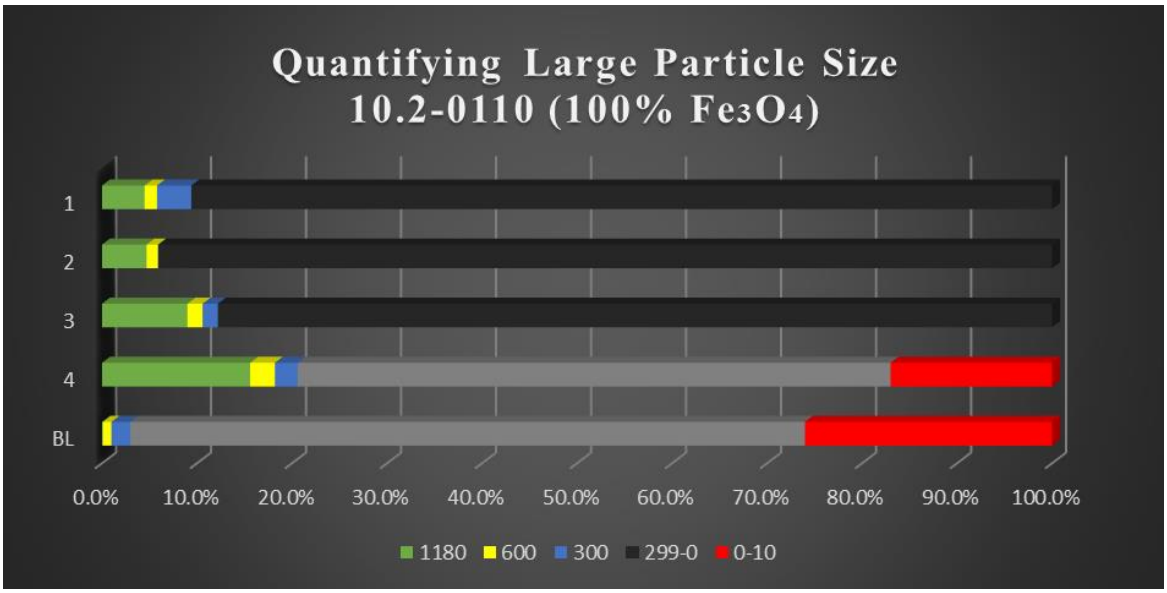

Figure 69 – Particle size data showing large and small size for baseline and location directly above the origin of the thermite.

Figure 70 presents the model data slightly different than the bar graph from the experimental results. The x-axis is the limits/bounds set within the model. The origin of the graph starts at the center of the thermite and the far right of the graph is the interior wall of the barrel. The y-axis is an increase in beta, the volume fraction times the density. As the model solves the differential equations it tracks the density throughout the system. Therefore where the values for beta increase/decrease, the density also increases/decreases.

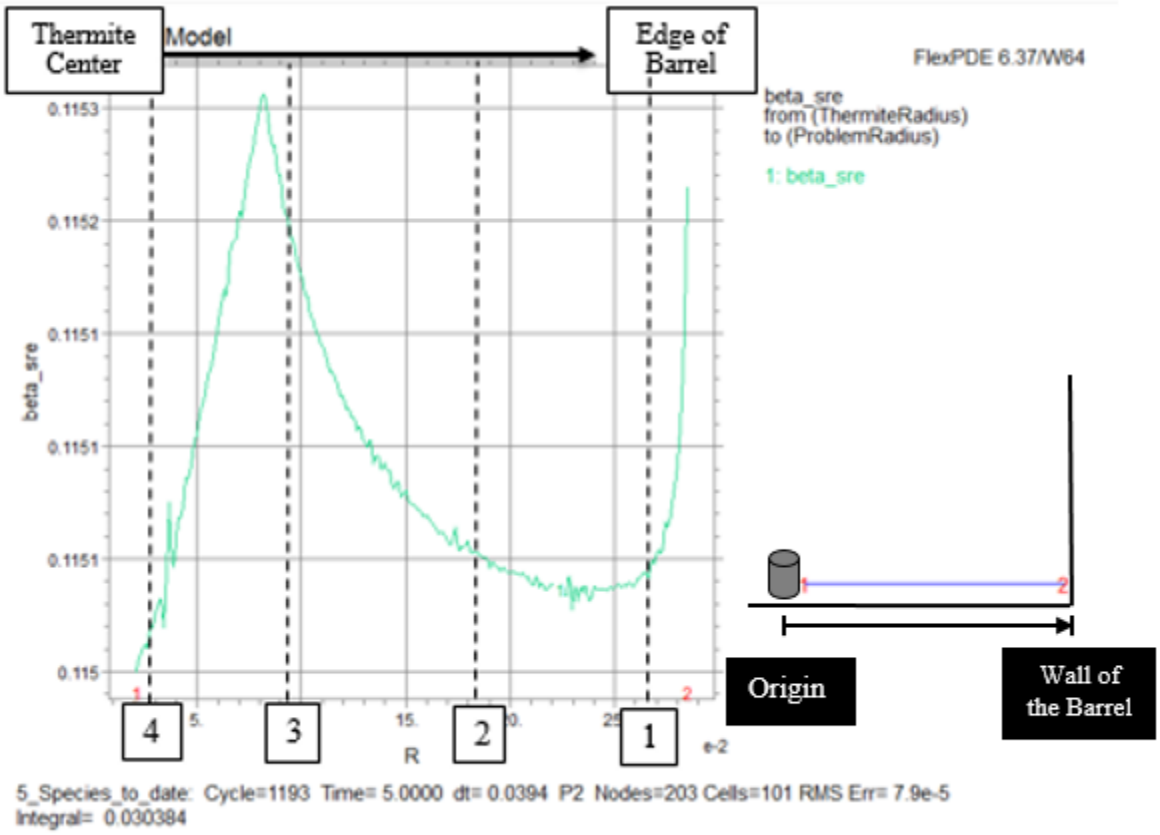

Figure 70 - Results from the model showing where the maximum density within the barrel can be expected

In order to better understand Figure 70 the sampling locations of the layers of the barrel are indicated on the bottom of the graph (4, 3, 2, and 1). Number 4 being the closest to the thermite (0.75" away) and number 1 being the top layer of Bt in the barrel (farthest away from the thermite charge).

Figure 71 shows a side by side comparison of the experimental data (Top) to the modeling data (Bottom), with promising results. From the experimental data it is seen that the majority of the clumping is achieved closer to the thermite charge (Layers 4 and 3), while there is an increase at the top of the barrel as well (Layer 1), while bypassing layer

2. The model shows the peak density will occur between layers 3 and 4, and also shows an increase as it approaches the wall of the barrel.

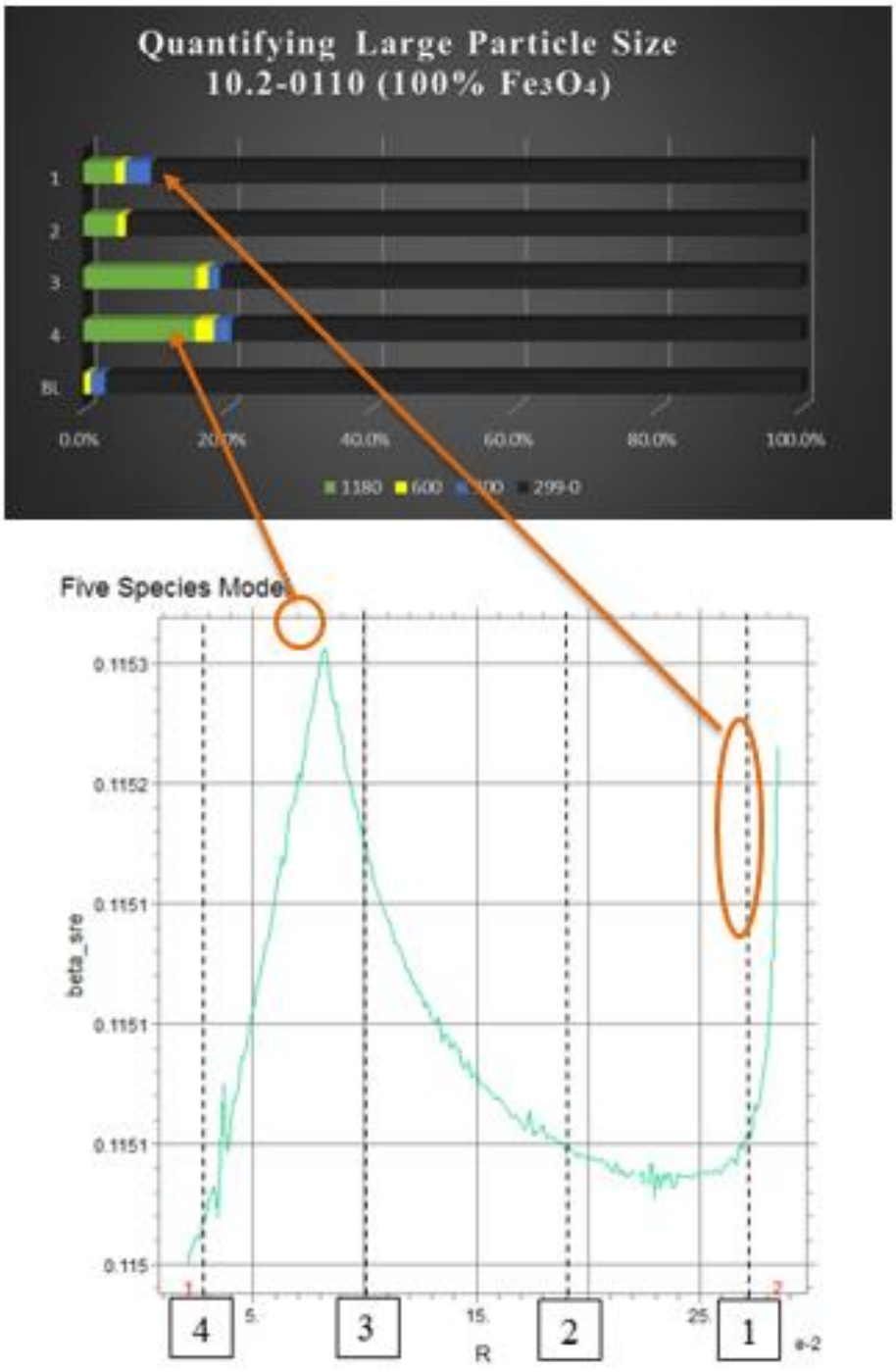

Figure 71 – Correlating data between the model and experiments show agreeable results.

The high temperatures are creating condensable gases, and as those condensable gasses cool, they re-condense. The model results capture where those re-condensable gases will have the highest density. These areas are highlighted in the orange circles in Figure 71, and correlate fairly well with experimental data.

As discussed in Chapter 5 different thermite compositions can be modeled by changing burn properties. When the burn time of the thermite is adjusted, the resulting density changes within the system can be seen below in Figure 72 and Figure 73.

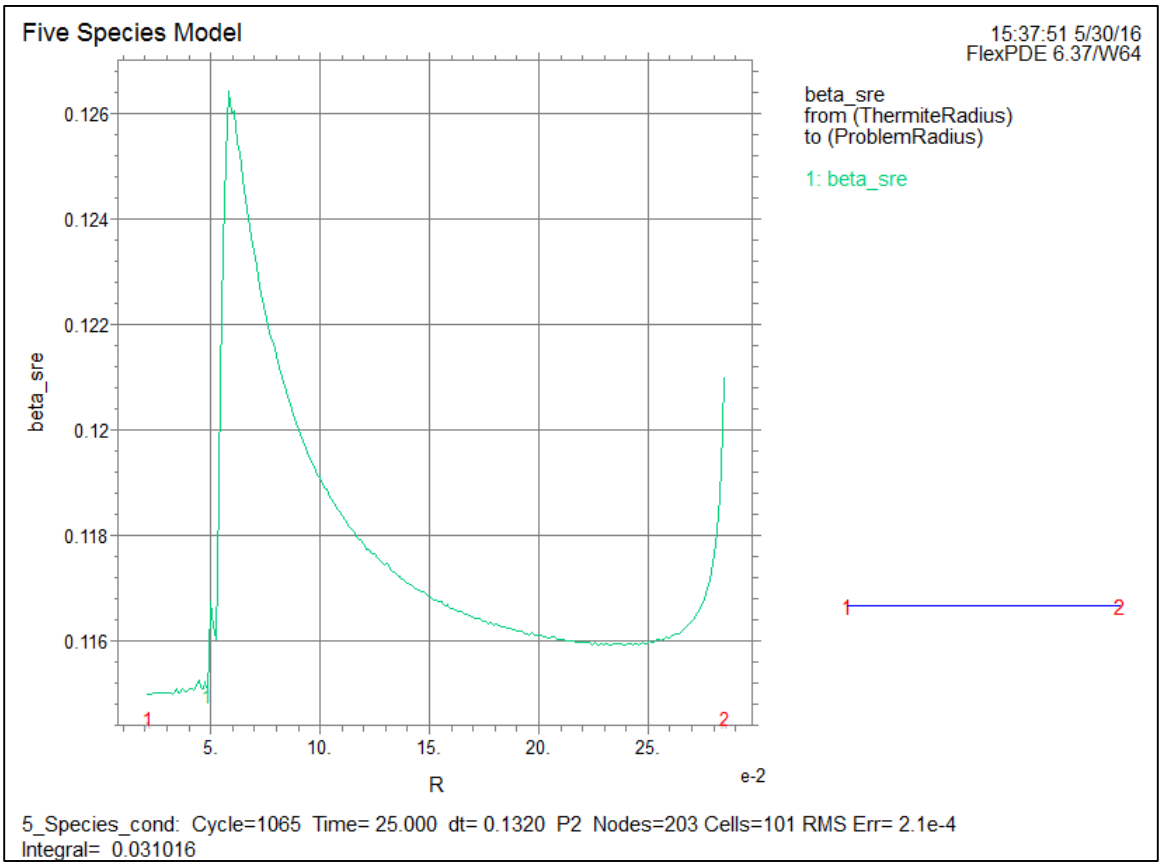

Figure 72 – Density results from the model with a thermite burn time of 1 second.

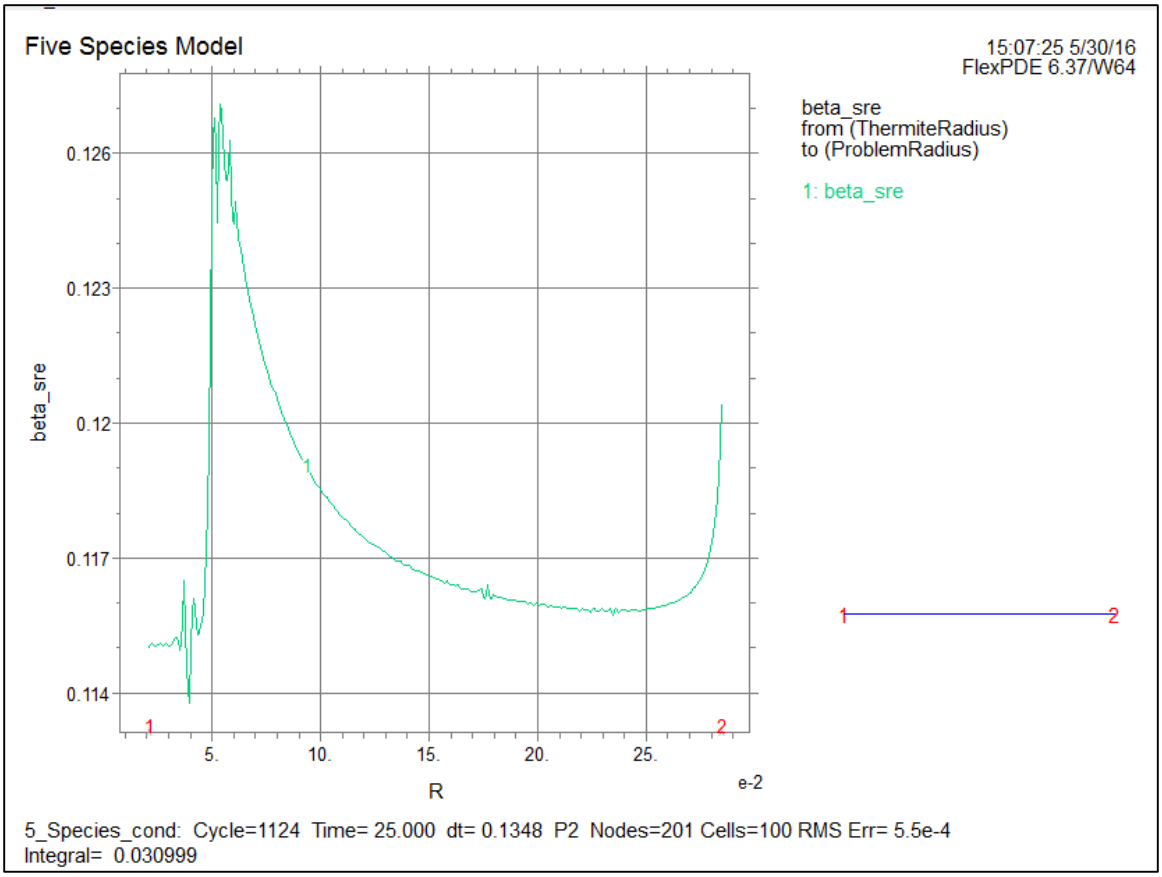

Figure 73 - Density results from the model with a thermite burn time of 5 seconds

The changes seen in the density due to altering the burn rate do not appear to change the modeling result as much as the burn rate effects the temperature. With a thermite burn increase to 5 seconds, there is a slight increase in density close to the thermite, and a slight decrease in density on the wall of the barrel. When coupled with the temperature profiles of the 1 second compared to the 5 second burn time, this makes sense. The temperatures for the 5 second burn were far less than a 1 second burn (300° C less). Assuming the same amount of energy is produced in both systems, the higher temperatures carry the re-condensable gases farther throughout the system, i.e. closer to the wall. Conversely the

lower temperatures show an increase in density closer to the origin due to the temperature gradients having a lower value.

Chapter 7: Conclusion

The objective of this thesis was to understand the fundamental phenomena that occurs when a high-energy heat source is placed inside a barrel of weaponized biological agent in the form of spores. The actual agent of concern is Bacillus Anthracis (Ba), but it is extremely dangerous and was not used for this type research. Rather, a strain of Bacillus, Bacillus Thuringiensis (Bt), was used as a simulant for Ba. The Bt was purchased as Javelin and mixed with silica to create a mixture similar to those of concern. With this simulant, a series of experiments and supporting numerical calculations were performed, with the goal of developing a sufficiently complex model to aid in development of concepts.

The experiments in this work were performed with a 10 gallon barrel filled with the simulant mixture. Different compositions of thermite were ignited inside the 10 gallon barrels of simulant, and data was taken to record the spatial temperature profiles as a function of time. After each experiment, a rigorous process was followed to quantify the aggregate size distribution at different locations in the barrel.

Since Bacillus spores are a living organism, they can be killed and/or rendered non-toxic to humans. It has been demonstrated that killing these spores with temperature is very difficult. Creating clumps of spores that are bigger than the human respirable limit (10 microns), proved to be a more attainable goal. When the spores are burned, a sticky material from their exospore is released. Additionally, as the spores and fill material burn, they created a combination of permanent gases and re-condensable gases. As these gasses re-condense in cooler parts of the barrel, they cause the material to stick together, creating clumps the size of marbles, functionally defeating the weaponized spores.

To better understand phenomena and predict performance of untested energetics, a detailed finite-element model (FEM) was developed to help optimize the design.

The model solves the coupled continuity and energy equations for 5 different species. Previous work shows that the properties of a bulk Bt mixture closely resemble that of a fluidized bed, which has a constant velocity profile. Consequently, for this work, it was assumed that the velocity is a time constant, but could vary with location. Supporting experiments were performed to measure a representative velocity profile to represent the momentum equation with the model.

The results of the model predictions agreed very well with the experimental data, indicating that the model accurately simulates the key aspects of the in-barrel phenomena. The analysis in this thesis is the first to capture the significance of the different type species in heat transport of this type of media, and it is the first work that correlates the created clumps of material with the re-condensation of vaporized organics within the mixture.

As expected, the location closest to the energetic, the origin, showed the highest temperatures, ranging from 700° C to 1000° C, which agreed well with the model predictions. Other temperature measurement locations also agreed very well with the model prediction. The ability of the model to accurately predict temperature at several locations for many different type thermites indicates the physics captured by the model are correct. In particular, the model's ability to track vapors being created, diffusing through the mixture, and then re-condensing is critical. This combined heat and mass transport is the dominate heat transport mechanism in this system, and has not captured by previous finite element conduction models.

Also in this work, reliable process was developed to quantify particle sizes down to 10 microns (respirable limit) after a thermite is ignited and burns inside a barrel. As shown, the model tracks the gases re-condensing throughout the mixture, which creates clumps. If, as postulated, the clumps are created by these re-condensed gases, the areas where the model predicts the greatest re-condensation should match with the experimental location with the greatest amount of clumping. Chapter 6 captures the correlation between the experimental data and modeling results in Figure 71.The graph shows the density of the re-condensed gas as a function of distance from the energetic source predicted by the model. This density represents the amount of the re-condensed gas. At about 8 cm from the source, the temperature drops below the vapor temperature of gasses, and they start to re-condense. Since re-condensation is fast compared to the diffusion velocity, the model actually predicts the peak re-condensation occurs at about 8 cm from the source. The results also shows the percent of particles above 300 microns measured after the experiment. The peak clumping measured in the experiment occurs closer to the source at almost 2 cm. This correlation between the model prediction and experimental measurement provides strong evidence that the model is sufficiently capturing the key mechanism causing clumping. Another interesting observation is that both the model and the experimental data show an increase in clumping about 20 to 25 cm from the source. That location is the top of the barrel, and both the experimental data and model accurately capture the gasses trapped and re-condensed at that location. Again, it is striking how accurate the model seems to predict the experimental measurements.

In summary, the validity of complex models, and the underlying assumptions, must be viewed skeptically unless validated with experimental data. A major accomplishment of this effort was that results from the model and the experiment match. From this, it is likely that the fundamental phenomena within this system are as follows:

(1) The heat transport is dominated by the mass transport of the gases as they diffuse and re-condense throughout the system.

(2) The clumping also is caused by the gases re-condensing throughout the system.

8. References

[1] A. Chemical, "Final report for contract F08630-03-C-0018, Agent Defeat Short Term Neutralization Data Collection and Modeling," 2006.

[2] G. D. R. A. P. J. T. David Moore, "Guidebook to Fungi," Cambridge University Press, 2011.

[3] G. Jenson, B. M. Hanson, J. Eilenberg and J. Mahillon, "The hidden lifestyle of Bacillus cereus and Relatives," Society for Applied Microbiology and Blackwell Publishing Ltd, 2003.

[4] D. A. Rasko, C. S. Han, M. R. Altherr and J. Ravel, "Genomics of the Bacillus Cereus Group of Organisms," Federation of European Microbiological Societies, 2005.

[5] Han, Cliff S. et al., "Pathogenomic Sequence Anlysis of Bacillus Cereus and Bacillus Thuringiensis Isolates Closely Related to Bacillus Anthracis," Journal of Bacteriology, May 2006.

[6] E. e. a. Helgason, "Bacillus anthracis, Bacillus cereus, and Bacillus thuringiensis—one species on the basis of genetic evidence," *Applied and environmental microbiology 66.6,* pp. 2627-2630, 2000.

[7] T. V. e. a. nglesby, "Anthrax as a biological weapon: medical and public health management," *Jama 281.18,* pp. 1735-1745, 1991.

[8] Y. Maeda and S. Koga, "Thermal Properties of Water in Bacillus cereus Spores and Vegetative Cells," *Netsusokutei,* vol. 8, no. 2, pp. 57-61, 1981.

[9] L. L. Wang, Y. M. Munir and Y. M. Maximov, "Thermite Reaction: their utilization in the synthesis and processing of materials," *Journal of material science,* no. 28, pp. 3693-3708, 1993.

[10] F. Shimojo, A. Nakano, R. K. Kalia and P. Vashishta, "Electronic processes in fast thermite chemical reactions: A first-principle molecular dynamics study," *Physical Review E,* vol. 77, no. 6, p. 066103, 2008.

[11] L. Duraes, B. F. Costa, R. Santos, A. Correia, J. Campos and A. Portugal, "Fe2O3/aluminum thermite reaction intermediate and final products characterization," *Material of Science and Engineering,* vol. A, no. 465, pp. 199-210, 2207.

[12] A. P. Snyder and J. P. Dworzanski, "Correlation of Mass Spectrometry Identified Bacterial Biomarkers from a Fielded Pyrolysis-Gas Chromatography-Ion Mobility Spectrometry Biodetector with the Microbiological Gram Stain Classification Scheme," Edgewood Chemical Biological Center Report Number ECBC-TR-415, September 2005.

[13] D. Lathouwers and J. Bellen, "Modeling of Biomass Pyrolysis for Hydrogen Production: The Fluidized Bed Reactor," California Institute of Technology, 2001.

[14] C. C. Pain, S. Mansoorzadeh, C. R. E. de Oliveira and A. J. H. Goddard, "Numerical Modeling of gas-solid fluidizing beds using the two-fluid appoach," John Wiley & Sond, Ltd., 2001.

[15] K. Zhang, S. Brandani, J. Bi and J. Jiang, "CFD simulation of fluidization quality in the three-dimensional fluidized bed," *Progress in Natural Science,* vol. 18, pp. 729-733, 2008.

[16] D. Lathouwers and Bellan, "Modeling and Simulation of Bubbling Fluidized Beds Containing Particle Mixtures," *Proceedings of the Combustion Institute,* vol. Volume 28, pp. 2297-2304, 2000.

[17] D. Lathouwers and J. Bellan, *Multiphase Flow Equations for Modeling Tar Production from Biomass Particle Pyrolysis in a Fluidized Bed Reactor,* Pasadena CA: Jet Propulsion Laboratory, California Institute of Technology.

[18] D. Lathouwers and J. Bellan, "Modeling of dense gas-solid reactive mixtures applied to biomass pyrolysis in a fluidized bed," *International Journal of Multiphase Flow,* no. 27, pp. 2155-2187, 2001.

[19] B. A. Craig and C. D. Shackelford, "Soil-Water Characteristic Curves and Dual Porosity of Sand-Diatomaceous Earth Mixtures," *Journal of geotechnical and geoenvironmental engineering,* no. September, pp. 790-800, 2001.

[20] A. Ray, "Finite Element Modeling and Simulation," Atlanta, 2006.

[21] W. P. Donovan, J. C. Donovan and J. T. Engleman, "Gene Knockout Demonstraties That vip3A Contributes to the Pathogenesis of Bacillus Thuringiensis toward Agrotic ipsilon and Spodoptera exigua," *Journal of Invertebrate Pathology,* vol. 78, pp. 45-51, 2001.

[22] D. Lathouwers and J. Bellan, "Modeling of dense gas-solid reactive mixture applied to bionmass pryrolysis in a fluidized bed," *Proceedings of the 2000 U.S. DOE Hydrogen Program Review,* p. 570, 2000.